

**3D FINITE ELEMENT MODELLING OF SURFACE EXCAVATION AND
LOADING OVER EXISTING TUNNELS**

**A THESIS SUBMITTED TO
THE GRADUATE SCHOOL OF NATURAL AND APPLIED SCIENCES
OF
MIDDLE EAST TECHNICAL UNIVERSITY**

BY

ONUR KAÇAR

**IN PARTIAL FULFILLMENT OF THE REQUIREMENTS
FOR
THE DEGREE OF MASTER OF SCIENCE
IN
CIVIL ENGINEERING**

JULY 2007

Approval of the thesis:

**3D FINITE ELEMENT MODELLING OF SURFACE EXCAVATION AND
LOADING OVER EXISTING TUNNELS**

submitted by **ONUR KAÇAR** in partial fulfillment of the requirements for the
degree of **Master of Science in Civil Engineering Department, Middle
East Technical University** by,

Prof. Dr. Canan Özgen
Dean, Graduate School of **Natural and Applied Sciences** _____

Prof. Dr. Güney Özcebe
Head of Department, **Civil Engineering** _____

Prof. Dr. Orhan Erol
Supervisor, **Civil Engineering, Dept., METU** _____

Examining Committee Members:

Prof. Dr. Yener Özkan
Civil Engineering Dept., METU _____

Prof.Dr. Orhan Erol
Civil Engineering Dept., METU _____

Prof.Dr. Ufuk Ergun
Civil Engineering Dept., METU _____

Assoc. Prof. Dr. Kemal Önder Çetin
Civil Engineering Dept., METU _____

Dr. Mutlu Akdoğan
Geoteknik Çözüm ve Proje _____

Date: _____

I hereby declare that all information in this document has been obtained and presented in accordance with academic rules and ethical conduct. I also declare that, as required by these rules and conduct, I have fully cited and referenced all the material and results that are not original to this work.

Name, Last Name: Onur KAÇAR

Signature:

ABSTRACT

3D FINITE ELEMENT MODELLING OF SURFACE EXCAVATION AND LOADING OVER EXISTING TUNNELS

KAÇAR, ONUR

M.Sc., Department of Civil Engineering

Supervisor: Prof. Dr. Orhan Erol

July 2007, 114 Pages

The influence of surface excavation and loading on the existing tunnels has been investigated using a Finite Element Method program, Plaxis 3D Tunnel. A parametric study has been carried out where the parameters were the depth of the surface excavation, the eccentricity of the excavation with respect to the tunnel axis, the height of the embankment fill and the stiffness of the soil. It is found that, excavations over the existing tunnels have a negative effect on the tunnel lining capacity since the unloading due to the excavation reduces the normal forces and increases the bending moments. On the other hand, it is found that surface loading within the limits considered in this study is not critical in terms of the tunnel stability due to the increase in normal forces and decrease in bending moments.

Keywords: Tunnel, numerical analysis, NATM

ÖZ

VAROLAN TÜNELLERİN ÜZERİNDEKİ KAZI VE YÜKLEMELERİN 3-BOYUTLU SONLU ELEMAN YÖNTEMİYLE MODELLENMESİ

KAÇAR, Onur

Yüksek Lisans, İnşaat Mühendisliği Bölümü

Tez Yöneticisi: Prof.Dr. Orhan Erol

Temmuz 2007, 114 Sayfa

Bu çalışmada, varolan tünellerin üzerinde yapılan kazı ve yüklemelerin etkileri, 3-boyutlu sonlu eleman yöntemi programı Plaxis 3D Tunnel kullanılarak araştırılmıştır. Parametrelerin, kazı derinliği, kazının tünel eksenine göre eksantrikliği, dolgu yüksekliği ve zeminin deformasyon modülünün olduğu parametrik bir çalışma yapılmıştır. Tünellerin üzerindeki kazıların, tünel kaplamalarının kapasitesine negatif etkisi olduğu görülmüştür. Bunun sebebi, kazıya bağlı yük boşalmasının eksenel kuvvetleri azaltması ve momentleri artırmasıdır. Diğer taraftan, bu çalışmada incelenen limitler içerisinde kalan yüzey yüklemelerinin tünel stabilitesini açısından kritik olmadığı görülmüştür. Bunun sebebi de eksenel kuvvetlerdeki artış ve momentlerdeki azalmadır.

Anahtar Kelimeler: Tünel, Numerik Yöntemler, YATM

To my Family

ACKNOWLEDGMENTS

I would like to express my deepest gratitude to my supervisor Prof. Dr. Orhan Erol for his guidance, advice, criticism and encouragement throughout the research.

I would like extend my sincere thanks to Assoc. Prof. Dr. K. Önder Çetin for his valuable suggestions, comments and help.

I would like to thank to the members of the Examining Committee for their suggestions and comments.

I would also like to thank to Res. Asst. Berna Unutmaz for her suggestions and help.

I would like to extend my thanks to Onur Kürüm, Erinç Bahçegül and Gül Çorbacioğlu for their endless support and help in software and format related problems. I would also like to thank to Engin Özkol, Mehmet Moralı and Özlem Dede for their valuable support.

TABLE OF CONTENTS

ABSTRACT.....	iv
ÖZ.....	v
ACKNOWLEDGMENTS.....	vii
TABLE OF CONTENTS.....	viii
CHAPTER	
1.INTRODUCTION.....	1
2.LITERATURE REVIEW AND BASIC CONCEPTS.....	4
2.1 Chronological View of Tunnels.....	4
2.2 Types of Tunnels.....	5
2.2.1 According to the Function	5
2.2.1.1 Railways	5
2.2.1.2 Metro Tunnels.....	5
2.2.1.3 Highway Tunnels	6
2.2.1.4 Water Conveyance Tunnels	6
2.2.2 According to the Construction Technique	7
2.2.2.1 Cut and Cover	7
2.2.2.2 Earth Boring&Pipe Jacking	7
2.3 NATM.....	8
2.3.1 NATM Philosophy	9
2.3.2 NATM Construction Technique	9
2.3.3 NATM in Rock.....	10
2.3.4 NATM in Soft Soil.....	11
2.4 Tunnel Design and Analysis.....	11
2.4.1 Stresses and Deformations in Tunnels	12
2.4.2 Surface Settlements.....	17
2.5 Numerical Methods	18
2.5.1 Beam Element Method with Elastic Support	19
2.5.2 Finite Element Method	20

2.5.3 Finite Difference Method	22
2.5.4 Boundary Element Method.....	23
2.5.5 Discrete Element Method.....	24
2.5.6 Hybrid and Complementary Methods.....	24
2.6 Soil Behavior and Constitutive Models	26
2.6.1 Mohr-Coulomb Model.....	28
2.6.2 Drucker-Prager Model	30
2.6.3 Cam-Clay and Modified Cam-Clay Models	31
2.7 2D and 3D Numerical Methods in Tunneling.....	33
2.7.1 Arching.....	35
2.7.2 Constitutive Modeling.....	36
2.7.3 Excavation Modeling	37
2.7.4 Modeling of Surface Excavation over Tunnels.....	37
3.PROBLEM STATEMENT AND METHODOLOGY	39
3.1 Geometry and Definition	42
3.2. Material Properties	51
3.3. Excavation Procedure	52
4.RESULTS AND DISCUSSION.....	54
4.1 Effect of Staged Construction on Forces in Tunnel Lining.....	54
4.2 Effect of Surface Excavation to the Tunnel Lining.....	56
4.3 Effect of Unsymmetrical Excavation to the Tunnel Lining.....	66
4.4 Effect of Surface Loading to the Tunnel Lining.....	77
5.CONCLUSION AND RECOMMENDATIONS.....	86
REFERENCES	88
APPENDICES.....	92
A TUNNEL LINING CAPACITY CALCULATION SAMPLE.....	92
B INTERACTION DIAGRAMS.....	93

LIST OF TABLES

TABLES

Table 3.1 Description and Properties of the Analysis.....	49
Table 4.1 Extreme Forces and Displacements for the Mid-Plane for Set1.....	58
Table 4.2 Extreme Forces and Displacements for the Mid-Plane for Set2.....	66
Table 4.3 Extreme Forces and Displacements for the Mid-Plane for Set3.....	78

LIST OF FIGURES

FIGURES

Figure 2.1 Several types of face excavation.....	10
Figure 2.2 Numerical methods and models for tunnel engineering.....	20
Figure 2.3 Models for tunnel engineering examples a) Beam Element Model with elastic Support. b) Finite Element Model.....	21
Figure 2.4 Impact of the numerical method on calculation results.....	25
Figure 2.5 Hybrid Method-Finite Element Method combined with Discrete Element Method.....	26
Figure 2.6 Real Soil Behavior involving hardening and softening.....	27
Figure 2.7 Mohr-Coulomb criterion in principal stress space a) Principal stress space, b) Mohr's diagram.....	29
Figure 2.8 Traces of Mohr-Coulomb failure surface in the deviatoric and triaxial planes. a) Deviatoric plane, b) Triaxial plane.....	30
Figure 2.9 a) Typical (p' ; V) plot of isotropic compression, swelling and recompression b) Idealized ($\ln p'$, V) plots in critical state	32
Figure 2.10 The Critical State Line in (a) (p' , q) plot and (b) (p' , V) plot (isotropic normal compression line is shown dashed in (b)).....	33
Figure 2.11 Failure surfaces in the deviatoric plane.....	34
Figure 2.12 Terzaghi's trap door experiments.....	35
Figure 3.1 Geometry of the problem.....	43
Figure 3.2 Tunnel cross section.....	43
Figure 3.3 Dimensions of the model and 3D mesh.....	44
Figure 3.4 Staged excavation and shotcrete application steps.....	45
Figure 3.5 Sign Convention.....	51
Figure 4.1 Normal forces in the tunnel lining a) Staged construction b) One-phase construction.....	55
Figure 4.2 Comparison of staged and one-phase construction.....	57
Figure 4.3 E vs. Axial Forces for Different Excavation Depths.....	58

Figure 4.4 H/B vs. Normal Forces for two extreme E values.....	59
Figure 4.5 E vs. Bending Moments for Different Excavation Depths.....	60
Figure 4.6 H/B vs. Moments for two extreme E values.....	61
Figure 4.7 Interaction diagrams for extreme values of H/B ratio and E value.....	62
Figure 4.8 Risk of failure for different H/B ratios and E values.....	63
Figure 4.9 E vs. Maximum Shear Forces for Different Excavation Depths.....	63
Figure 4.10 E vs. Vertical Displacement for Different Excavation Depths.....	65
Figure 4.11 E vs. Horizontal Displacement for Different Excavation Depths.....	65
Figure 4.12 E vs. Axial Forces for Different Excavation Eccentricities.....	67
Figure 4.13 e/B vs. Normal Forces for two extreme E values.....	68
Figure 4.14 E vs. Bending Moments for Different Excavation Eccentricities.....	69
Figure 4.15 e/B vs. Moments for two extreme E values.....	69
Figure 4.16 Interaction diagrams for extreme values of e/B ratio and E value.....	71
Figure 4.17 Risk of failure for different e/B ratios and E values.....	72
Figure 4.18 E vs. Maximum Shear Forces for Different Excavation Eccentricities.....	72
Figure 4.19 E vs. Vertical Displacements for Different Excavation Eccentricities.....	73
Figure 4.20 E vs. Horizontal Displacements for Different Excavation Eccentricities.....	74
Figure 4.21 Axial force distribution in the tunnel lining for Analysis30 (e=20m, E=600 MPa).....	75
Figure 4.22 Moment distribution in the tunnel lining for Analysis30 (e=20m, E=600 MPa).....	75
Figure 4.23 Shear Force distribution in the tunnel lining for Analysis30 (e=20m, E=600 MPa).....	76

Figure 4.24 Vertical displacement distribution in the tunnel lining for Analysis30 ($e=20\text{m}$, $E=600\text{ MPa}$).....	76
Figure 4.25 Horizontal displacement in the tunnel lining for Analysis30 ($e=20\text{m}$, $E=600\text{ MPa}$)	77
Figure 4.26 E vs. Axial Forces for Different Fill Heights.....	78
Figure 4.27 h/B vs. Normal Forces for two extreme E values.....	80
Figure 4.28 E vs. Bending Moments for Different Fill Heights.....	80
Figure 4.29 h/B vs. Moments for two extreme E values.....	81
Figure 4.30 Interaction diagrams for extreme values of h/B ratio and E value.....	82
Figure 4.31 Risk of failure for different e/B ratios and E values.....	83
Figure 4.32 E vs. Maximum Shear Forces for Different Fill Heights.....	84
Figure 4.33 E vs. Vertical Displacements for Different Fill Heights.....	84
Figure 4.34 E vs. Horizontal Displacements for Different Fill Heights.....	85

CHAPTER 1

INTRODUCTION

Tunnels are the vital elements for the every day life of the people especially in heavily crowded urban areas. Tunnels are built to move people or materials in a defined route where the movement without a tunnel is impossible or it is impractical or inadequate. The mountains, rivers, dense population areas can only be passed with tunnels in some cases. Tunnels are used for different purposes such as transportation, water conveyance and storage. Railway tunnels, highway tunnels and pedestrian tunnels are used for the transportation of the people. Water conveyance tunnels are built for transportation of water from the mountainous areas to the urban areas or to collect and transport the wastewater to the wastewater treatment plants. The detailed information about the tunneling history and the types of tunnels will be given in the proceeding chapter.

Tunnels have been built for thousands of years. In the last century, the need of use of underground space to overcome the difficulties encountered by construction of the railways and highways in mountainous areas has increased the number and the quality of tunnel constructions. From engineering point of view, many advances have been made to handle with the problems in difficult areas. Several methods and approaches have been developed to design and analyze the tunnels. Most of them however suffer from the lack of ability to consider all of the aspects of the tunnel construction. In the beginning of the last century, the tunnels were built based on the past experience. Then some empirical methods have been proposed but they could not take all the geotechnical parameters and construction process into account. There are also several analytical approaches in the tunnel design and analysis. However, they have a lot of limitations. They can not reflect the sequential excavation and construction

procedure and the time dependent behavior of shotcrete and soil with accuracy. They are based generally on simple parameters and the complex parameters are neglected. Although this decreases the predictive capacity of the method, it provides a fast and cheap way of a first order approximation of the tunnel analysis or design.

Tunneling is a 3D problem and the construction sequence and the time effects play an important role in the analysis and design of the tunnels. Beginnings from the 1960's numerical methods have been used in tunneling engineering to consider these facts. 2D numerical methods are suitable for some cases but they are not as accurate as 3D models are. The simplifications made by performing 2D numerical analysis make the calculations easier and less time consuming but they are not able to simulate the construction sequence and 3D effects such as arching. The use of numerical methods in tunnel engineering became popular especially in the last twenty years. The innovations in the computer technology and the new programs developed for the tunnel engineering purposes made the numerical methods the leading approach in tunnel engineering. Among the others, Finite Element Method is probably the most popular numerical method. All numerical methods have advantages and disadvantages when compared with the others. The type of the numerical method to be employed in the analysis should be determined according to the type of the tunnel, construction procedure, soil type and the nature of the problem. Different numerical methods have been described in the following chapter and the strength and the weaknesses of these methods have been defined.

The tunnels in urban areas are not located generally in great depths in the soil. Therefore, the effects of the surface activities can easily reach the tunnel and the stability of the tunnel can be damaged. In urban areas, new structures can be built or the existing structures can be replaced with new ones over the routes of the existing tunnels. As a result of these constructions some excavations or loadings can take place. In this study,

the effects of the surface excavations and loadings to the existing tunnels have been investigated. For this purpose, a finite element method software package, Plaxis 3D Tunnel, has been utilized. All the analysis for modeling the whole tunnel construction and for modeling the excavations and loadings after the completion of the tunnel has been carried out by using this program.

A typical metro tunnel constructed by using NATM technique has been simulated according to the usual construction sequence. Four different Young's Modulus values for the soil have been assigned. The geometry of the excavations and loadings has been changed and a parametric study has been carried out.

In the following chapters, firstly, some basic concepts are discussed. The history, general types and some well known analysis methods of tunnels has been discussed. The NATM tunnels are discussed in detail because of the scope of the study. After that, the numerical method types and their area of use are described. The general concepts in numerical modeling are discussed. Following this, the problem has been defined and the modeling part is described in detail. After that the results of the analysis are presented and discussed.

CHAPTER 2

LITERATURE REVIEW AND BASIC CONCEPTS

2.1 Chronological View of Tunnels

The tunneling and underground construction history extends up to the prehistoric era. The first underground constructions were for defense and mining purposes. Megaw and Bartlett (1981) state that the earliest examples are the salt mine in Hallstatt (B.C. 2500) and flint mines in France and Portugal (B.C. 2000).

Another use of tunnels in ancient times was water supplying. Using tunnels as water conveyors had many advantages such as decreasing the amount of evaporation and being difficult to be damaged by enemies. The pioneers of canal building were Greeks and Romans. An early example from Greece tunneling is the water supply canal of Eupalinus of Magara in B.C. 687. Also several canals and tunnels were built in 'Fertile Crescent' (Egypt, Palestine, Syria, and Iraq).

Shinha (1989) states that Greeks made a great contribution to tunneling by using advanced surveying techniques and deriving the tunnel from both portals toward the middle of the tunnel, which decreased the consumed time. He also argues that, during Renaissance era, gunpowder has been utilized in tunneling and conventional methods such as shovels, picks and water has been replaced by blasting.

Marc Isambard Brunel's great Thames tunnel was the first shield driven tunnel and also it was the first tunnel driven under a tidal river. (Megaw and Bartlett, 1981)

After that time, several improvements have been made and today there are many types of shields and tunnel boring machines. The tunneling activities in Alps in Europe had so many contributions to tunneling in terms of improving the existing methods and also by developing new methods.

2.2 Types of Tunnels

Tunnels can be categorized in several ways. The aim of the tunnel, the method of construction or the hosting medium can be the features of the tunnel on which the classification is based. In the following pages some types of tunnels are introduced and brief information on these tunnels has been given.

2.2.1 According to the Function

Tunnels are constructed for different purposes. The function can be a good classification criterion as described as follows. These descriptions are a summary of the related chapter by Megaw and Bartlett (1981).

2.2.1.1 Railways

Railways tunnels can be hosted in any kind of ground. The main circumstances where railway tunnel are needed can be listed as mountain ranges, hills and subaqueous crossings. The typical railway tunnel is about 5m x 7m for a single-track tunnel and about 8.5m x 7m high in case of twin tracks.

The gradient should be less than 1%. The horseshoe form is the most common type. However, also circular form with segmental concrete cast iron lining has also been constructed. (Megaw and Bartlett, 1981)

2.2.1.2 Metro Tunnels

Metro tunnels are different from railway tunnels in several aspects. Metro tunnels are constructed in urban areas, but it is not rare to encounter subaqueous sections or hills.

The gradients can be steeper due to the fact that no heavy good trains are included in metro lines.

Cut-and-cover method is preferred where it is possible to construct the tunnel in a shallow depth without significant disturbance of the streets and urban activities. When the city is a heavily congested one, deeper tunneling is necessary. (Megaw and Bartlett, 1981)

2.2.1.3 Highway Tunnels

In highway tunnels curves can be sharper and the gradient can be much more higher compared with the railway tunnels.

Dimensions of highway tunnels increase with increasing technology of vehicles. Road widths for two lanes has been increased to 7.3- 7.5 m in many modern tunnels from a value of 4.9 m in early Blackwall Tunnel (1897) Since the diameters in circular tunnels have also increased, the excavated area increased as the square of the diameter.

The construction methods for highway tunnels are numerous such as, shield drives. TBM's, drill and blast, cut-and-cover etc.

2.2.1.4 Water Conveyance Tunnels

The basic features of tunnels to convey water or sewage are smoothness and water tightness.

Smoothness is important in cases where water flow should be maximized or head loss is to be minimized. Water tightness gains importance in cases where water pressure is very high or there is a possibility of inflow in drinking water tunnels. (Megaw and Bartlett, 1981)

2.2.2 According to the Construction Technique

2.2.2.1 Cut and Cover

Cut and cover tunneling is usually thought of as trench excavation in soft ground. However, boulders of all sizes may be encountered; and where, for instance, gravity sewers must conform to a required hydraulic gradient, the trench may pass into rock. The choice of trench support system may be governed by the mixed face condition rather than by the soil condition. Where soldier piles and lagging are the preferred supports, the soldier piles must penetrate sound rock for toe support. If this is not reliable, then the toes of the piles must be tied back to the rock with long rock bolts. Alternatively, the trench in overburden may be made wider than that in rock.

When soldier piles are driven in boulders, it is at least difficult to maintain their proper position. It is therefore appropriate in bouldery ground to predrill the piles so that boulders can be broken up using a large churn drill bit.

The potential need for dewatering must be taken into account in all cut and cover construction. Any water permitted to flow unfiltered into an excavation will result in loss of ground and consequent unsymmetrical loading of the walls of the excavation and settlement of adjacent sidewalks and structures. (McCusker, 1989)

2.2.2.2 Earth Boring & Pipe Jacking

Earth boring and pipe jacking are related operations and are commonly confused with one another. Earth boring methods are usually confined to relatively small diameter pipe installations of limited length. Pipe jacking has reached a level of sophistication allowing it to be used for the entire construction of substantial projects, such as a 15-km interceptor sewer project with pipe size up to 3.25 m in Egypt. (McCusker, 1989)

The basic methods are:

Auger Boring: The soil is removed by using an auger within the jacked pipe. The leading edge of the first pipe is commonly fitted with a cutter or shoe, both to protect the pipe and to assist in breaking down the excavated soil. Ground stability in weak soils is controlled by adjusting the distance between the end of pipe and the head of the auger.

Pipe Jacking: Auger boring is a form of pipe jacking, in that the pipe is jacked at the same time as the excavation progresses. However, in pipe jacking, the jacking of the pipe is not itself a part of the excavation process. Although augers may still be used, their primary function is spoil removal. The cutting action is separate and is usually controlled by an operator present at the cutting head. All types of excavator shields may be used, including shields fitted with sand shelves, with or without mechanical excavators; rotary head TBM's; slurry shields.

2.3 NATM

The new Austrian tunneling Method (NATM) emerged in the years 1957 to 1965. (Kolymbas,2005). The basic concepts has been developed by two Austrian tunneling experts, Rabcewitz and Muller-Salzburg. The Tunnel has been named as NATM in order to distinguish it from the Old Austrian tunneling Method. The main idea in NATM is heading the tunnel conventionally and applying shotcrete support sparingly and following the principles of the observational method. (Kolymbas,2005)

According to ICE (1996) NATM is a philosophy and also a construction technique and the distinction between them must be made. This confusion in NATM is addressed to the modifications and developments by the philosophy set by Rabcewicz. ICE (1996) made a distinction between NATM

philosophy and NATM construction technique by stating their key features as follows.

2.3.1 NATM Philosophy

- The strength of the ground around a tunnel should be fully mobilized.
- The mobilization is achieved by allowing sufficient ground deformation
- Initial support with appropriate load-deformations characteristics should be installed.
- Instrumentation is installed to monitor the deformations of the initial support system and the distribution of the load upon it. Where appropriate, variations in primary support and in sequence of excavation are made based on the monitoring results. (ICE,1996)

2.3.2 NATM Construction Technique

The key features of the construction technique often referred to as NATM are:

- The tunnel is sequentially excavated and supported, and the excavation sequences and face areas can be varied. (Typical partial face excavations are shown in Figure1.)
- The primary support is provided by the sprayed concrete in combination with some or all of the following.
 - a) steel mesh
 - b) steel arches (normally lattice girders)
 - c) ground reinforcement (e.g. rock bolts, spiling).
- Cast insitu concrete lining is installed as permanent lining which is designed separately

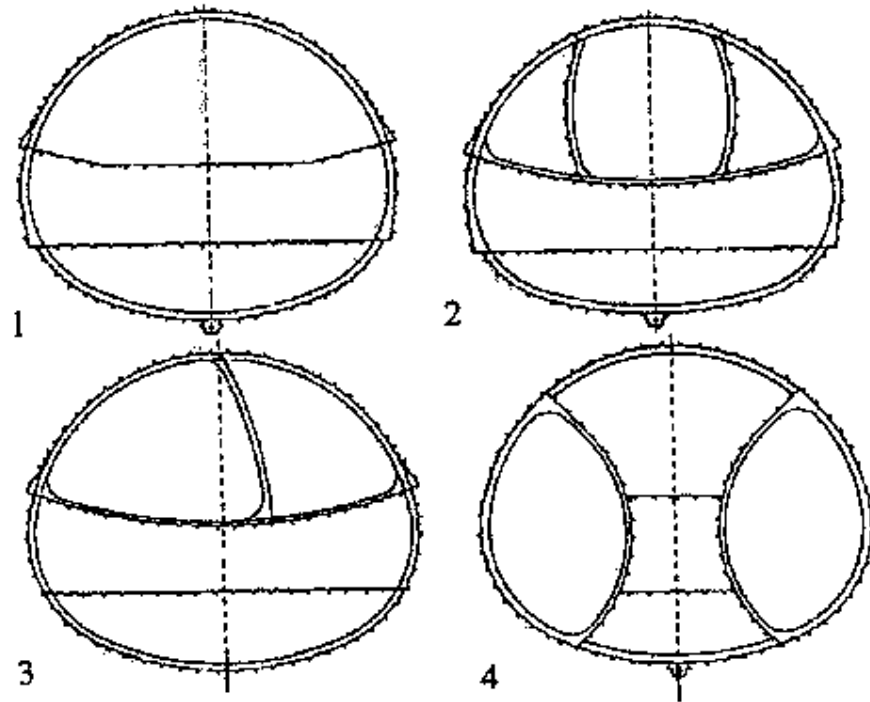


Figure 2.1 Several types of Face excavation (Kolymbas,2005)

2.3.3 NATM in Rock

The original NATM principles were developed from the experiences of tunnel construction in Alps. Since the tunneling medium was rock, the design procedures and construction technique are developed in such a way that they were adequate for rock tunneling under high overburden stresses.

During the construction through Alps, it was found that, if the primary lining is very stiff or if it is installed too early without allowing sufficient deformation, the stresses developed on the lining is too high. In order to avoid this high stress concentration on the lining, more flexible primary

support (sprayed concrete in combination with rock bolts or steel arcs) could be used. It was also perfectly safe and economic due to the mobilization of the rock strength. (ICE 1996)

2.3.4 NATM in Soft Soil

When tunneling is considered, soft soil can be defined as the type of ground which requires an immediate support following the excavation. Utilization of sprayed concrete as primary support in soft soil tunneling is a relatively new concept when compared with rock tunneling. (ICE 1996) Soft ground tunneling in urban areas is of great importance since the settlements due to tunneling activities may damage the overlying structures and some precautions should be taken in order to limit the settlements.

NATM applications in soft soil differ from the applications in rock both in the excavation sequence and in the completion of the primary support. The staged excavation should be limited to an extent in terms of dimensions and duration in order to reduce the settlement which is one of the most important problems encountered in soft soil tunneling. By taking these limitations into account it is obvious that the items stated in the NATM philosophy section are not applicable in soft soil. NATM in soft ground in urban areas can be defined as the primarily application of shotcrete as temporary support and a following installation of the permanent support in a later date. The sequence of the excavation, the dimensions of the excavated face can be varied according to the monitoring results.

2.4 Tunnel Design and Analysis

Underground structures have been built since thousand of years. Most of these underground structures have been constructed by using the past experience. Although several methods have been proposed and used in the literature, a specific method for all construction and material types is not available. This fact may be due to the complex nature of tunnel design. The stresses and deformations on the tunnel and also in the subsurface depend

greatly on the construction technique, hosting ground, liner type, construction sequence and workmanship and it is also time dependent. There are several methods to design and analyze the tunnels from very simple empirical methods to very complex numerical methods. In the proceeding chapters some of these methods will be briefly discussed. It should be noted that all of these methods have limitations in some extend and their applicability to specific cases should be checked.

2.4.1 Stresses and Deformations in Tunnels

Terzaghi (1946) has proposed an empirical design tool for tunnels in rock. He assumed a tunnel with a depth greater than 1.5 times B+H where B is the width of tunnel and H is the height of the tunnel. He used nine types of rock to establish this design table. The definitions of these rock types are more qualitative than quantitative. Therefore, this classification system is highly designer dependent. (Sinha, 1989)

In 1974, Barton, Lien and Lunde introduced a “Q” system and recommended a value of roof load in kg/cm² which is as follows:

$$P_{roof} = \frac{2.0J_n^{1/2} - Q^{1/3}}{3J_r} \quad (2.1)$$

Where

$$Q = \frac{RQD}{J_n} \cdot \frac{J_r}{J_a} \cdot \frac{J_w}{SRF} \quad (2.2)$$

RQD = Rock quality designation

J_n =Joint set number

J_a =Joint alteration number

J_w =Joint water reduction factor

SRF =Stress reduction factor

By determining this value, support category is chosen by using the tables proposed by Barton et al.

In 1974, Bieniawski proposed the Rock Mechanics Rating system. This system is developed by assigning rating values to six parameters of rock which are:

1. Uniaxial compressive strength of intact rock
2. Rock quality designation
3. Spacing
4. Orientation
5. Condition of Discontinuities
6. Ground water conditions.

RMR is the sum of all these ratings. Bieniawski proposed a table in which the recommended support types and the properties of these support types based on these RMR values can be found. (Sinha, 1989)

Another way of determining the stresses at the tunnel is the one derived from the theory of stress distribution around a circular opening. This formula is derived by inserting the horizontal stress in tunnels:

$$\sigma_h = k \cdot \sigma_v \quad (2.3)$$

into the well known Kirsch equation. The obtained equations are:

$$\sigma_r = \frac{1}{2} \sigma_v \left[(1+k) \left(1 - a^2 / r^2 \right) + (1-k) \left(1 - 4a^2 / r^2 + 3a^4 / r^4 \right) \cos 2\theta \right] \quad (2.4)$$

$$\sigma_t = \frac{1}{2} \sigma_v \left[(1+k) \left(1 + a^2 / r^2 \right) - (1-k) \left(1 + 3a^4 / r^4 \right) \cos 2\theta \right] \quad (2.5)$$

$$\tau_{rt} = \frac{1}{2} \sigma_v \left[(-1+k) \left(1 + 2a^2 / r^2 \right) - 3a^4 / r^4 \cos 2\theta \right] \quad (2.6)$$

σ_r is the radial stress, σ_t is the tangential stress and τ_{rt} is shear stress.

Another method in tunnel design is the Flexibility and Stiffness Method where the flexibility Ratio and Compressibility ratios are defined as:

$$F = \frac{\frac{E_m}{(1+v_m)}}{\frac{6E_s I_s}{(1-v_s)^2 r^3}} \quad (2.7)$$

$$C = \frac{\frac{E_m}{(1+v_m)(1-2v_m)}}{\frac{E_s t_s}{(1-v_s)^2 r}} \quad (2.8)$$

E= Modulus of Elasticity

v= Poisson's ratio

r = Radius of opening

I= Moment of Inertia

t= thickness

Subscripts:

m= medium

s= support

Einstein and Schwartz (1980) have defined the thrust and moment in the lining for two different soil-lining interaction conditions:

For Full Slip Case:

$$\frac{T}{PR} = \frac{1}{2}(1+k)(1-a_0) + \frac{1}{2}(1-k)(1-2a_2) 2 \cos 2\theta \quad (2.9)$$

$$\frac{M}{PR^2} = \frac{1}{2}(1-k)(1-2a_2) 2 \cos 2\theta \quad (2.10)$$

$$\frac{U_s E}{PR(1+v)} = \frac{1}{2}(1+k)a_0 - (1-k)[(5-6v)a_2 - (1-v)] 2 \cos 2\theta \quad (2.11)$$

$$\frac{V_s E}{PR(1+v)} = \frac{1}{2}(1-k)[(5-6v)a_2 - (1-v)] \sin 2\theta \quad (2.12)$$

T= Thrust

P= Vertical Pressure

k= horizontal pressure/vertical pressure

R= radius of opening

M=moment

v= Poisson's ratio of host medium

θ = angle measured from spring line

U_s = radial deformation of support

E= modulus of elasticity of host medium

$$a_0 = \frac{C_1 F_1 (1-v)}{C_1 + F_1 + C_1 F_1 (1-v)} \quad (2.13)$$

$$a_2 = (F_1 + 6)(1-v) / [2F_1(1-v) + 6(5-6v)] \quad (2.14)$$

where

$$C_1 = ER(1-v_s^2) / E_s A_s (1-v^2) \quad (2.15)$$

$$F_1 = ER^3(1-v_s^2) / E_s I_s (1-v^2) \quad (2.16)$$

Where

v_s = Poisson's ratio of support

A_s = area of support

E_s =modulus of elasticity of support

I_s =moment of inertia of support

For No Slip Case:

$$\frac{T}{PR} = \frac{1}{2}(1+k)(1-a_0) + \frac{1}{2}(1-k)(1+2a_3) \cos 2\theta \quad (2.17)$$

$$\frac{M}{PR^2} = \frac{1}{4}(1-k)(1-2a_2+2b_2)\cos 2\theta \quad (2.18)$$

$$\frac{U_s E}{PR(1+v)} = \frac{1}{2}(1+k)a_o + \frac{1}{2}(1-k)[4(1-v)b_2 - 2a_3]\cos 2\theta \quad (2.19)$$

$$\frac{V_s E}{PR(1+v)} = -(1-k)[a_3 + (1-2v)b_2]\sin 2\theta \quad (2.20)$$

The symbols are same as before and

$$a_3 = b_1 b_2 \quad (2.21)$$

$$b_1 = \frac{(6+F_1)(C_1)(1-v) + 2F_1 v}{3F_1 + 3C_1 + 2C_1 F_1 (1-v)} \quad (2.22)$$

$$b_2 = \frac{C_1(1-v)}{2[C_1(1-v) + 4v - 6b_1 C_1(1-v)]} \quad (2.23)$$

Bobet (2001) made a study on analytical solutions for liner displacements and stresses. He assumed the liner and ground as elastic and a circular cross section with plane strain conditions in a direction perpendicular to the cross section of the tunnel. He also assumed a depth to radius ratio larger than 1.5 and the ground as homogeneous and isotropic. His study is based on the relative Stiffness Method proposed by Einstein and Schwartz (1979). He considered the cases; shallow tunnel in dry ground, saturated ground and saturated ground with air pressure. He also developed a formula for the surface settlements.

Verruijt (1997) proposed a complex variable solution for circular tunnels in elastic half plane. He used the complex variable method with the homogeneous linear elastic material model. He utilized the boundary conditions that the upper boundary of the half plane is free of stresses, and

that at the boundary of the tunnel the displacements are prescribed. He obtained the stresses and displacements by solving the equations with the defined boundary conditions:

$$\sigma_{xx} + \sigma_{yy} = 2\{\phi'(z) + \overline{\phi'(z)}\} \quad (2.24)$$

$$\sigma_{yy} - \sigma_{xx} + 2i\sigma_{xy} = 2\{z\phi''(z) + \psi'(z)\} \quad (2.25)$$

$$2\mu(\mu_x + i\mu_y) = K\phi(z) - z\overline{\phi'(z)} - \overline{\psi(z)} \quad (2.26)$$

In 2005, Nam and Bobet investigated the loading and the displacements of the primary and secondary supports under different drainage conditions. They combined the numerical results with analytical solutions in order to achieve a design methodology for the design of the support of deep tunnels under the water table.

They concluded that if the pore pressure increases behind the secondary support, the primary support is unloaded and the secondary support is loaded, where the first one moves outwards and the second one moves inwards. They state that the load increment in the secondary support is comparatively larger than the load decrement in the primary support. However their solutions are not applicable to all cases due the assumptions made to obtain these solutions.

2.4.2 Surface Settlements

Tunneling induced surface settlements gain more importance in tunneling as increasing number of tunnels are being constructed in urban areas. Methods to estimate the surface settlements should be developed and the mechanism under this phenomenon should be clearly investigated in order to minimize the effects of these settlements to the overlying structures.

The most widely used method for estimating the surface settlements is the empirical method proposed by Peck (1969) and Schmidt (1969).

In this method the settlement profile is approximated by the Gaussian distribution curve:

$$S = S_{\max} \exp\left(-\frac{x^2}{2i^2}\right) \quad (2.27)$$

Where S is the settlement, S_{\max} is the maximum settlement above the tunnel centerline, i is the distance between tunnel centerline and the inflexion point of the curve and x is the horizontal distance from the tunnel centerline in the transverse direction.

In 1995, Verruijt and Booker made a study on evaluating the settlements due to deformation of a tunnel with analytical methods. They extended the solution of Sagaseta (1987) by considering the ground loss not only for the incompressible case and by including the effect ovalization. This solution is based on the assumption of linear elastic soil and therefore it has some limitations. The settlements determined by using this method are generally larger than the observed ones.

In 1998, Loganathan and Paulos made an attempt to find an analytical solution for tunneling induced ground movements in clays. They used the closed form solution derived by Verruijt and Booker by incorporating the redefined definition of the traditional ground loss parameter.

2.5 Numerical Methods

The use of numerical methods in geomechanics is getting more and more popular in recent years. As much more powerful computers are available in the market with affordable prices, the codes for numerical methods are

getting more complex and can simulate the real construction conditions, geological data and site better. As a result of this, due the complex nature of tunnel design and analysis, numerical methods are widely used among tunnel designers, researchers and experts.

Potts and Zdravkovic (2001) state that the field conditions can be simulated more accurately if the utilized constitutive models can represent the soil behavior accurately and if the boundary conditions set are correct.

The human factor is at least as important as the items stated above. Most of the numerical codes are user friendly developed in recent years. Although it simplifies the whole numerical simulation and calculation process, it has also very important disadvantages. These codes might be also used by in experienced people. Because of the complex nature of the numerical analysis, the operator must be aware of the constitutive models used, have a knowledge in soil and rock mechanics and should be familiar with the numerical code employed. (Potts and Zdravkovic, 2001)

The type of the computational method to be utilized should depend on the complexity of the problem. The use of numerical tools for a simple problem is inefficient in terms of time and effort. (Gnilsen, 1989)

Gnilsen (1989) lists the numerical methods used in tunnel engineering as in Figure2.2.

2.5.1 Beam Element Method with Elastic Support

The model for the Beam Element Method, known also as “Coefficient of Subgrade Reaction Method” can be seen in Figure2.3.

By this simple method, the tunnel support is simulated by elastic beams and the hosting ground is simulated by spring elements.

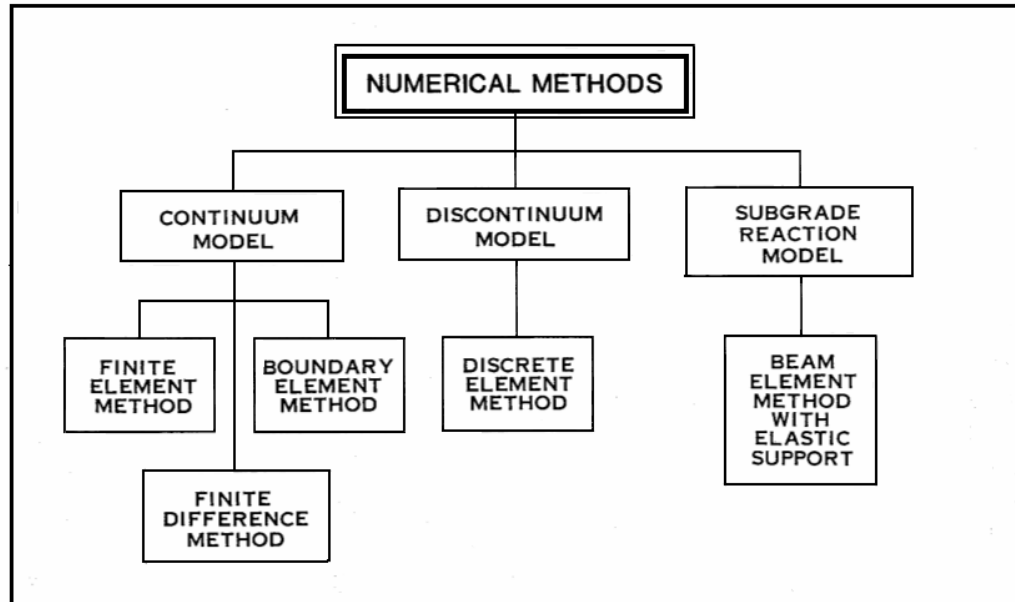


Figure 2.2 Numerical Methods in tunnel engineering (Gnilsen, 1989)

These spring elements are perpendicular to the lining simulating the normal forces exerted on the tunnel lining. Tangential spring elements can also be used in order to simulate the shear stresses between the hosting ground and the lining. The springs in tension are eliminated in an iterative way in order to simulate the real conditions properly. Due the simplicity of the model, the calculation time and storage capacity are extremely low compared with the other numerical methods. On the other hand, this method can only model very simplified tunnel conditions. The simulation does not include the interaction of the soil bodies each represented by a spring element. (Gnilsen, 1989)

2.5.2 Finite Element Method

Finite Element Method is one of the most widely used numerical methods in geomechanics and also in tunnel engineering. It is a continuum model but discontinuities can be also modeled individually. (Gnilsen, 1989)

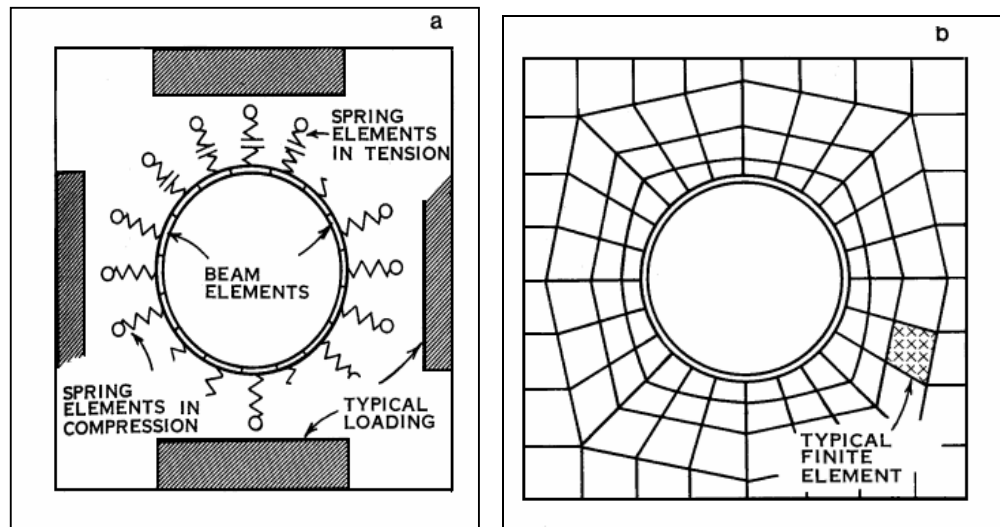


Figure 2.3 Models for Tunnel engineering examples a) Beam Element Model with elastic Support. b) Finite Element Model. (Gnilsen, 1989)

The reason of the popularity of FEM can be addressed to the fact that it was the first numerical method with enough ability to include the material non-homogeneity, complex boundary conditions and non-linear deformability. (Jing and Hudson, 2002)

The main idea of FEM is as follows: The hosting ground is discretized into a limited number of smaller elements. These elements are connected at nodal points. The stress, strain and deformation to be analyzed are caused by changing the original subsurface conditions (Gnilsen, 1989). The stresses and strains generated in one element effects the interconnected elements, and so forth.

The stress-strain relationships of the elements are modeled mathematically by creating a global stiffness which relates the unknown quantities with known quantities and the results are obtained by solving this matrix. The

equations to be solved are highly complex and as the number of the elements in the model increase, the calculation time and the storage capacity increase dramatically.

By using FEM, complex conditions can be simulated due the capability of simulation of advanced constitutive models, non-homogeneities, stage by stage construction and time effect.

However; the finite element method is formulated based on continuum assumptions. Complete detachment of elements, sliding and large scale openings can not be included. The global stiffness matrix can be ill-conditioned if many fracture elements are incorporated. (Jing and Hudson, 2002)

The output of the analysis is typically also complex and it makes the assessment of the results difficult. A post-processor may be utilized in order to overcome this difficulty. (Gnilsen, 1989)

2.5.3 Finite Difference Method

This method is also based on continuum assumptions and the subsurface is discretized into a number of elements like in Finite Element Method. The main difference between Finite Difference Method and Finite Element Method lies by the determination of the unknown quantities.

In Finite Difference Method, it is assumed that for a determined small time interval, the disturbance on a given point is only experienced by its immediate neighbors. (Gnilsen, 1989)

In Finite Difference Method, the mesh elements are solved separately and as a result of this the storage capacity need is reduced since no matrix formation is required.

The solution is achieved by using Newton's law of motion and the constitutive law of the in situ material. The acceleration in mesh points are integrated to obtain the mesh point velocity from which strain changes are determined subsequently. These strain changes are used to evaluate the stress increments in the mesh points. (Gnilsen, 1989)

Finite Difference Method is the most direct technique among the numerical methods and it enables more straightforward simulation of complex constitutive models without iterative solutions. (Jing&Hudson, 2002)

By using Finite Difference Method, large modules can be created without using very complex computing tools and it is more efficient in dynamic problems and non-linear and large strain situations but weaker in linear simulation and static conditions in contrast to Finite Element Method (ICE,1996)

Material heterogeneity, complex boundary conditions and fractures are also shortcomings of Finite Difference Method. (Jing and Hudson, 2002)

2.5.4 Boundary Element Method

The use of the Boundary Element Method is growing in tunnel engineering. The Boundary element Method models the ground as a continuum and a discretization on the excavation boundary is applied. The medium inside these boundaries is modeled by partial differential equations. The unknown quantities are determined by integrating these partial differential equations. (Gnilsen, 1989)

The main advantage of Boundary Element Method is the simpler mesh generation. As a result of this data input and data output are much simpler compared with FEM and FDM. Moreover, the solutions are continuous (Jing and Hudson) Boundary Element Method is highly capable of simulating the

situations where the defined boundaries are very important. (Gnilsen, 1989)
On the other hand, BEM has some shortcomings such as simulating the material heterogeneity or non-linear behavior. (Jing and Hudson, 2002). Also the construction procedures and sequences and time dependent behavior can not be simulated easily. (Gnilsen, 1989)

2.5.5 Discrete Element Method

In this method the hosting ground is modeled as individual rigid blocks. In other words the ground is not modeled as a continuum. This model can be used in situations where the deformations of the blocks are negligible compared with the movements of the rigid blocks along the joints. (Gnilsen, 1989)

The basic difference between DEM and continuum based methods is that the contact patterns between components of the system are continuously changing with the deformation process for the former, but are fixed for the latter. (Jing and Hudson, 2002)

This method is more suitable for the situations where the hosting ground is composed of highly jointed rock masses. Large block movements can be analyzed more efficiently compared with most continuum models. The computer capacity requirement is also moderate. However, the direction and location of the joints are needed as an input parameter which can not be determined easily without constructing the tunnel. (Gnilsen, 1989)

2.5.6 Hybrid and Complementary Methods

As stated in the previous sections, all numerical models have some advantages and disadvantages. The efficiency of the model depends on the nature of the problem. The type of the numerical method to utilize in the analysis of the problem should be determined only after examining the real conditions sufficiently and understanding the capability of the available numerical methods.

Tunnel engineering works are very complex and can not be simulated easily. Although a numerical model fits best to the situation of concern, it may not reflect all the real conditions properly. Figure 4 represents the roof displacement of a tunnel analyzed with different methods by Laabmayr and Swoboda. (1978)

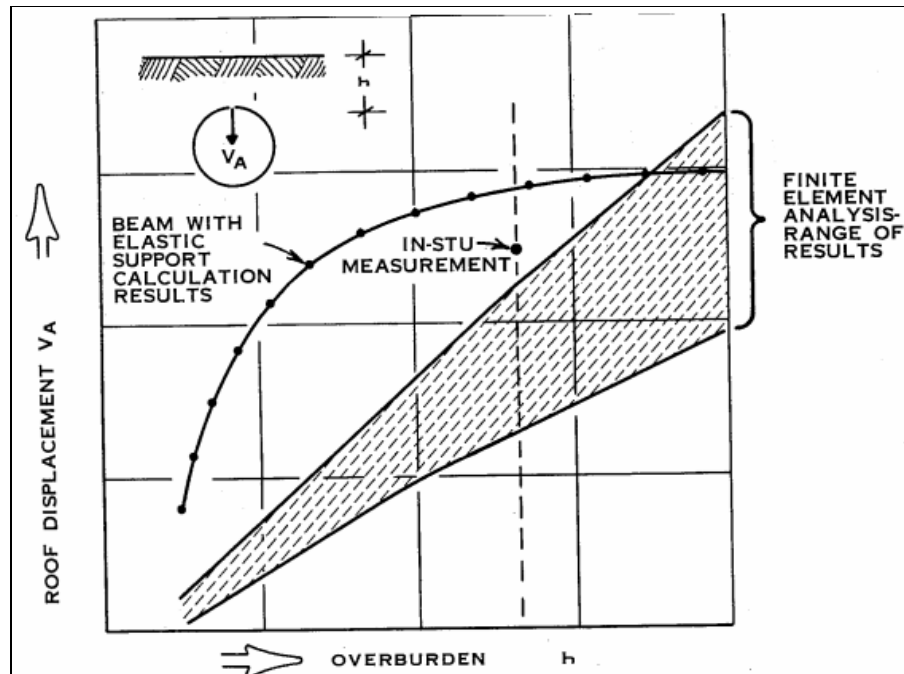


Figure 2.4 Impact of the numerical method on calculation results (Laabmayr and Swoboda, 1978 in Gnilsen, 1989)

To overcome these difficulties, different numerical methods are combined. These hybrid models have basically two advantages;

- By combining numerical methods, the strengths of the each method is preserved whereas the shortcomings of the methods are eliminated.
- The combination of the individual methods and their associated methods may create a new method which simulates the problem more accurately. (Gnilsen, 1989)

For example Finite Element Method can be combined with Beam Element Method as illustrated in Figure 2.5.

The Finite element Method is employed by calculating the stress, strain and deformation of the ground and the primary lining. It is assumed that the permanent lining is installed at a later time, which is consistent with real conditions, and the forces on the permanent lining are calculated with Beam Element Method.

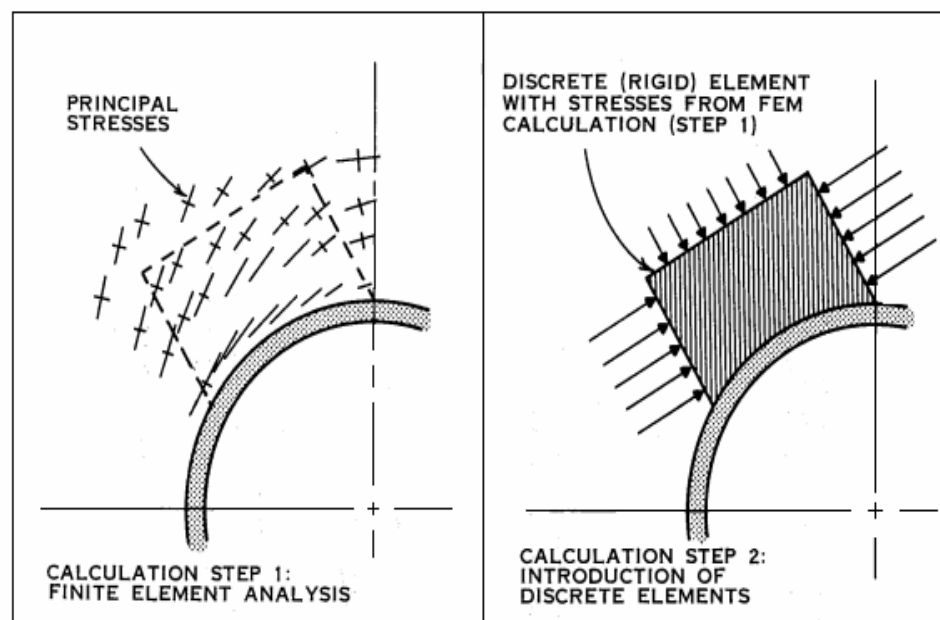


Figure 2.5 Hybrid Method-Finite Element Method combined with Discrete Element Method

2.6 Soil Behavior and Constitutive Models

Stress-strain behavior, strength parameters and failure surfaces are the key features of the stability problems in geotechnical engineering. (Chen, 1975) There have been several models proposed in order to reflect the actual soil behavior in the literature. Some of these models are very simple like the ones based on the elastic behavior whereas some of them are so complex that they can only be used in numerical calculations and not for practical purposes.

In this study, the failure criterion based on elasto-plastic behavior will be discussed due to the fact that they are widely used and engineers and researchers are familiar with them.

The stress-strain behavior for most of the soils can be shown with Figure 2.6.

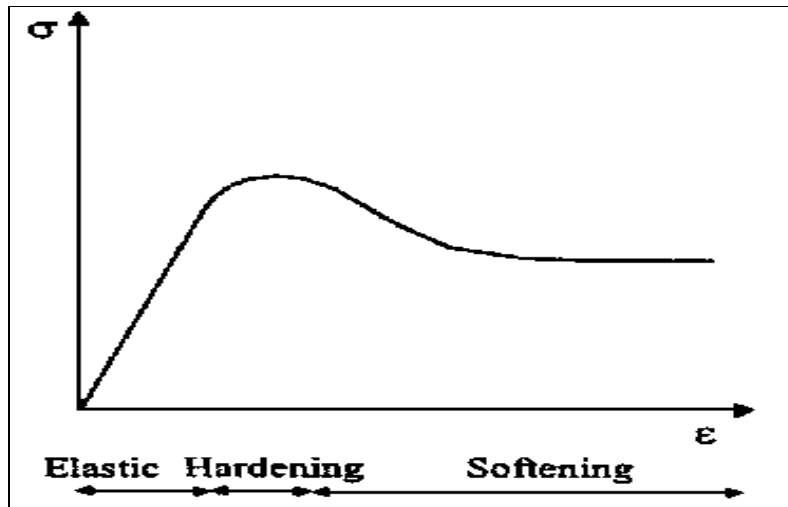


Figure 2.6 Real Soil Behavior involving hardening and softening (Potts&zdravkovic, 2001)

This Figure represents an elasto-plastic behavior in which the elastic portion is assumed to be linear and includes strain hardening and softening.

In the presented behavior, the strain increments are dependent on the current stress level and therefore strain increments directions may not coincide with the incremental stress directions. (Potts and zdravkovic, 2001)

The strain hardening and softening rules are not included in simple elasto-plastic models and therefore they only reflect the peak strength and strain. However there are also models accounting the strain softening and hardening rules.

2.6.1 Mohr-Coulomb Model

In the Mohr-Coulomb model, the failure of the soil is assumed to happen if the shear stress τ at any point in the soil reaches an amount that is a linear function of the cohesion c and the normal stress σ . (Chen and Liu, 1990).

This linear function is given as:

$$\tau = c + \sigma \tan \phi' \quad (2.28)$$

where c and ϕ' are material constants.

The failure condition can be expressed in terms of principal stresses as follows σ_1 , σ_2 and σ_3 being the principal stresses and $\sigma_1 > \sigma_2 > \sigma_3$

$$\sigma_1 \frac{(1 - \sin \phi)}{2c \cos \phi} - \sigma_3 \frac{(1 + \sin \phi)}{2 \cos \phi} = 1 \quad \text{for } c \neq 0 \quad (2.29)$$

In terms of stress invariants

$$f(J_1, J_2, \theta) = -\frac{1}{3} I_1 \sin \phi + \sqrt{J_2} \sin \left(\theta + \frac{\pi}{3} \right) - \frac{1}{\sqrt{3}} \sqrt{J_2} \cos \left(\theta + \frac{\pi}{3} \right) \sin \phi - c \cos \phi = 0 \quad (2.30)$$

Mohr-coulomb criterion in principal stress space is illustrated in Figure2.7.

Mohr-Coulomb criterion has two shortcomings. First, the meridians in the triaxial plane (Figure2.8) and the failure envelope in Mohr's diagram are straight lines. This implies that ϕ does not depend on confining pressure which is only valid for a limited range of confining pressures. Another shortcoming of Mohr-Coulomb criterion is the intermediate principal stress-

independent failure assumption. Also the failure surface has corners which make the use of this criterion in numerical analysis difficult. (Chen&Liu, 1990)

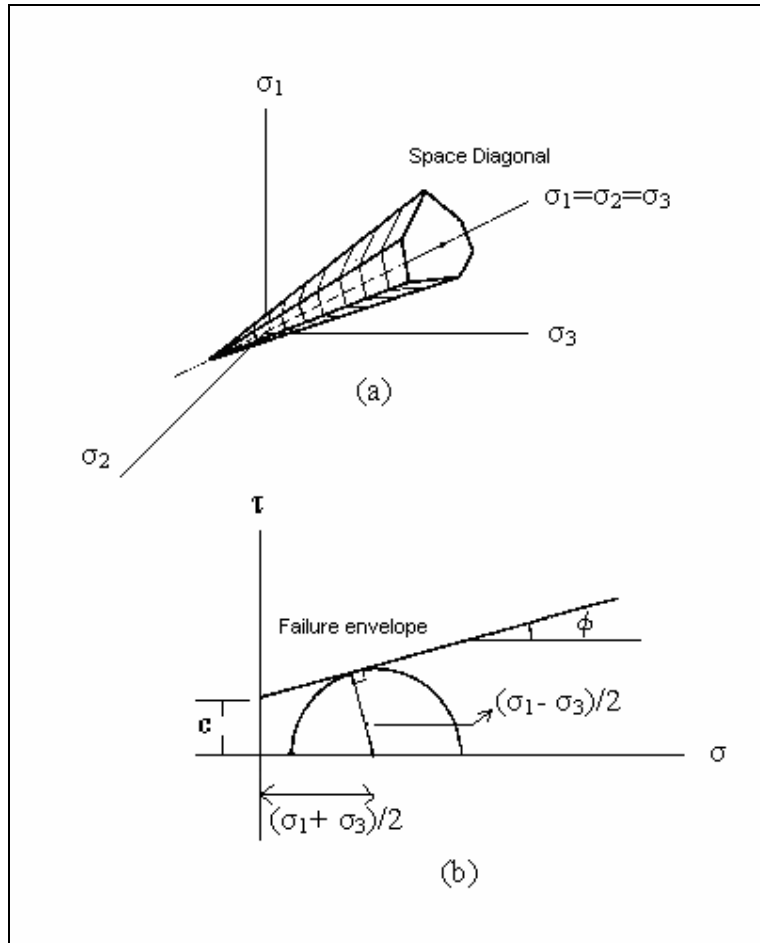


Figure 2.7 Mohr-Coulomb criteria in principal stress space and Mohr's diagram. a) Principal stress space, b) Mohr's diagram (Chen&Liu, 1990)

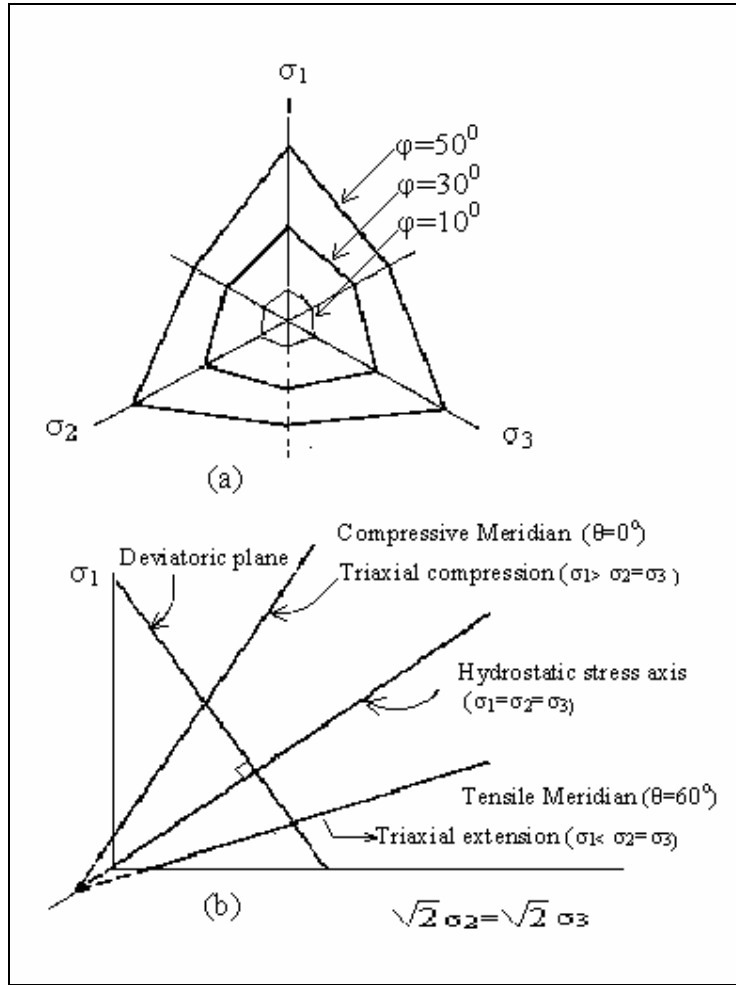


Figure 2.8 Traces of Mohr-Coulomb failure surface in the deviatoric and triaxial planes. a) Deviatoric plane, b) Triaxial plane

2.6.2 Drucker-Prager Model

Drucker-Prager model is an extended version of von Mises model. This criterion can be expressed in terms of stress invariants as follows;

$$f(J_1, J_2) = \sqrt{J_2} - \alpha I - k \quad (2.31)$$

Where k and α are material constants.

The Drucker-Prager model is a simple model and therefore advantageous. The only two parameters can be determined from conventional triaxial tests. (Chen and Liu, 1990)

These parameters can also be related with the Mohr-Coulomb parameters. There are several ways of this approximation. Here is an approximation for load carrying capacity problems based on the conditions (1) plane strain deformation and (2) same rate of dissipation of mechanical energy per unit volume. (Chen and Lui, 1990)

$$\alpha = \frac{\tan \phi}{(9 + 12 \tan^2 \phi)^{\frac{1}{2}}} \quad (2.32) \quad k = \frac{3c}{(9 + 12 \tan^2 \phi)^{\frac{1}{2}}} \quad (2.33)$$

Drucker-Prager model has a smooth failure surface and it makes this model suitable for three dimensional numerical applications. Also the effect of hydrostatic pressure on soil strength is included even for a limited range of hydrostatic pressure. Moreover, the influence of the intermediate principal stress is considered. However, the accuracy of this influence depends strongly on the selection of the material constants k and α (Chen&Liu, 1990)

2.6.3 Cam-Clay and Modified Cam-Clay Models

Cam clay is an elasto-plastic constitutive model developed by Roscoe and Schofield (1963). The modified Cam clay model is then proposed by Roscoe and Burland (1968).

The Cam clay and modified Cam clay models are formulated for a soil which is subjected to triaxial test.

The state of the soil during this triaxial test is described by the following parameters. (Britto and Gunn, 1987)

$$p' = \frac{\sigma'_a + 2\sigma'_r}{3} = \frac{\sigma_a + \sigma_r}{3} - u \quad (2.34)$$

$$q = \sigma'_a - \sigma'_r = \sigma_a - \sigma_r \quad (2.35)$$

$$V = 1 + e \text{ (Specific Volume)} \quad (2.36)$$

When the soil is subjected to isotropic compression the behavior is as shown in Figure 2.9. In part (b) of the Figure 2.9, the idealized behavior is also illustrated.

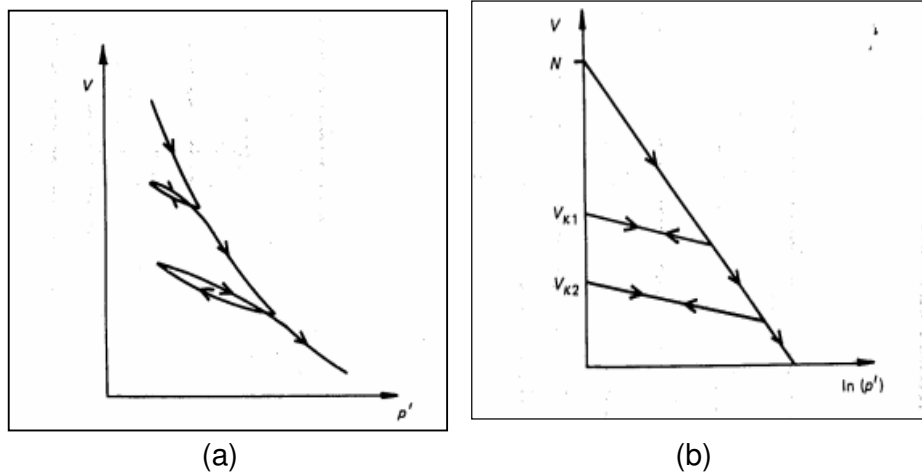


Figure 2.9 a) Typical (p' ; V) plot of isotropic compression, swelling and recompression
b) Idealized ($\ln p'$, V) plots in critical state theory (Britto&Gunn, 1987)

(The virgin compression line and the recompression lines are assumed to be linear and their equations are as follows:

$$V = n - \ln(p') \quad \text{isotropic virgin compression line} \quad (2.37)$$

$$V = V_k - K \ln(p') \quad \text{recompression lines} \quad (2.38)$$

N is a constant for a particular soil.

Figure 2.10 represents the Critical State Line (CSL) in p' , V , q space. CSL is the state of the soil at which the soil can be sheared with no change in imposed stresses or volume of the soil. The line is the intersection of two planes defined by

$$q = Mp' \quad (2.39)$$

$$V = \Gamma - \lambda \ln(p') \quad (2.40)$$

where M and Γ are material constants.

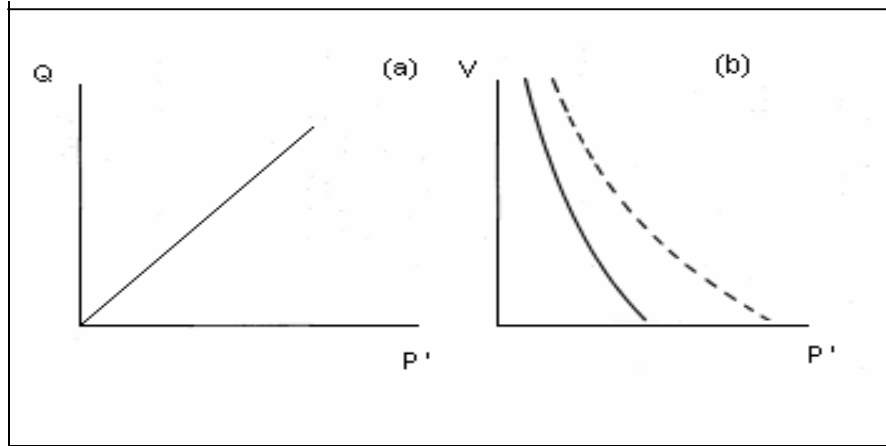


Figure 2.10 The Critical State Line in (a) (p', q) plot and (b) (p', V) plot (isotropic normal compression line is shown dashed in (b)) (Britto&Gunn)

Since the critical state formulations are based on triaxial test results and use p' and q , an approximation in full stress space is needed. There have been several attempts to define the shape of the yield surface and plastic potential in the deviatoric plane. Figure 2.11 shows the best known failure surfaces of Lade and Matsuoaka-Nakai. (Potts and Zdravkovic, 2001)

2.7 2D and 3D Numerical Methods in Tunneling

Since the early applications in the mid 1960's, numerical methods in tunnel engineering have been widely used with a steady growth. This is most probably due to the fact that numerical methods are capable of simulating the excavation and construction steps which is a drawback for analytical solutions. (Gioda and Swoboda, 1999)

Although 3D numerical analysis of tunnels can simulate the excavation/construction process, 2D numerical studies in tunneling are much more popular than the 3D analysis. (Galli&Leonardi, 2004)

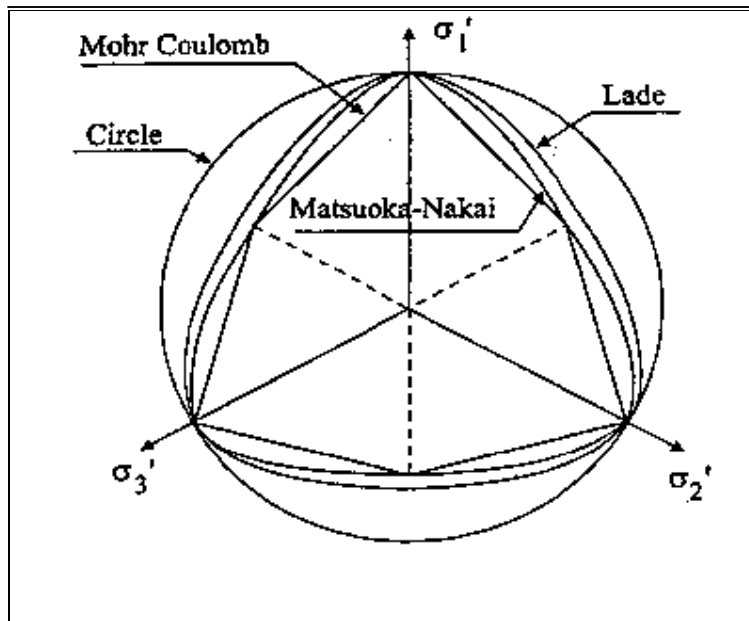


Figure 2.11 Failure surfaces in the deviatoric plane (Potts&Zdravkovic, 2001)

Oreste et al. (1999) made a comparison between 2D and 3D analysis using Finite Difference Method with programs Flac2D and Flac3D and showed that 3D numerical modeling is necessary to evaluate the stresses and displacements around low overburden tunnels. (Farias et al., 2003)

Nakai et al. (1997) investigated the settlements and earth pressures due to tunnel excavation by utilizing 2D and 3D elastoplastic finite element analyses and also 3D and 2D model tests. They also investigated the dilatancy effects by using sand and clay as the hosting medium. They concluded that in order to predict the deformation and earth pressure in tunneling, 3D analysis is necessary in which the construction process and mechanical properties of the soil including soil dilatancy are properly taken into account. They achieved this by using elastoplastic constitutive models for clay and sand, named t_{ij} -clay model and t_{ij} -sand model proposed by Nakai and Matsuoka (1986) and Nakai (1989)

2.7.1 Arching

Arching can be defined as the stress redistribution which results in many cases in a decrease in loading over the deflecting or yielding areas of a structure and an increase over adjoining rigid and stationary parts.

There has been many experimental studies to examine stress distribution and arching, the most famous being conducted by Terzaghi in 1936 using a deflecting trapdoor in the base of a soil bin. He found that the pressure acting on a long trapdoor was independent of the state of stress in the soil located more than two or three door widths above the door. The experiments were concerned with a plane strain condition, with only two plane surfaces of sliding. In a three-dimensional situation, for example a circular door, the equivalent distance is one to one-and-a-half diameters. The results of one of Terzaghi's experiments are given in Figure 2.12.

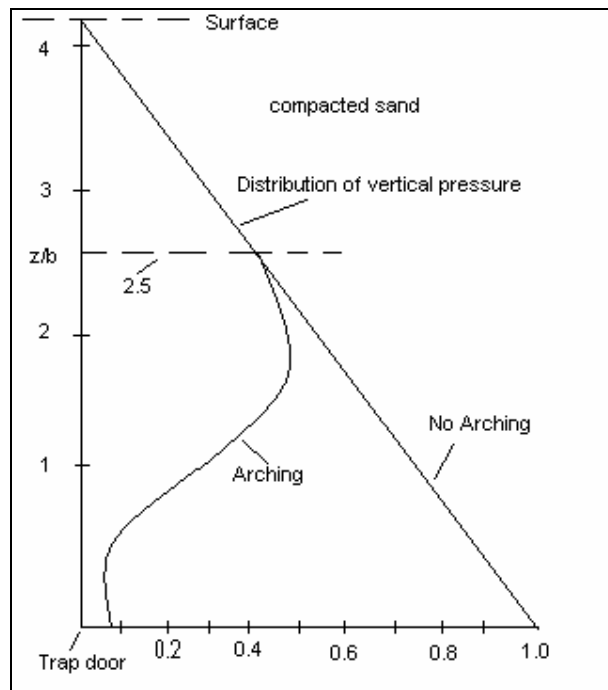


Figure 2.12 Terzaghi's trap door experiment

Arching effect is very important in numerical modeling in tunnel engineering. As the arching is a 3D event, only a 3D analysis can include the effect of arching by calculating the stress field in the hosting medium.

2.7.2 Constitutive Modeling

Constitutive model is one of the main components of numerical modeling. As described before, there are a lot of available models from very simple ones to highly complex ones.

Main&Herle made a study on the effect of constitutive models in numerical analyses of Heathrow Express trial tunnel. They utilized two traditional models (Mohr-Coulomb; Modified Cam-Clay) and four models of different complexity (isotropic and anisotropic nonlinear elasticity with perfect plasticity, combined isotropic and kinematic hardening plasticity and hypoplasticity.)

Their results show that the deformations in tunnels could be predicted more precisely when the constitutive model used takes the following phenomena into account; nonlinearity of the stress-strain curve, anisotropic behavior with different response in at least two perpendicular directions and path-dependent stiffness. However they also report that the combined isotropic and kinematic hardening plasticity did not perform well and even relatively simple models can be used successfully if applied in suitable problems.

In 2002, Bohac et al. performed FEM calculations for the Mrazovka Tunnel in Prague. Their study focuses on the effects of the constitutive model for the filling of the joints which intersect the tunnel profile at several locations. They used three material models for evaluating the deformations of the tunnel and its overburden. These models are a model with constant E , a model with stress dependent E and a third model with stress and strain dependent E .

They concluded that the surface settlements were not highly material model dependent since only the weak zone was modeled with different material models. On the other hand, they report a 50% larger deformation of the crown with the stress-strain dependent model in comparison with the linear elastic model.

2.7.3 Excavation Modeling

Another important factor in numerical modeling is the excavation modeling. There are numerous approaches to model the tunnel excavation in 2D numerical models like the ones suggested by Potts&Addenbrooke (1997) and Rowe (1983).

Potts&Addenbrooke simulate the ground loss by a technique in which the soil removal is carried out in small increments and the procedure is stopped when the prescribed amount of ground loss is achieved. Rowe's approach is more complex. In this procedure beam elements and soil elements are modeled with separate meshes. There is a gap between these meshes which simulates the ground loss. After unloading the volume and activation of the support elements, the gap is closed.

The methods explained above or other methods used in 2D simulation are too complex to use in 3D numerical modeling. Therefore simpler methods are being utilized in the literature in 3D analysis. For instance Augarde et al. used an approach in which the removal of the elements in the tunnel and simultaneously activation of lining elements are followed by uniform hoop shrinkage to develop the required amount of ground loss.

2.7.4 Modeling of Surface Excavation over Tunnels

Dolezalova (2001) investigated the effects of an deep excavation over an existing tunnel complex in Prague. She used 2D FEM to model both the tunnel construction and the surface excavation. She found that the some connections could be detached and the water tightness could be damaged. The predictions made on the basis of this analysis were in good agreement with the field measurements.

In 2002, Abdel-Meguid, Rowe and Lo made a study on the effects of the surface excavation for York-Mills Centre on the Toronto Transit Commission tunnels. They used 3D and 2D FEM models and compared the results with

the site data. They found that the excavation produces tensile stresses in the top fibers of the lining and compressive stresses in the lower fibers. They also found that the 3D results are similar with the measurements unlike the 2D model.

CHAPTER 3

PROBLEM STATEMENT AND METHODOLOGY

Tunnels are vital elements of transportation and infrastructure in urban areas. The tunneling induced ground settlement is the major problem in tunneling activities in urban areas. These settlements can damage the overlying structures and they should be reduced to an acceptable value by different methods such as grouting.

On the other hand, the impacts of surface construction and excavation to the existing tunnels have not yet been examined sufficiently. As the service lives are concerned, it is highly possible that the new structures will be built and existing structures will be replaced by new ones on the routes of tunnels. For example, for the construction of an underground car park or for the 3-4 storey basement construction, excavations up to 10-15 m are possible. A surface fill is also possible on the route of the existing tunnel. This fill may be due to a highway construction or due to a retaining wall construction.

In this study, the situations described above, namely excavation and loading over the existing tunnels are investigated in terms of the changes of the forces and moments in the tunnel lining. The study covers the numerical simulation of the tunnel construction and thus obtaining the initial forces and moments in the tunnel lining and numerical simulation of the excavation and loading over the tunnel. The excavation and loading situations are investigated separately since the possibility that both an excavation and loading taking place simultaneously in the same area is very low.

A 3D FEM commercial package “Plaxis 3D Tunnel” has been utilized in order to carry out the parametric analysis. The Plaxis 3D Tunnel program is developed especially for the analysis of different type of tunnels under different geotechnical conditions. Although it is very suitable for tunnel analyses, numerous kinds of complex soil-structure interaction problems can be assessed by employing Plaxis 3D Tunnel since it is equipped with different features which enable the realistic simulation of the specific problem in hand. In the Plaxis 3D Tunnel reference manual (2001), the capabilities and properties of the program are given in detail. In the following pages a short review of this manual is given:

Plaxis 3D Tunnel program consist of four basic components; namely Input, Calculation, Output and Curves. In the Input program the boundary conditions, geometry of the problem, all structural components such as retaining walls, tunnel lining, geogrids or anchors with appropriate material properties are defined. The soil and the interfaces can be modeled with different levels of complexity. The plates can be used to model walls, tunnel and liners. The plates are modeled with Mindlin Beam theory. In this theory, shear deformations are also calculated in addition to the out-of-plane bending. The Shear Stiffness is calculated based on the assumption that the plate has a rectangular section.

The volume elements are 15-node wedge elements and they are composed of 6-node triangles in x-y direction and 8-node quadrilaterals in z-direction. Higher order element types are not employed in 3D analysis since it would result in a dramatic increase in the memory consumption and calculation time. The plates, walls and shells are modeled with 8-node plate elements and 16-node interface elements are used to model the soil-structure interaction. The 2D mesh generation in Plaxis is fully automatic and the 3D mesh generation is semi automatic. The size of the mesh elements can be adjusted by using a general mesh size varying from very coarse to very fine and also by using local refinements.

The 2D model should contain all the structural elements and the geometry components even if they will not be used in the initial stages of the calculation. The program does not allow entering an input such as a structural element or soil cluster after the mesh is generated. After defining a new element or geometry portion, the mesh should be regenerated and the calculations performed before should be repeated with the new input.

After that the 2D model mesh is generated, the distance between the z-planes are defined by the user and a 3D mesh is generated based on the 2D meshes in each of the specified z-planes. In staged construction, the objects in the desired slice can be activated, deactivated or the properties can be changed. The number of mesh elements in 3D model depends on the number of the mesh elements in 2D model, the length of the slices and the total length of the tunnel in z-direction. Very fine meshes in 2D model should be avoided in order to reduce the number of elements in 3D model; and also to reduce the memory consumption and calculation time to the acceptable limits.

After fully defining the geometry and generating the mesh in 3D, initial stresses are applied by using either the K_0 -procedure or gravity loading. The calculation procedure can be performed automatically but there is also an option for manual control. The stages of the construction are defined by activating and deactivating the objects in the slices and a simulation of the construction process can be achieved. A construction period can also be specified for each construction stage. However the material model type for the soil should have been specified as Hardening-soil model. The number of the iterations can be specified both as manually and automatically.

The most important calculation type in Plaxis 3D tunnel is the staged construction as far as the tunnel construction simulation is concerned. In order to carry out this type of calculation, a 3D model with all active and inactive structural and geotechnical objects should be defined. In every

stage of the calculation the material properties, the geometry of the problem, loading type and water pressures can be redefined. These changes generally cause substantial out-of-balance forces. These out-of-balance forces are stepwise applied to the finite element mesh using a *Load advancement ultimate level procedure*. During these calculations, a multiplier that controls the staged construction process (ΣM_{stage}) is increased from zero to the ultimate level which is generally 1.0. The constructions which are not completed fully can be modeled by using this feature. (Plaxis 3D Tunnel reference manual, 2001).

3.1 Geometry and Definition

The geometry of the problem and the tunnel cross section are given in Figure 3.1 and Figure 3.2 respectively. It is typical shape in NATM tunnels. The tunnel has a height of 10m and a width of 11 m. The cover depth of the tunnel is 20 m as shown in Figure 3.1. The excavation and loading geometries are in a range which is common in civil engineering practice. The excavation is 24m in width and 40 m in length. The shorter side of the excavation is in the same direction with the tunnel length. The fill is 24m in width and 36m in length in the most lower level and 6m in the top. The depth of the excavation, the height of the fill and the eccentricities of excavation with respect to the tunnel axis has been changed throughout the study in order to assess the influences of these parameters to the forces and displacements on the tunnel lining. The tunnel is not in the center in x-direction since some of the excavations and embankment loadings throughout the study are eccentric. The symmetry of the tunnel could not be utilized in this study and the whole tunnel has been modeled rather than only modeling the left or the right half of the tunnel since the excavations and loadings were eccentric.

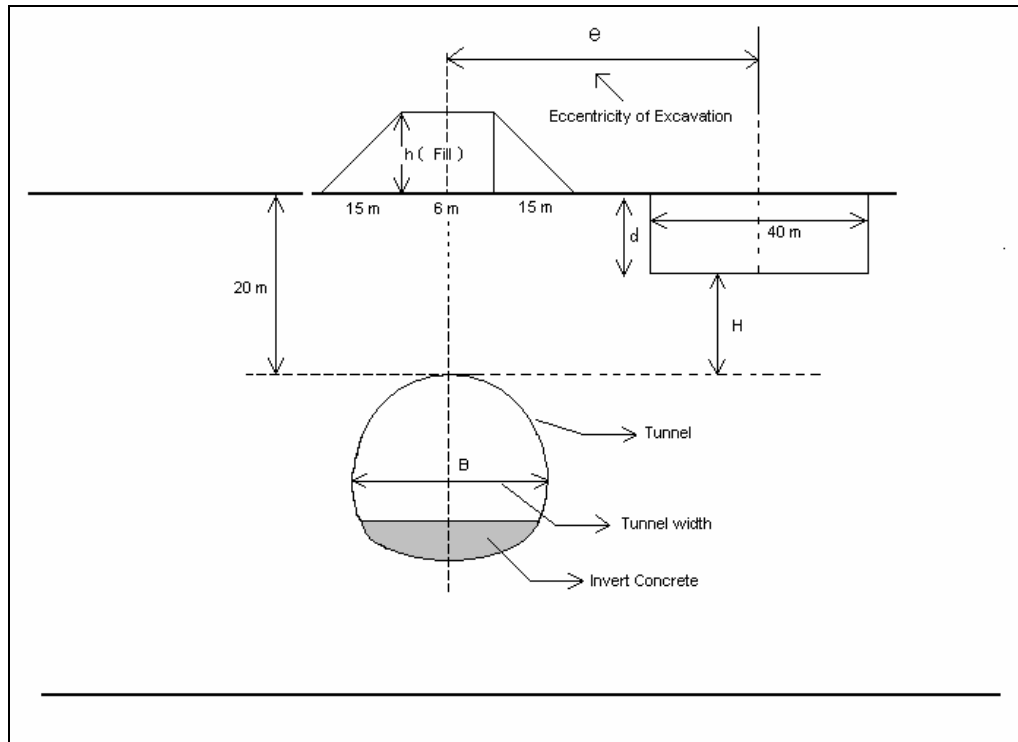


Figure 3.1 Geometry of the problem (not to scale)

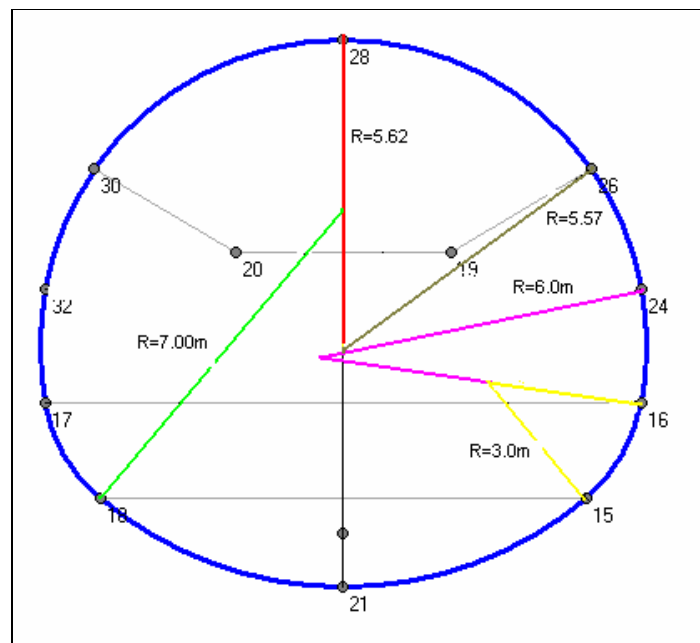


Figure 3.2 Tunnel cross section

The width of the model is 100m, the height is 70m and the length of the model is 90 m. In the model, there is a distance of about 55m between the tunnel centerline and the geometry boundary in x-direction and a distance of about 44.5m in negative y direction. The distances are far enough to reduce the boundary effects. The tunnel model is fixed in at both sides in x direction, at the front and rear planes in z direction, at the bottom in x and y directions. (Figure 3.3)

The mesh is generated automatically and some refinements have been applied in order to get smaller mesh sizes in the tunnel vicinity where the stresses and deformations are concentrated. The mesh is then extended in z direction. The mesh consists of 7740 elements and 22670 nodes. (See Figure 3.3)

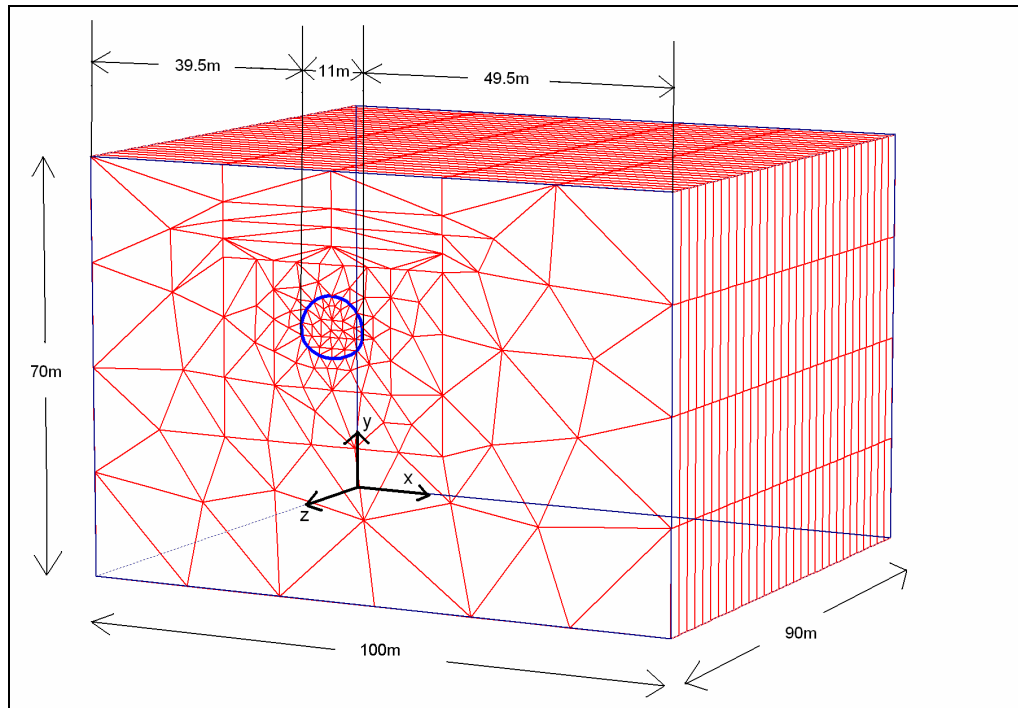


Figure 3.3 Dimensions of the model and 3D mesh

The slices are set as 3 m in z direction. In the staged construction, the advancement of top heading, bench and invert excavations are assumed to 3 meters. Although this value is a little bit higher than the common practice, shorter advancements, i.e. shorter slice lengths, result in excessive run times and memory consumption. In this study, each stage of the calculations took about 20 minutes and a full run has been completed in about 24 hours. The sequential excavation and shotcrete application steps are shown in Figure 3.4 The tunnel length is taken as 90 meters which is suitable to be able to evaluate the distribution of the deformations and stresses due to the surface excavation and construction along the tunnel. These effects are given in Chapter 4.

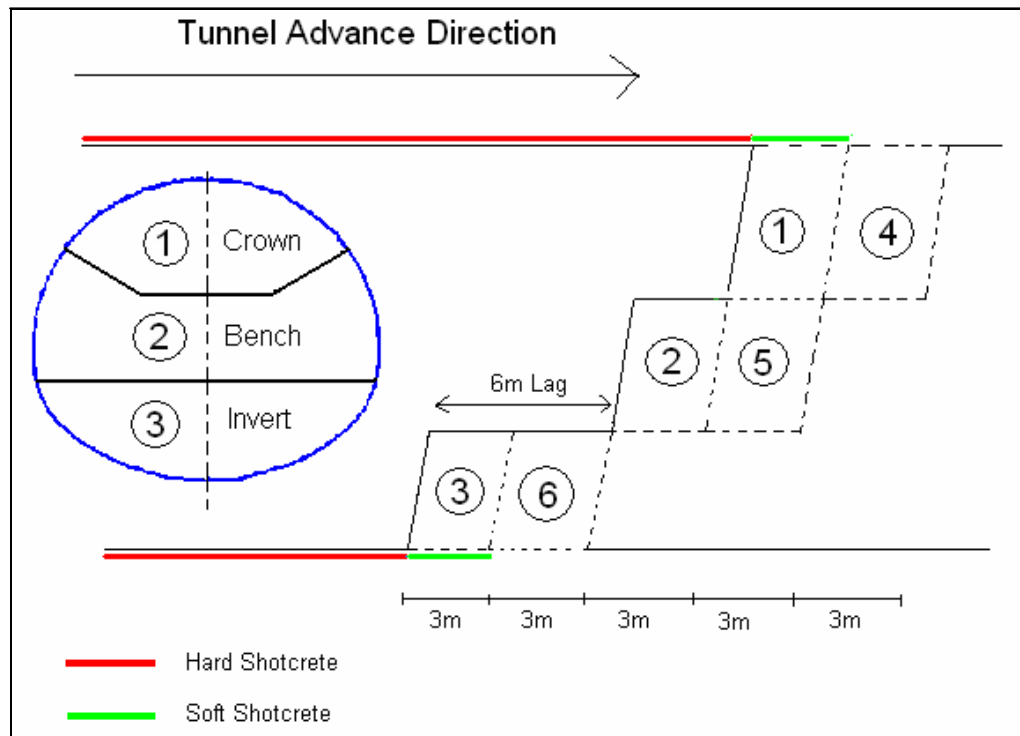


Figure 3.4 Staged excavation and shotcrete application steps

The hosting medium is assumed to be consisting of only one type of soil. In this study the hosting medium is extremely weathered soft rock like soil. It is assumed that no water table is encountered in the problem domain. All the analyses are performed by considering the drained conditions.

The Mohr-coulomb material model has been utilized for the modeling of the soil behavior. Mohr-coulomb model is a simple model with very well known parameters. Although there are more sophisticated models which include the creep effects and non-linearity of the material to a more complex level, Mohr-Coulomb model can be used satisfactorily in a parametric study like this, provided that parameters are chosen appropriately. The modulus of elasticity used for the soil is the unloading/reloading modulus. Since tunneling is an unloading process rather than loading, the used moduli are 3 times greater than the initial loading modulus. Actually, the behavior of the soil is highly non-linear and the model used for the soil should be capable of making a distinction between the loading and unloading/reloading. The elasticity modulus of the soil is stress dependent and the loading history has a great influence on the soil non-linear behavior. On the other hand, the more complex the material model, the more difficult is the evaluating and assessing of the parameters. The number of the parameters needed increase with the complexity of the problem and these parameters make no sense to most of the engineers and researchers.

The shotcrete is modeled as a linear elastic material. A distinction has been made between the soft shotcrete and the hardened shotcrete. The moments and forces in the tunnel lining depend greatly on the stiffness of the tunnel lining. This effect is included in the analysis by assigning to the tunnel lining first the soft shotcrete material properties and then by changing these properties in the next step with the properties of a hardened shotcrete. The main parameter for the linear elastic materials in Plaxis 3D Tunnel is the Young's Modulus E . The Young's Modulus for the shotcrete has been evaluated by using the empirical formula suggested by American Concrete Institute which relates the Young's Modulus with the compression strength of the concrete:

$$E=4900\sigma^{1/2} \quad (3.1)$$

Where σ is the 28 day compression strength of the concrete.

The compression strengths are chosen 5 MPa for soft shotcrete and 30 MPa for hard shotcrete. The Compressive strength of the hard shotcrete is actually higher than 30 MPa; however the value has been reduced in order to take the possible poor workmanship and the immediate cracking of the shotcrete when it hardens into account.

The final lining of the tunnels are actually not the main load carrying components in short term. They are designed for the long term since the shotcrete is degraded in time and it loses its load carrying capacity. The final linings are designed also by considering the possible changes in the water table or changes in the geometry of the overlying soil. In this study, the final lining is designed only for the loads from the surrounding soil and no factor of safety has been used. The reason is that in this study the changes of the loads and deformations in the final lining are concerned rather than the safety of the final lining. The material factors used for the calculations of the final lining are 1.5 and 1.15 for concrete and steel respectively. The final lining is assumed to be reinforced concrete.

In the analysis, the final lining is modeled by assigning the concrete parameters to the primary lining and it is assumed that in the long term, the primary lining has been degraded and there is a full contact between the final lining and the surrounding soil. The steel used in the reinforcement is not taken into account by the material properties assigned to the final lining. However, it is used for the calculation of the load carrying capacity of the lining. Since the loads and deformations are different for different elasticity modulus of the soil, the area of the steel used for different models is not the same. For $E_{\text{soil}} = 150$ MPa and for $E_{\text{soil}} = 300$ MPa, the steel area for 1 m of the lining is taken as 8 cm^2 and for $E_{\text{soil}} = 600$ MPa and $E_{\text{soil}} = 900$ MPa the steel area is taken as 6 cm^2 . The steel used for the models with lower elasticity modulus of the soil have bigger areas since the forces and the

deformations on the tunnel lining decreases with increasing elasticity modulus of the soil. The material properties are given in section 3.2. A sample calculation of the load carrying capacity of the tunnel lining and the interaction diagram are given in Appendix A.

After completion of the tunnels, the excavations and loadings are carried out by deactivating the pre-specified soil clusters and by activating the pre-specified loadings. The loading due to the embankment fill material has been modeled with distributed load. The unit weight of the fill material is assumed to be 18 kN/m^3 and the intensity of the distributed load is determined by the total weight of the fill material. Following the calculation of the stresses and deformations in the final lining, another stage in which the excavation or the loading is carried out, has been defined. At this stage, the displacements of the tunnel lining due to the tunnel construction have been reset to zero. By using this feature of Plaxis 3D Tunnel program, the displacements only due to excavation or loading can be determined more easily, whereas the stress field is not changed. Totally, 48 runs for the excavations and loadings have been carried out.

These runs can be divided basically into 3 sets. In the first set, excavations with depths $d=6\text{m}$, 9m , 12m and 15m and with no eccentricity for 4 different elasticity modulus of the soil have been modeled. In the second set, the excavation depth d is kept constant as 9m and the calculations are performed for $e=10\text{m}$, 20m , 30m and 40m eccentricities of the excavation. These calculations are repeated for 4 elasticity modulus, again. In the modeling of the excavations, the excavations were not supported. The soil is relatively strong and there was no need to support these excavations. However, if the soil would be not so strong, it could be necessary to support the sides of the excavation. In the third set, a fill with no eccentricity with different heights h has been modeled. The fill heights are $h=5\text{m}$, 10m and 15m . These calculations are performed again for 4 different elasticity modulus, namely 150 MPa , 300 MPa , 600 MPa and 900 MPa . (Table 3.1)

Table3.1: Description and properties of the analysis

Set 1

	E (MPa)	Excavation Depth, d (m)	Excavation Eccentricity, e (m)
Analysis 1	150	0	0
Analysis 2	150	6	0
Analysis 3	150	9	0
Analysis 4	150	12	0
Analysis 5	150	15	0
Analysis 6	300	0	0
Analysis 7	300	6	0
Analysis 8	300	9	0
Analysis 9	300	12	0
Analysis 10	300	15	0
Analysis 11	600	0	0
Analysis 12	600	6	0
Analysis 13	600	9	0
Analysis 14	600	12	0
Analysis 15	600	15	0
Analysis 16	900	0	0
Analysis 17	900	6	0
Analysis 18	900	9	0
Analysis 19	900	12	0
Analysis 20	900	15	0

Table3.1: (Continued) Description and properties of the analysis
Set 2

	E (MPa)	Excavation Depth, d (m)	Excavation Eccentricity, e (m)
Analysis 21	150	9	10
Analysis 22	150	9	20
Analysis 23	150	9	30
Analysis 24	150	9	40
Analysis 25	300	9	10
Analysis 26	300	9	20
Analysis 27	300	9	30
Analysis 28	300	9	40
Analysis 29	600	9	10
Analysis 30	600	9	20
Analysis 31	600	9	30
Analysis 32	600	9	40
Analysis 33	900	9	10
Analysis 34	900	9	20
Analysis 35	900	9	30
Analysis 36	900	9	40

Set 3

	E (MPa)	Fill Height , h (m)	Fill Eccentricity (m)
Analysis 37	150	5	0
Analysis 38	150	10	0
Analysis 39	150	15	0
Analysis 40	300	5	0
Analysis 41	300	10	0
Analysis 42	300	15	0
Analysis 43	600	5	0
Analysis 44	600	10	0
Analysis 45	600	15	0
Analysis 46	900	5	0
Analysis 47	900	10	0
Analysis 48	900	15	0

The sign convention for normal forces and bending moments in Plaxis 3D Tunnel is given in Figure 3.5. The compressive forces are taken as negative and tensile forces are taken as positive. In results section of the study (Chapter4), the sign convention is consistent with Plaxis 3D Tunnel in the tables. However, in the diagrams, for illustrative simplicity, the absolute values of the forces are taken.

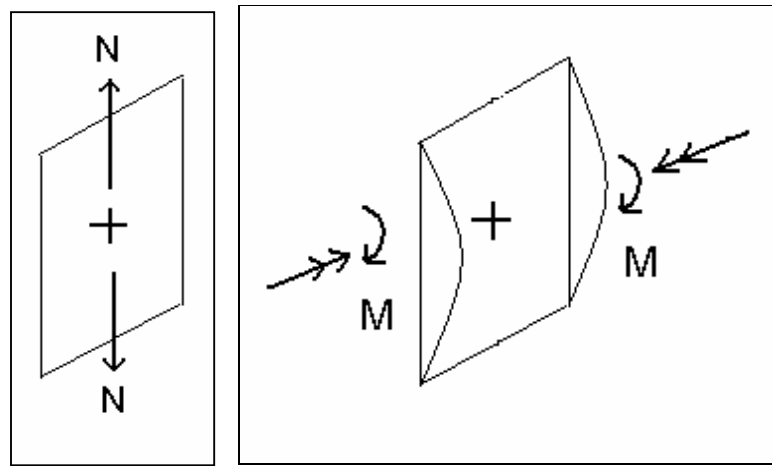


Figure 3.5 Sign Convention

3.2. Material Properties

Geotechnical properties of the soil:

$$\phi' = 30^\circ$$

$$c' = 60 \text{ kPa}$$

$$\gamma = 21 \text{ kN/m}^3$$

$$\nu = 0.3$$

$$E = 150 \text{ MPa}, 300 \text{ MPa}, 600 \text{ MPa}, 900 \text{ MPa}$$

Properties of the shotcrete:

Thickness: 30cm

$E = 10960000 \text{ kPa}$ for soft shotcrete

$E = 26840000 \text{ kPa}$ for hard shotcrete

$$\gamma = 24 \text{ kN} / \text{m}^3$$

$$\nu = 0.2$$

Properties of Concrete: (BS25)

$E = 30250000 \text{ kPa}$

$$\nu = 0.2$$

$$\gamma = 24 \text{ kN/m}^3$$

3.3. Excavation Procedure

Each analysis consists of 94 consecutive stages. In this chapter only the beginning and the end of the stages are presented as the intermediary stages are the same.

Initial stage: Generation of the initial stresses by using the K_0 procedure.

Stage 1: Excavation and soft shotcrete application of crown (slice1)

Stage 2: Excavation and soft shotcrete application of crown (slice2);
application of hard shotcrete to the crown (slice1)

Stage 3: Excavation and soft shotcrete application of bench (slice1);
application of hard shotcrete to the crown (slice2)

Stage 4: Excavation and soft shotcrete application of crown (slice3);
application of hard shotcrete to the bench (slice1)

Stage 5: Excavation and soft shotcrete application of bench (slice2);
application of hard shotcrete to the crown (slice3)

Stage 6: Excavation and soft shotcrete application of crown (slice4);
application of hard shotcrete to the bench (slice2)

Stage 7: Excavation and soft shotcrete application of bench (slice3);
application of hard shotcrete to the crown (slice4)

Stage 8: Excavation and soft shotcrete application of invert (slice1);
application of hard shotcrete to the bench (slice3)

Stage 9: Excavation and soft shotcrete application of crown (slice5);
application of hard shotcrete to the invert (slice1)

Stage 10: Excavation and soft shotcrete application of bench (slice4);
application of hard shotcrete to the crown (slice5)

Stage 11: Excavation and soft shotcrete application of invert (slice2);
application of hard shotcrete to the bench (slice4)

Stage 12: Excavation and soft shotcrete application of crown (slice6);
application of hard shotcrete to the invert (slice2)

,

,

,

Stage 84: Excavation and soft shotcrete application of crown (slice30);
application of hard shotcrete to the invert (slice26)

Stage 85: Excavation and soft shotcrete application of bench (slice29);
application of hard shotcrete to the crown (slice30)

Stage 86: Excavation and soft shotcrete application of invert (slice27);
application of hard shotcrete to the bench (slice29)

Stage 87: Excavation and soft shotcrete application of bench (slice30);
application of hard shotcrete to the invert (slice27)

Stage 88: Excavation and soft shotcrete application of invert (slice28);
application of hard shotcrete to the bench (slice30)

Stage 89: Excavation and soft shotcrete application of invert (slice29);
application of hard shotcrete to the invert (slice28)

Stage 90: Excavation and soft shotcrete application of invert (slice30);
application of hard shotcrete to the invert (slice29)

Stage 91: Application of hard shotcrete to the invert (slice30)

Stage 92: Application of final lining to all slices

Stage 93: Application invert concrete to all slices

Stage 94: Surface excavation or surcharge load application (slices 12, 13,
14, 15, 16, 17, 18, and 19)

CHAPTER 4

RESULTS AND DISCUSSION

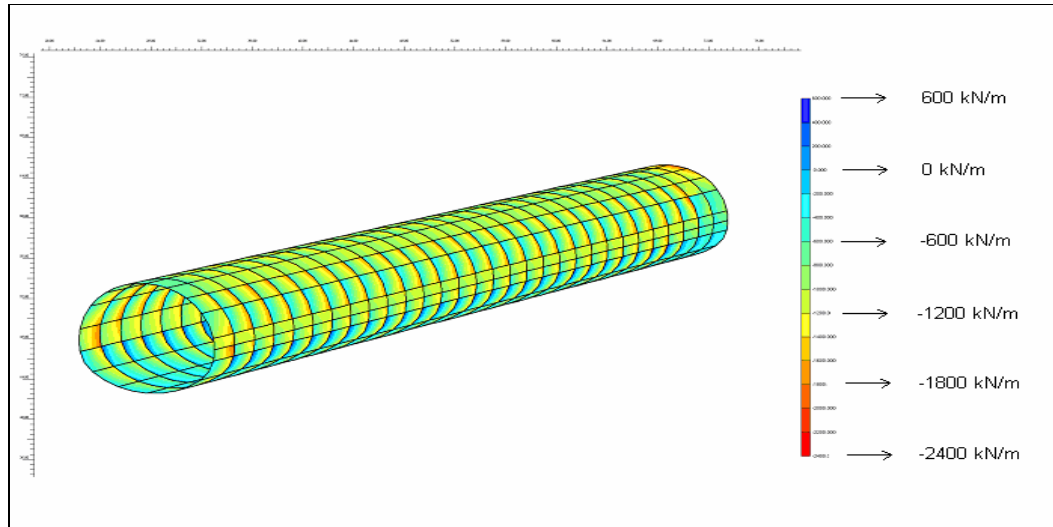
The results of the analyses and their interpretation are presented in this chapter. The results are given both in tabular and in graphical forms. In this chapter, the typical or the most extreme cases are presented graphically in terms of interaction diagrams and force distribution in tunnel final lining. The rest of the results which are great in quantity are given in appendices.

4.1 Effect of Staged Construction on Forces in Tunnel Lining

The main idea behind the staged excavation modeling is to simulate the real construction procedure and thus take the arching effect and the effects of the sequential construction to the 3D model into account. It has been shown by various studies that the forces and deformations are different for the staged excavation and for the one-phase excavation. In this study, a sample calculation has been carried out in order to see the effects of staged excavation to the forces in the tunnel lining. This is achieved by comparing the results of a staged excavation analysis with the results of a one-phase excavation. Both analysis have been made for $E=150$ MPa and surface excavation depth, $d=15$ m. The results are different for these two cases.

The extreme normal force in the mid-plane for the staged construction analysis is -1460 kN/m before the excavation and -820 kN/m after the excavation. The decrease of the normal force is about 44%. On the other hand, the extreme normal force for the one-phase construction is -2510 kN/m before the excavation and -1980 kN/m after the excavation. The decrease in normal force is 21%. The difference between the normal forces of these two cases is 1050 kN/m. This difference is due to the arching effect which is shown in Figure 4.1. For staged construction case, the arching effect can be seen in the rear planes of the slices. Since no arching effect

occurs in front of the plane, the normal forces are different in front and the rear side of the same plane. For the one-phase construction case, no arching occurs and as it is shown in Figure 4.1 b, the normal forces are higher.



a)

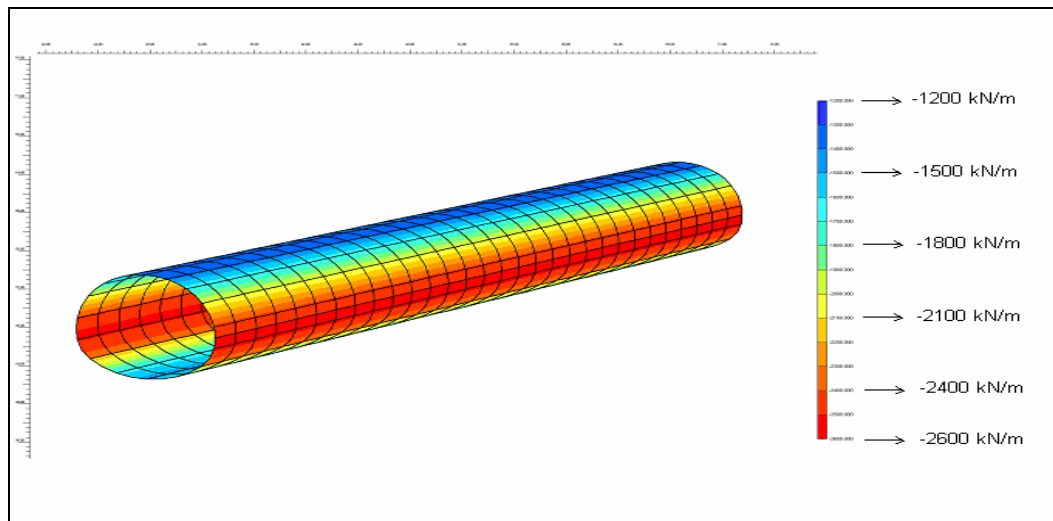


Figure 4.1 Normal forces in the tunnel lining a) Staged construction b) One-phase construction

The difference between the bending moments is higher in terms of percentage. For the staged construction case, the bending moments are -63.83 kNm/m and -203.48 kNm/m before and after the excavation, respectively. These values are -180.58 kNm/m and -271.70 kNm/m for the one-phase case. The latter case results in about 3 times greater bending moments before the excavation and about 1.3 times greater bending moments after the excavation.

The shear forces in these two cases before the excavation are similar. It is -159.56 kN/m for the staged construction case and -168.43 kN/m for the one-phase construction case. However, there is a 50% difference between these values after the excavation. The values for these shear forces are -400.3 kN/m and -599.59 kN/m for the staged construction case and one-phase construction case, respectively. The forces on the tunnel lining for staged construction case and for one-phase construction case are shown in Figure 4.2.

From these results, it can be concluded that the staged excavation modeling is not only necessary for evaluating the forces in the tunnel lining after the completion of the construction, but the changes in these forces greatly depend on the staged construction modeling.

4.2 Effect of Surface Excavation to the Tunnel Lining

In this section, the effects of a surface excavation which is symmetrical with respect to the tunnel axis have been investigated. Four different excavation depths, namely $d=6\text{m}$, $d=9\text{m}$, $d=12\text{m}$ and $d=15\text{m}$ are used. The tabular form of the results is shown in Table 4.1. The normal forces are reduced when an excavation is carried out on the ground surface. The magnitude of this decrease depends both on soil stiffness and also on the excavation depth. The E vs. Axial Force diagram is almost linear before the excavation and the slope gets steeper especially in lower E values when the excavation depth increases. (See Figure 4.3.)

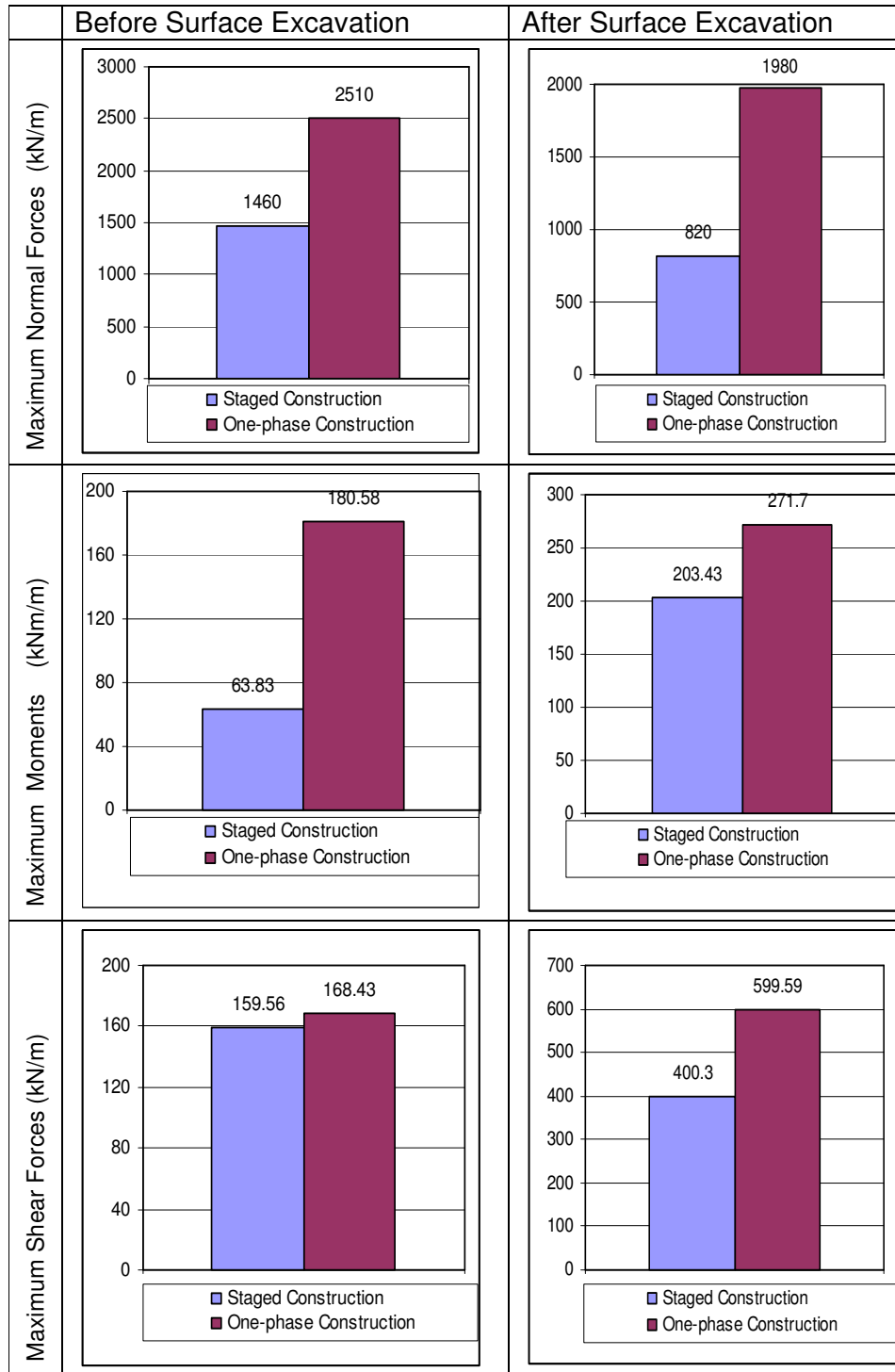


Figure 4.2 Comparison of staged construction and one-phase construction

Table 4.1 Extreme Forces and Displacements for the Mid-Plane

Set 1

Analysis	Normal Force (kN/m)	Bending Moment (kNm/m)	Shear Force (kN/m)	Vertical Displacement (mm)	Horizontal Displacement (mm)
Analysis1	-1460	-63,83	-159,56	N/A	N/A
Analysis 2	-1150	-116,43	-179,97	9,68	2,42
Analysis 3	-958,64	-148,64	-262,44	15,12	3,97
Analysis 4	-860,1	-180,55	-344,76	20,55	5,36
Analysis 5	-819,73	-203,48	-400,3	24,9	5,83
Analysis 6	-1360	-37,92	-96,8	N/A	N/A
Analysis 7	-1010	-63,9	-104,55	5,23	1,23
Analysis 8	-838,43	-80,16	-151,9	8,23	2,05
Analysis 9	-760,25	-97,14	201,58	11,35	2,82
Analysis10	-711,11	-109,97	239,53	14,04	3,27
Analysis11	-1260	-21,29	-58,81	N/A	N/A
Analysis 12	-927,68	-32,34	-57,6	2,8	0,58
Analysis 13	-772,92	-40,12	-79,47	4,44	1,00
Analysis 14	-622,48	-47,98	-113,28	6,2	1,4
Analysis 15	-569,27	58,54	-143,36	7,76	1,67
Analysis 16	-1190	-16,27	-39,72	N/A	N/A
Analysis 17	-878,04	-22,41	-39,18	1,94	0,37
Analysis 18	-720,94	-26,85	-53,26	3,09	0,64
Analysis 19	-585,99	34,15	79,54	4,33	0,9
Analysis 20	-530,04	42,35	103,04	5,49	1,09

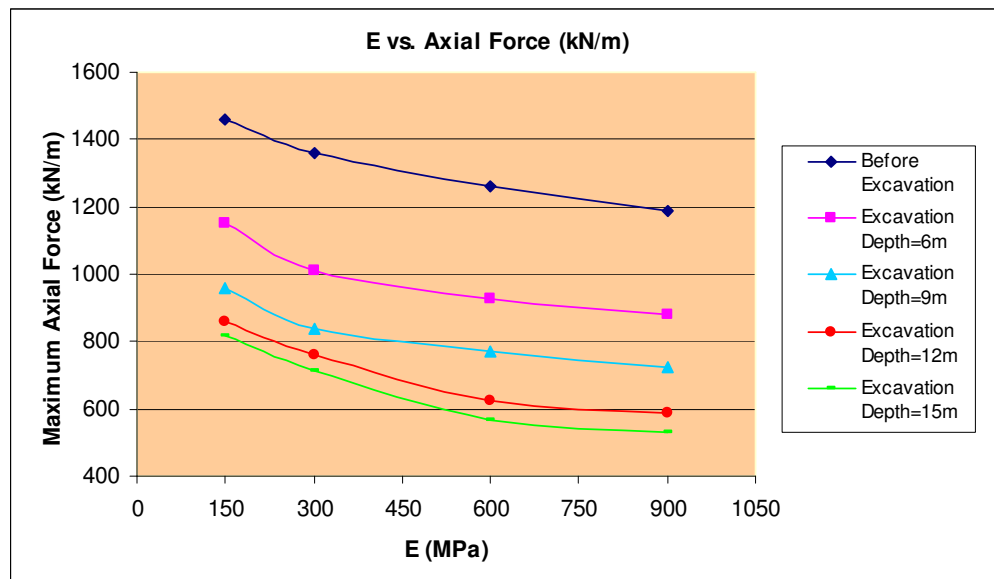


Figure 4.3 E vs. Axial Forces for Different Excavation Depths

For $E = 150$ MPa; the normal forces decrease by 21%, 34%, 41% and 44% from the initial value of the normal force which is -1460 kN/m, for excavation depths $d=6$ m, $d=9$ m, $d=12$ m, and $d=15$ m respectively. These values are 26%, 38%, 44% and 48% for $E=300$ MPa; 26%, 39%, 51% and 55% for $E=600$ MPa; 26%, 39%, 51% and 55% for $E=900$ MPa. As it can be understood from these results and from Figure 4.3, the change in the axial forces do not vary so much as the excavation depth gets closer to the tunnel depth. The results also show that for $E>600$ MPa, the percentage of the change of the normal forces are very similar. Figure 4.4 shows the normal forces for different H/B ratios. In the figure two extreme cases, $E=150$ MPa and $E=900$ MPa are shown.

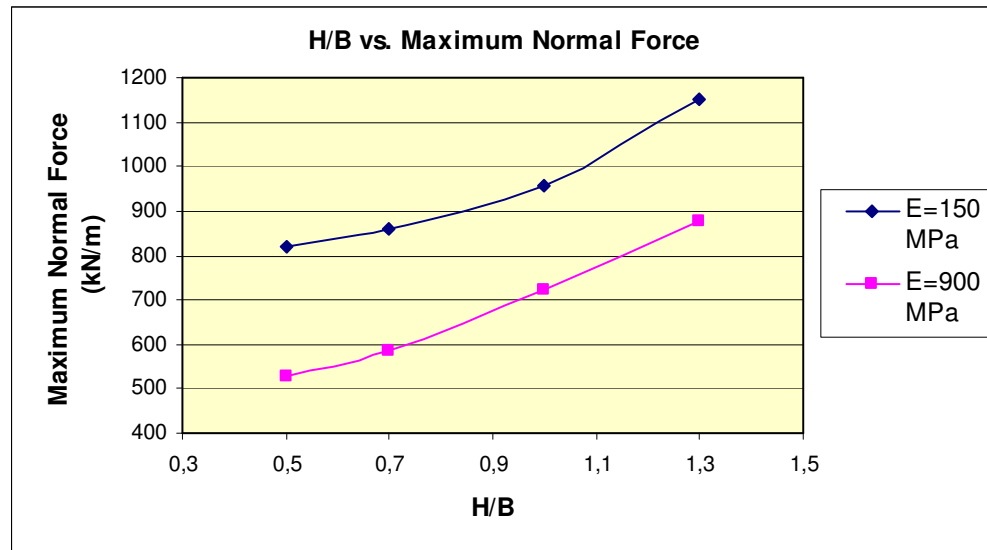


Figure 4.4 H/B vs. Normal Forces for two extreme E values

The bending moments are increasing with increasing depth (decreasing H/B ratio) in opposite to the normal forces. The magnitude of the bending moment for $E=150$ MPa is -116.43 kNm/m, -148.64 kNm/m, -180.55 kNm/m and -203.48 kNm/m for excavation depth $d=6$ m, 9m, 12m and 15m, respectively. The increase of the bending moments from the initial value, -63.83 kNm/m, are 82%, 133%, 183% and 219% for the excavations depths

$d=6\text{m}$, 9m , 12m and 15m , respectively. These increases as percentage for the other E values are; 69%, 111%, 156% and 190% for $E=300\text{ MPa}$; 52%, 88%, 125% and 175% for $E=600\text{ MPa}$; 38%, 65%, 110% and 160% for $E=900\text{ MPa}$. (Figure 4.5) The interesting point here is that the sign of the moment has been changed from negative to positive for the cases $E=600\text{ MPa}$ and $d=15\text{m}$; $E=900\text{ MPa}$ and $d=12\text{m}$; $E=900\text{ MPa}$ and $d=15\text{m}$. It can be seen also from these results that the moments can be increased up to 3 times when the excavation depth is 15m . On the other hand, the rate of the increase in the bending moments decreases with increasing magnitudes of the Young's Modulus. Figure 4.6 shows the bending moments for two extreme E values for different H/B ratios. It can be seen from the figure that the rate of decrease of the maximum moments with increasing H/B ratios is higher for $E=150\text{ MPa}$ as compared to $E=900\text{ MPa}$.

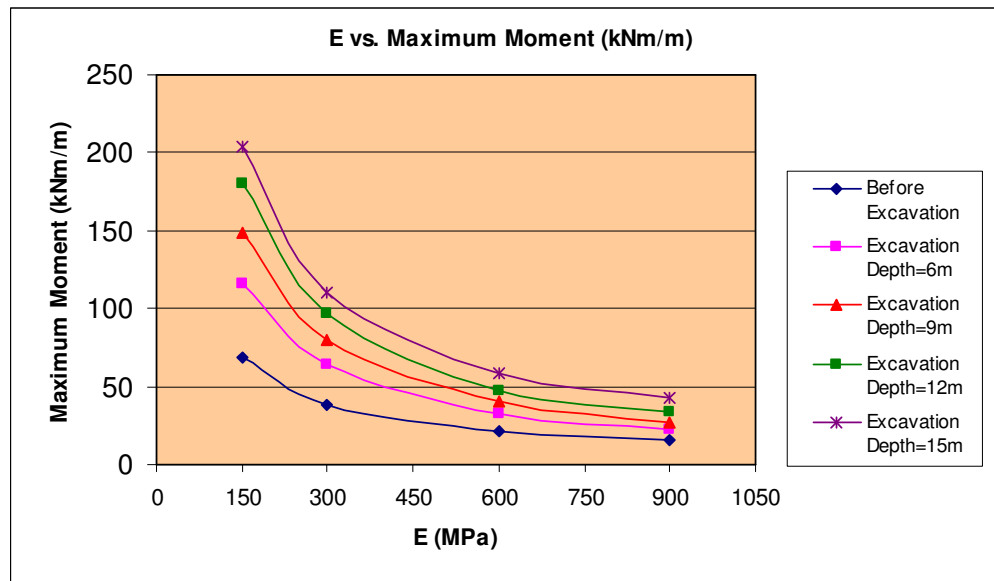


Figure 4.5 E vs. Bending Moments for Different Excavation Depths

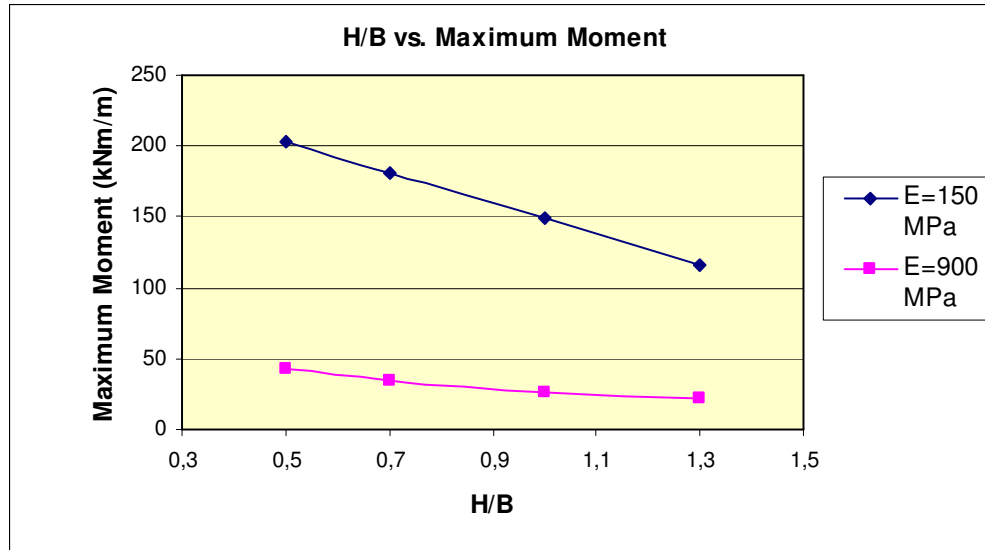


Figure 4.6 H/B vs. Moments for two extreme E values

The normal force and the bending moment couples in the mid-plane are shown in the interaction diagrams in Figure 4.7. Two extreme cases with $H/B=0.5$ and $H/B=1.3$ for $E=150$ MPa and $E=900$ MPa are presented. As it can be seen from the figure, the number of the force couples that move outside the interaction diagram is highest for $E=150$ and $H/B=0.5$ case. If a normal force and moment couple lie on the outer side of the interaction diagram, it can be said that there exist some forces in the tunnel lining which can not be supported safely by the tunnel lining. The rest of the interaction diagrams are presented in Appendix B. Figure 4.8 illustrates the risk of failure of the tunnel lining for all H/B and E values. The figure shows that the failure risk increases with decreasing H/B ratios and E values.

The shear forces increase with increasing excavation depth and decrease with the increasing Young's Modulus. The increase of the shear forces from the initial value -159.56 kN/m for $E=150$ MPa are 13%, 64%, 116% and 151% for excavation depth $d=6$ m, 9m, 12m and 15m, respectively. The increases for $E=300$ MPa are 8%, 57%, 108% and 147% from the initial value -96.8 kN/m for $d=6$ m, 9m, 12m and 15m, respectively. The shear force before the excavation is -58.81 kN/m for $E=600$ MPa and the value

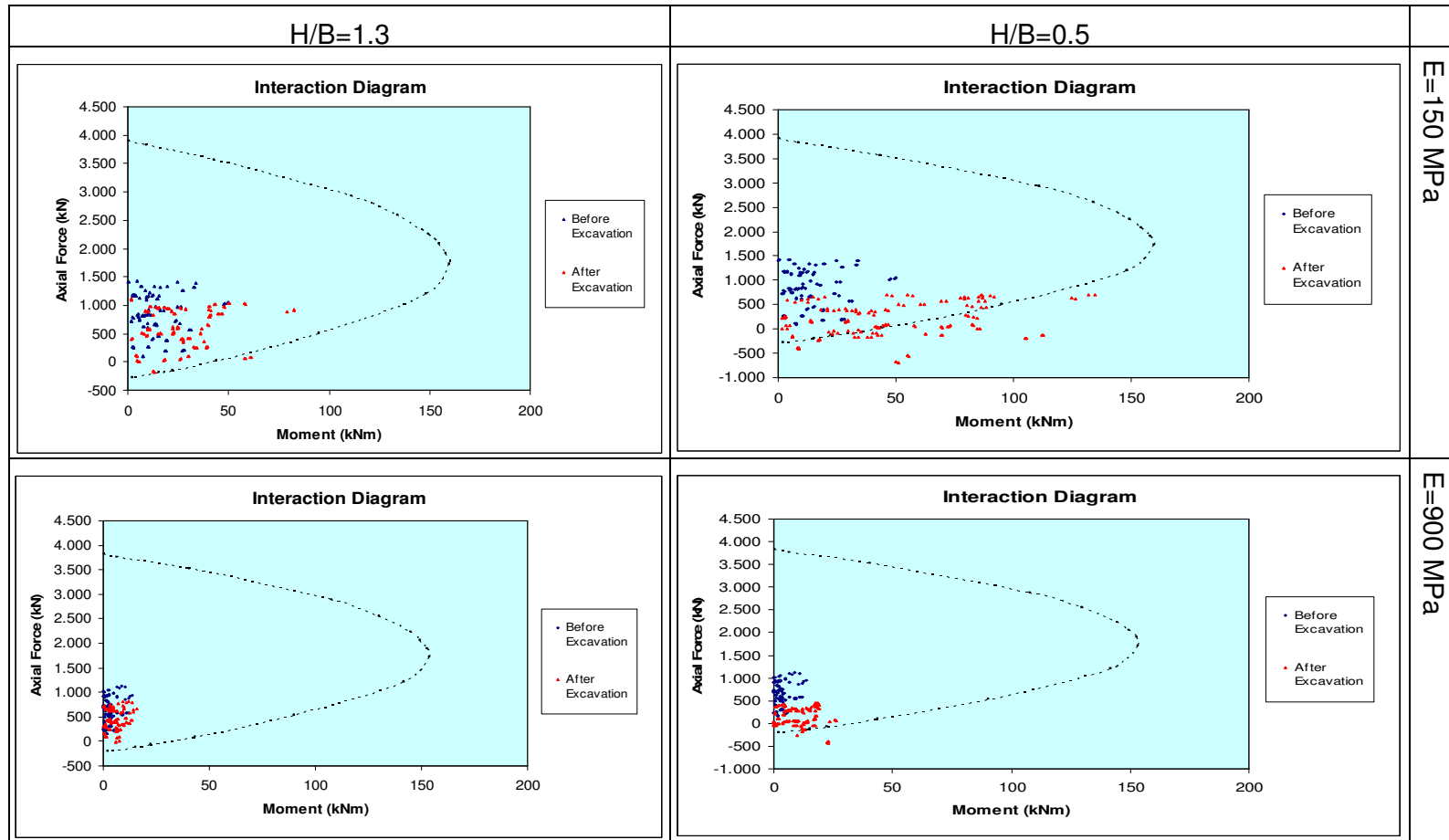


Figure 4.7 Interaction Diagrams for extreme values of H/B ratio and E

	E=150 MPa	E=300 MPa	E=600 MPa	E=900 MPa
H/B=0.5	X	X	X	X
H/B=0.7	X	X	X	X
H/B=1.0	X	X	X	✓
H/B=1.3	X	✓	✓	✓
✓ = The capacity of the lining not exceeded (No Failure)		X = The capacity of the lining exceeded (Failure)		

Figure 4.8 Risk of failure for different H/B ratios and E values

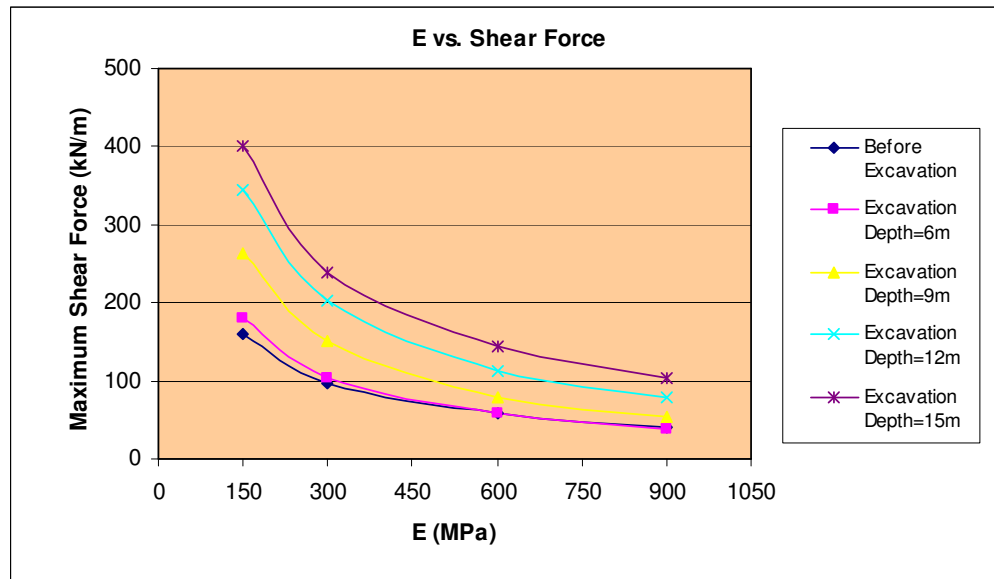


Figure 4.9 E vs. Maximum Shear Forces for Different Excavation Depths

decreases by 2% for $d=6\text{m}$ and increases 35%, 93% and 145% for $d=9\text{m}$, 12m and 15m respectively. The initial value of the shear force for $E=900\text{ MPa}$ is -39.72 kN/m and this value decreases by 1% for $d=6\text{m}$ and increases by 34%, 100% and 161% for $d=6\text{m}$, 9m and 12m respectively. By inspecting these results and Figure 4.9, it can be seen that the excavation with a depth $d=6\text{m}$ has very little effect on the shear force. However, for the greater values of the excavation depth, i.e. for smaller values of H/B ratios, the shear force changes significantly

The vertical and horizontal displacements due to the excavations are determined by resetting these displacements before the excavation and thus the obtained displacements are caused only by the excavation. Vertical and horizontal displacements increase with increasing excavation depth and decrease with increasing Young's Modulus. The vertical displacements for $E=150\text{ MPa}$ are 9.68mm , 15.22mm , 20.55mm and 24.9mm for $d=6\text{m}$, 9m , 12m and 15 m respectively. These values are for $E=300\text{ MPa}$, 5.23mm , 8.23mm , 11.35mm and 14.04 mm for $d=6\text{m}$, 9m , 12m and 15m respectively. For $E=600\text{ MPa}$, these displacements are 2.8mm , 4.44mm , 6.2mm and 7.76mm for $d=6\text{m}$, 9m , 12m and 15m respectively. When the case with $E=900\text{ MPa}$ is considered, the vertical displacements are 2.8mm , 4.44mm , 6.2mm and 7.76mm for $d=6\text{m}$, 9m , 12m and 15 m respectively. (Figure 4.10) Horizontal displacements are smaller than the vertical displacements as it can be seen in Table 4.1 and in Figure 4.11. The difference of the horizontal displacements for 12m and 15m are very close. For $E=150\text{ MPa}$, the horizontal displacements are 2.42mm , 3.97 mm , 5.36mm and 5.83 mm for $d=6\text{m}$, 9m , 12m and 15m . For $E=300\text{ MPa}$ the displacements are 1.23 , 2.05mm , 2.82mm and 3.27 ; for $E=600\text{ Mpa}$ they are 0.58mm , 1mm , 1.4mm and 1.67mm ; for $E=900\text{ MPa}$ horizontal displacements are 0.37mm , 0.64mm , 0.9mm and 1.09 mm for $d=6\text{m}$, 9m , 12m and 15 m respectively. The horizontal displacements are small in magnitude and in most of the situations they are not the primary concern.

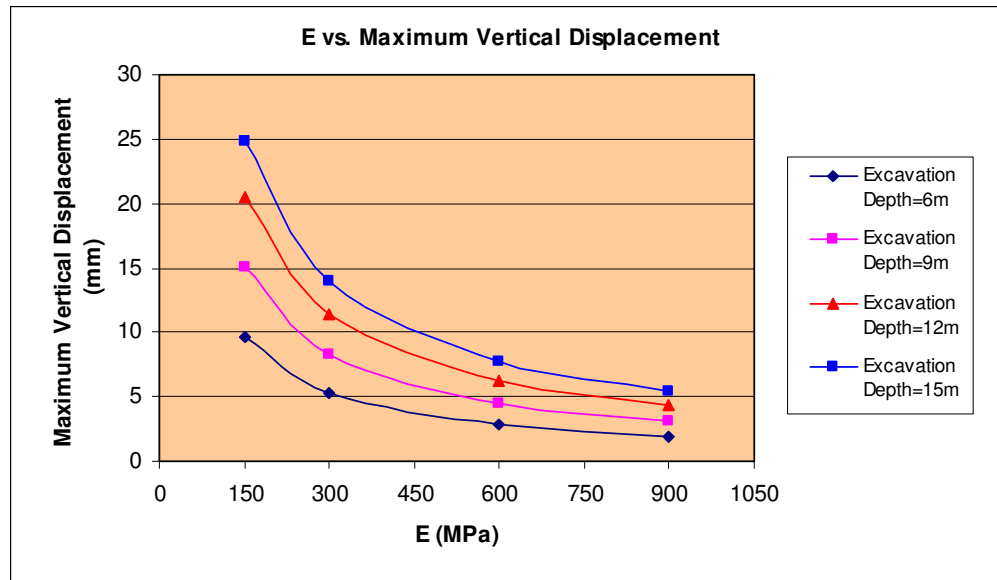


Figure 4.10 E vs. Vertical Displacements for Different Excavation Depths

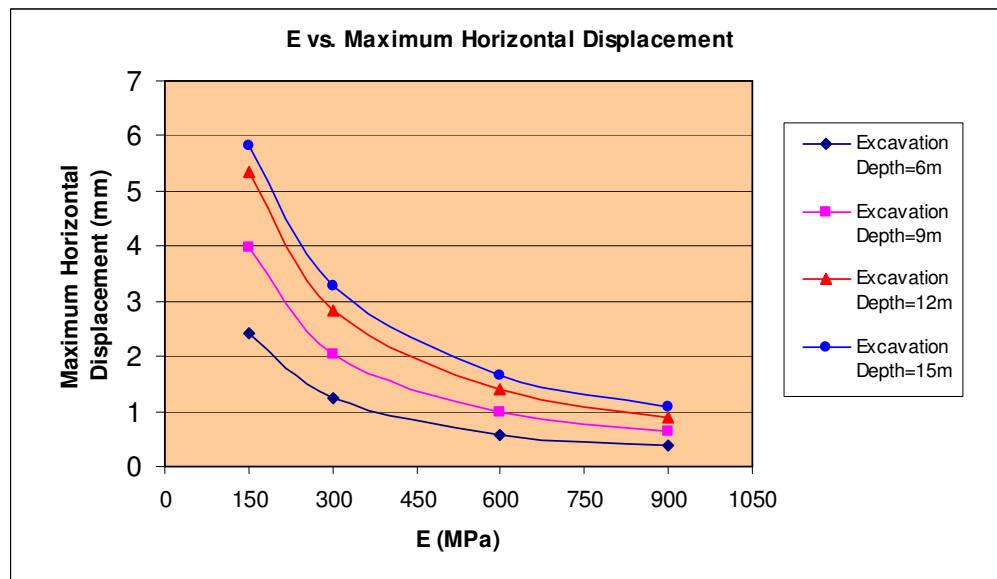


Figure 4.11 E vs. Horizontal Displacements for Different Excavation Depths

4.3 Effect of Unsymmetrical Excavation to the Tunnel Lining

In this section, the effects of excavations which are not symmetrical with respect to the tunnel lining have been investigated. The depth of the excavation is kept constant as 9m and different eccentricities of the excavations with respect to the tunnel lining have been studied. The eccentricities are $e=10\text{m}$, $e=20\text{m}$, $e=30\text{m}$ and $e=40\text{m}$. The tabular form of the results is presented in Table 4.2

Table 4.2 Extreme Forces and Displacements for the Mid-Plane

Set 2

Analysis	Normal Force (kN/m)	Bending Moment (kNm/m)	Shear Force (kN/m)	Vertical Displacement (mm)	Horizontal Displacement (mm)
Analysis 21	-1060	-145,51	-266,33	14,08	4,3
Analysis 22	-1290	-119,61	-192,43	10,56	3,64
Analysis 23	-1370	-87,7	-150,31	6,42	2,94
Analysis 24	-1390	-67,19	-151,01	3,57	2,36
Analysis 25	-935,55	-78,61	-155,8	7,63	2,18
Analysis 26	-1140	-66,4	-113	5,65	1,82
Analysis 27	-1250	-50,15	-100,94	3,39	1,53
Analysis 28	-1320	-39,27	-101,39	1,87	1,22
Analysis 29	-869,02	-37,23	-84,76	4,1	1,07
Analysis 30	-1060	33,24	-63,48	2,99	0,89
Analysis 31	-1170	-25,6	-59,58	1,77	0,8
Analysis 32	-1250	22,56	-60,46	0,97	0,63
Analysis 33	-802,43	27,47	-56,58	2,84	0,69
Analysis 34	-985,18	24,76	-43,35	2,06	0,59
Analysis 35	-1100	17,76	41,49	1,21	0,54
Analysis 36	-1180	16,67	-40,6	0,66	0,43

The normal forces in this set are smallest for $e=10\text{m}$, i.e. the decrease in the normal forces is highest. If the eccentricity gets larger, in other words if the e/B ratio increases, the rate of the decrease of the normal forces decreases. (See Figure 4.12) The values of normal forces before the excavation and for $e=40\text{m}$ are very similar, especially for $E=600\text{ MPa}$ and $E=900\text{ MPa}$. The normal forces for $E=150\text{ MPa}$ are -1060 kN/m , -1290 kN/m , -1370 kN/m

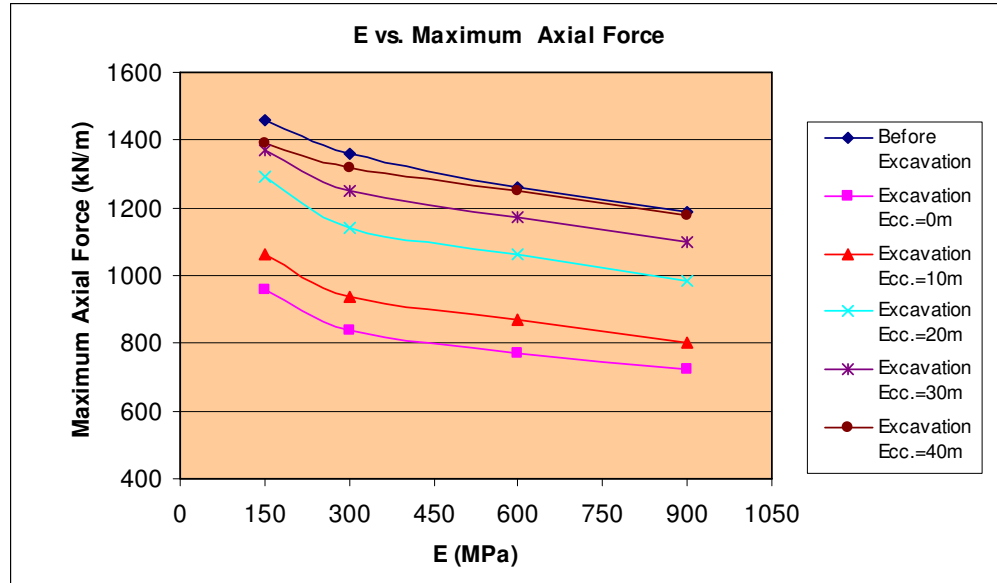


Figure 4.12 E vs. Axial Forces for Different Excavation Eccentricities

and -1390 kN/m and the changes from the initial value -1460 kN/m are 27%, 12%, 6% and 5% for $e=10\text{m}$, 20m , 30m and 40m respectively. For $E=300\text{ MPa}$, the normal forces are -935.55 kN/m, -1140 kN/m, -1250 kN/m and -1320 kN/m and the decreases from the initial value -1360 kN/m are 31%, 16%, 8% and 3% for $e=10\text{m}$, 20m , 30m and 40m , respectively. For $E=600\text{ MPa}$, the normal forces are -869.02 kN/m, -1060 kN/m, -1170 kN/m and -1250 kN/m and the changes from the initial normal force -1260 kN/m are 31%, 16%, 7% and 0.8% for $e=10\text{m}$, 20m , 30m and 40m respectively. The difference between the initial value and the value for excavation eccentricity $e=40\text{m}$ is almost zero. For $E=900\text{ MPa}$, the normal forces are -802.43 kN/m, -985.18 kN/m, -1100 kN/m and -1180 kN/m and the changes from the initial value -1190 kN/m are 33%, 17%, 8% and 0.8% for $e=10\text{m}$, 20m , 30m and 40m respectively. The effect of excavation to the normal forces diminishes when the eccentricity reach 40m . Figure 4.13 shows the normal (axial) forces for different e/B ratios. Only two extreme E values are considered.

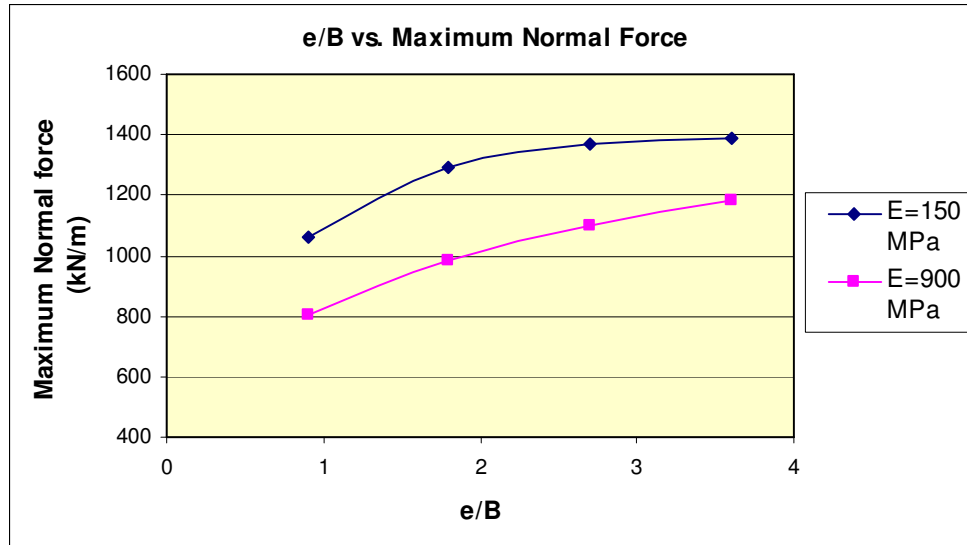


Figure 4.13 e/B vs. Normal Forces for two extreme E values

Figure 4.14 shows the bending moments after an excavation with different eccentricities. As it can be seen from the figure, the bending moments are very close to each other when the Young's Modulus is 600 MPa or 900 MPa. The bending moments before the excavation and for the case with $e=40$ m are almost identical and it can be concluded that the effects of the excavation diminishes for bending moments beyond the $e=40$ m as in the case of normal forces. The initial value of the bending moment for $E=150$ MPa is -63.83 kNm/m and the changes are for $e=10$ m, 20 m, 30 m and 40 m; 128%, 87%, 37% and 5%, respectively. The changes from the initial value -37.92 kNm/m for $E=300$ MPa are 107%, 75%, 32% and 4% for $e=10$ m, 20 m, 30 m and 40 m respectively. In Figure 4.15, the bending moments for e/B ratios and two extreme E values are given. The rate of decrease of bending moments with increasing e/B ratio is higher for soft soil.

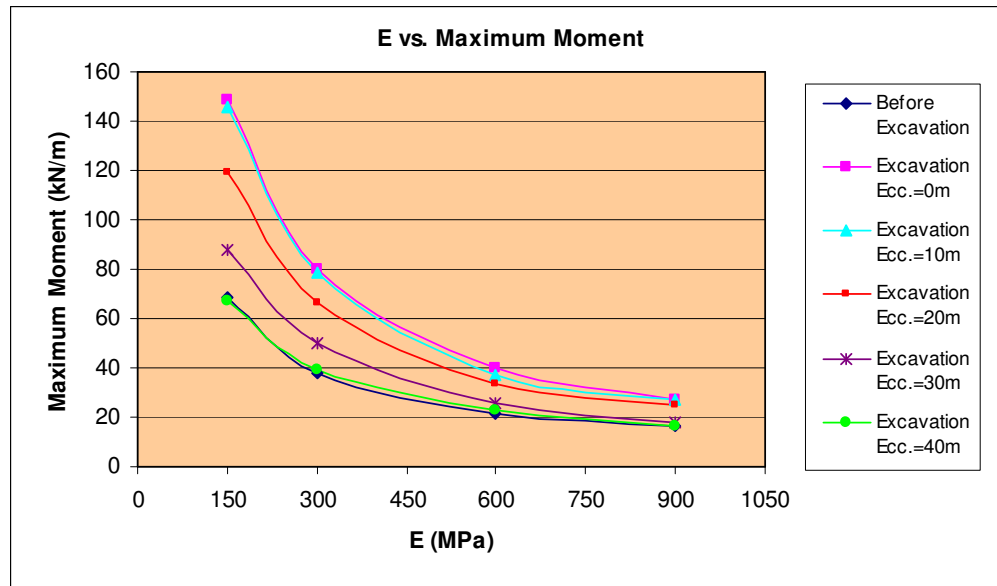


Figure 4.14 E vs. Bending Moments for Different Excavation Eccentricities

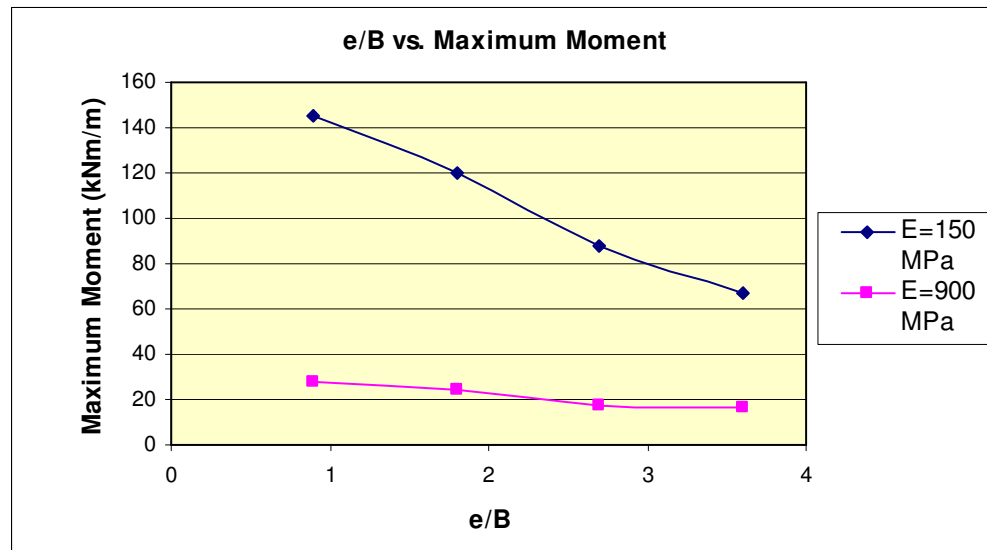


Figure 4.15 e/B vs. Moments for two extreme E values

The normal force and the bending moment couples in the mid-plane are shown in the interaction diagrams in Figure 4.16. Two extreme cases with $e/B=0.9$ and $e/B=3.6$ for $E=150$ MPa and $E=900$ MPa are illustrated. The figure shows that the risk of failure due to the surface excavation decreases with the increasing eccentricity or e/B ratio. Moreover, the stiffer the soil, the lower is the risk of exceeding the tunnel liner capacity. The only failure case is the case with $E=150$ MPa and $e/B=0.9$ Figure 4.17 illustrates the risk of failure of the tunnel lining for all e/B and E values.

The change of the shear forces in this case are interesting since the forces increase in some cases and decrease in other cases for different values of eccentricities and Young's Modulus. The increases are large in magnitude whereas the decreases are very small (Figure 4.18). The initial value, i.e. the shear force value before the excavation is -159.56 kN/m for $E=150$ MPa and the changes of this value due to the excavation are 67%, 21%, -6% and -5% (- sign indicates a decrease) for excavation eccentricities $e=10$ m, 20m, 30m and 40 m respectively. The percentage of the changes of shear forces from the initial value -96.8 kN/m for $E=300$ MPa are 61%, 17%, 4% and 5% for $e_e=10$ m, 20m, 30m and 40m respectively. The changes for $E=600$ MPa are 44%, 8%, 1% and 1% for $e=10$ m, 20m, 30m and 40m again whereas the initial value of the shear force is -58.81 kN/m. For $E=900$ MPa, the initial value is -39.72 kN/m and the changes are 42%, 9%, 4% and 2% for $e=10$ m, 20m, 30m and 40m respectively. As it can be seen from Figure 4.18, the shear forces do not change after that the excavation eccentricity e reaches 30m.

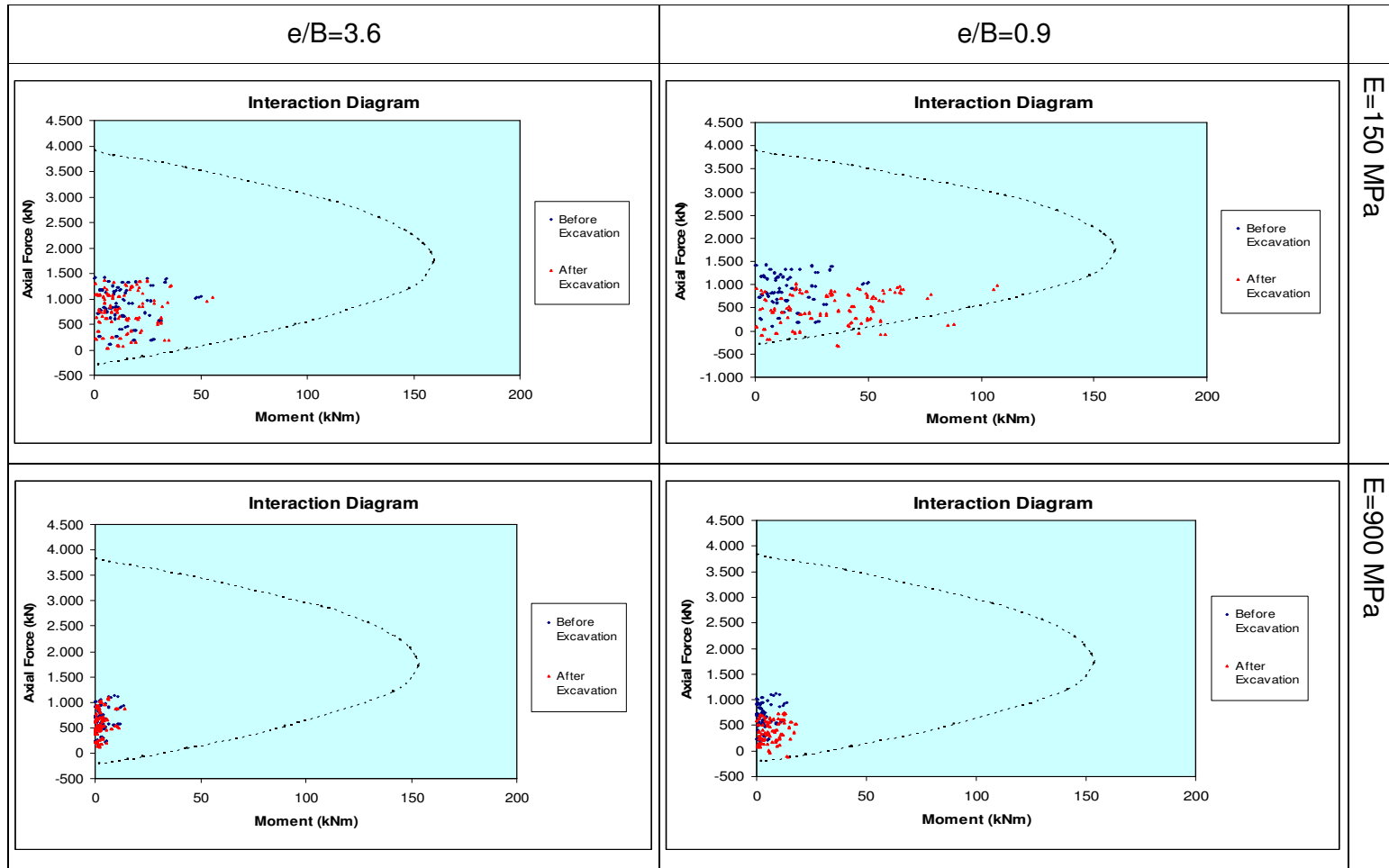


Figure 4.16 Interaction Diagrams for extreme values of e/B ratio and E



	E=150 MPa	E=300 MPa	E=600 MPa	E=900 MPa
e/B=0.9	✗	✗	✗	✓
e/B=1.8	✗	✓	✓	✓
e/B=2.7	✓	✓	✓	✓
e/B=3.6	✓	✓	✓	✓
 = The capacity of the lining not exceeded (No Failure)		 = The capacity of the lining exceeded (Failure)		

Figure 4.17 Risk of failure for different e/B ratios and E values

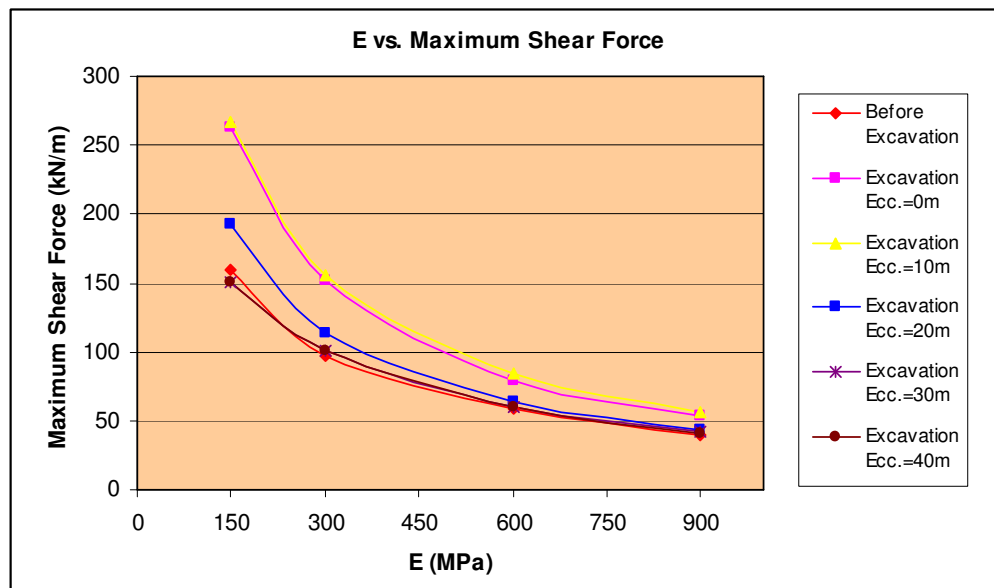


Figure 4.18 E vs. Maximum Shear Forces for Different Excavation Eccentricities

Excavation induced vertical and horizontal displacements decrease with increasing excavation eccentricity and with increasing Young's Modulus. The vertical displacements for $E=150$ MPa are 14.08mm, 10.56mm, 6.42mm and 3.57mm for $e=10$ m, 20m, 30m and 40 m respectively. When the case with $E=900$ MPa is considered, the vertical displacements are 2.84mm, 2.06mm, 1.21mm and 0.6mm for $e=10$, 20m,30m and 40 m respectively. (See Figure 4.19) Horizontal displacements are smaller than the vertical displacements as it can be seen in Table 4.2 and in Figure 4.20. For $E=150$ MPa, the horizontal displacements are 4.3mm, 3.64mm, 2.94mm and 2.36mm for $e=10$ m,20m,30m and 40m, respectively. For $E=900$ MPa horizontal displacements are 0.69mm, 0.59mm, 0.54mm and 0.43mm for $e=10$ m, 20m, 30m and 40 m respectively.

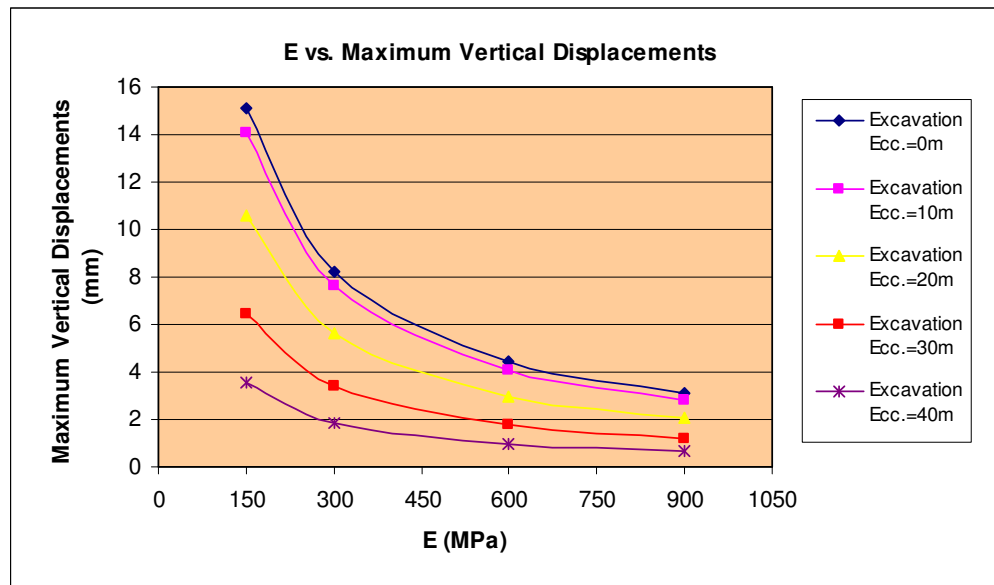


Figure 4.19 E vs. Vertical Displacements for Different Excavation Eccentricities

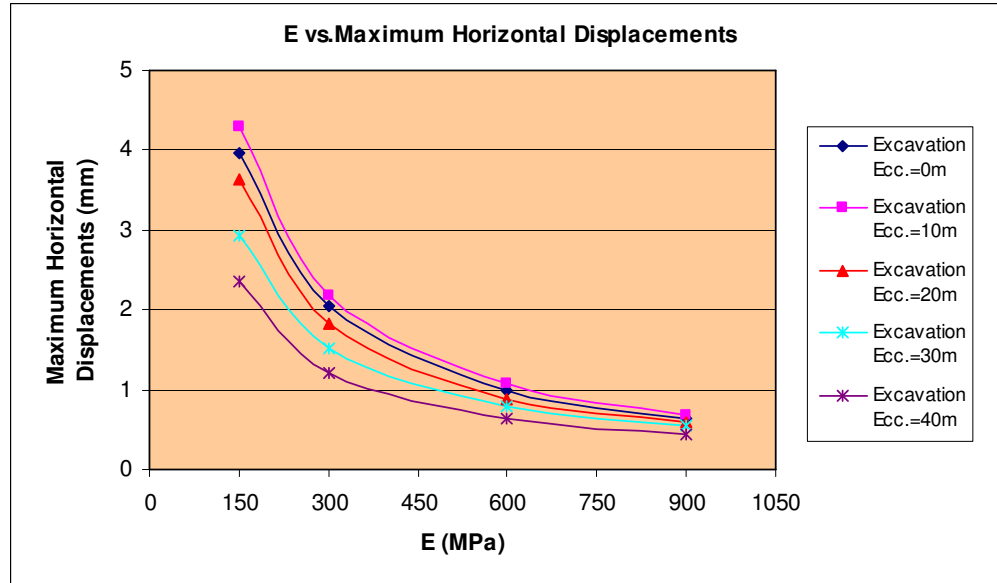


Figure 4.20 E vs. Horizontal Displacements for Different Excavation Eccentricities

The unsymmetrical excavations do not only change the magnitudes of the forces and deformations in the tunnel lining, they also change the force and deformation distribution around the tunnel lining. In Figures 4.21, 4.22, 4.23, 4.24 and 4.25, the change of the force and moment distribution around the tunnel lining for an unsymmetrical excavation with $e=20\text{m}$ and $E=600\text{ MPa}$ is given.

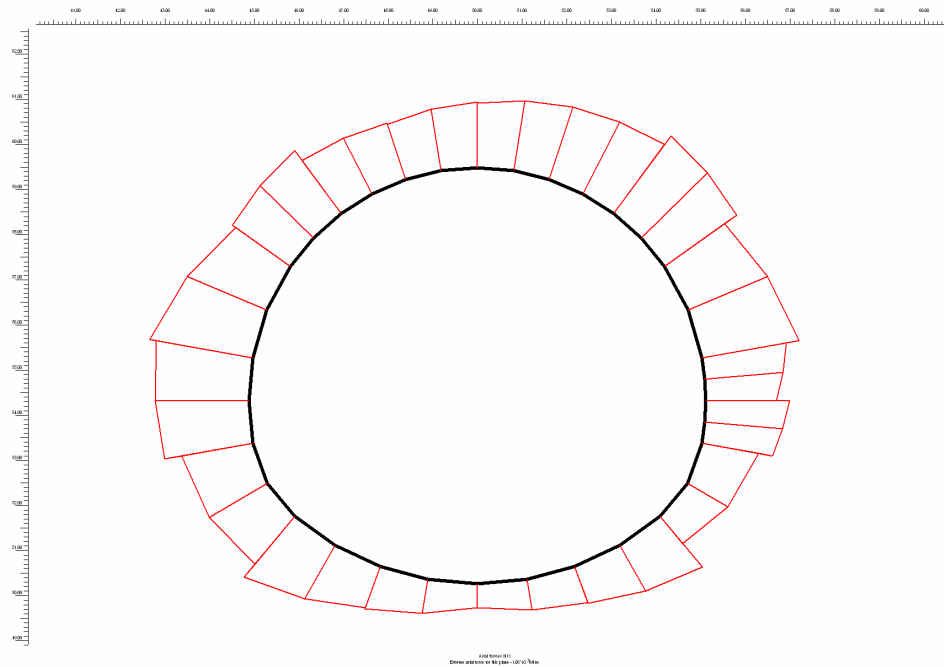


Figure 4.21 Axial force distribution in the tunnel lining for Analysis30 (e=20m, E=600 MPa)

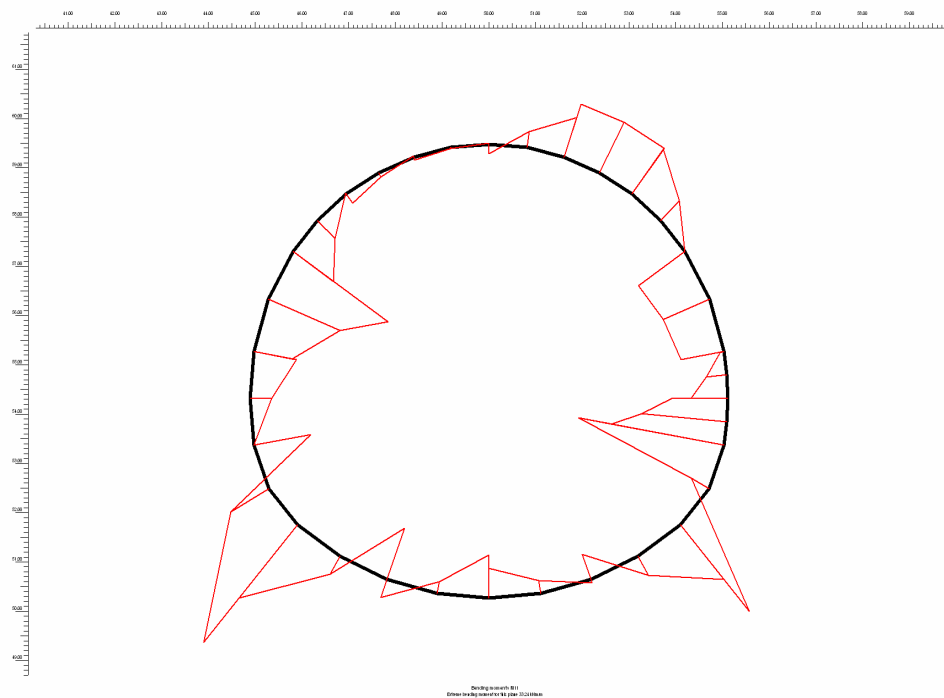


Figure 4.22 Moment distribution in the tunnel lining for Analysis30 (e=20m, E=600 MPa)

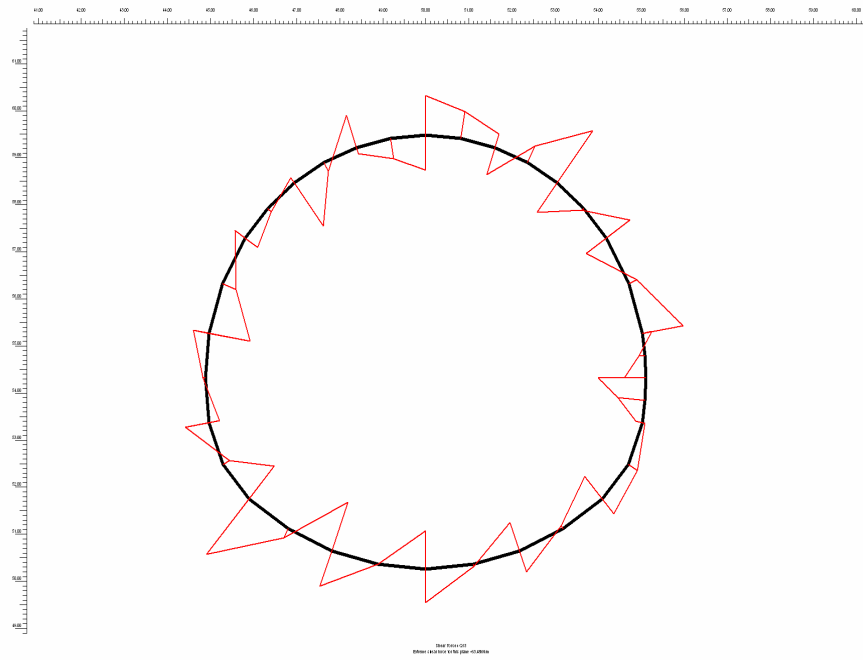


Figure 4.23 Shear Force distribution in the tunnel lining for Analysis30 (e=20m, E=600 MPa)

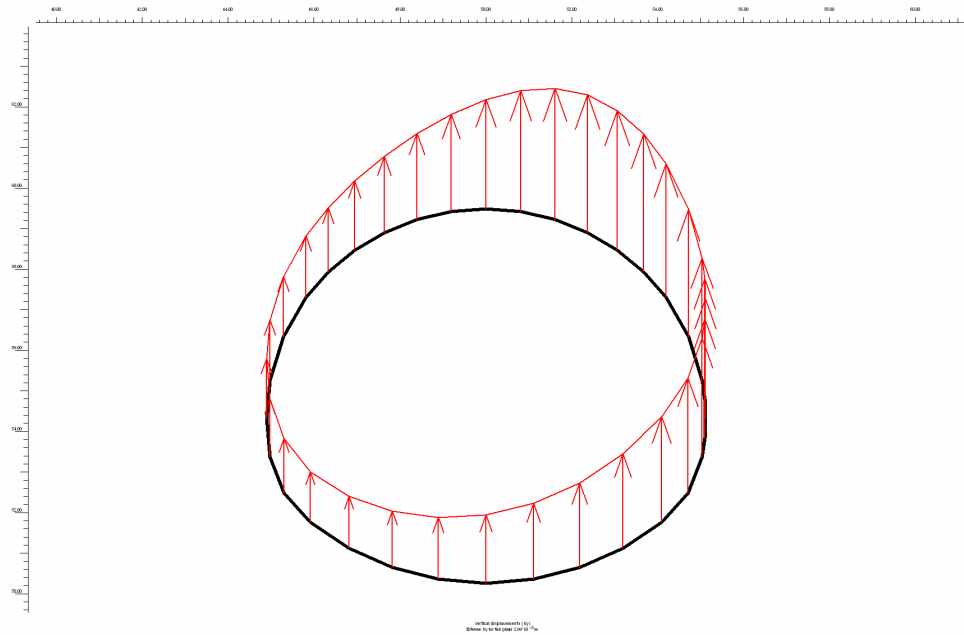


Figure 4.24 Vertical displacement distribution in the tunnel lining for Analysis30 (e=20m, E=600 MPa)

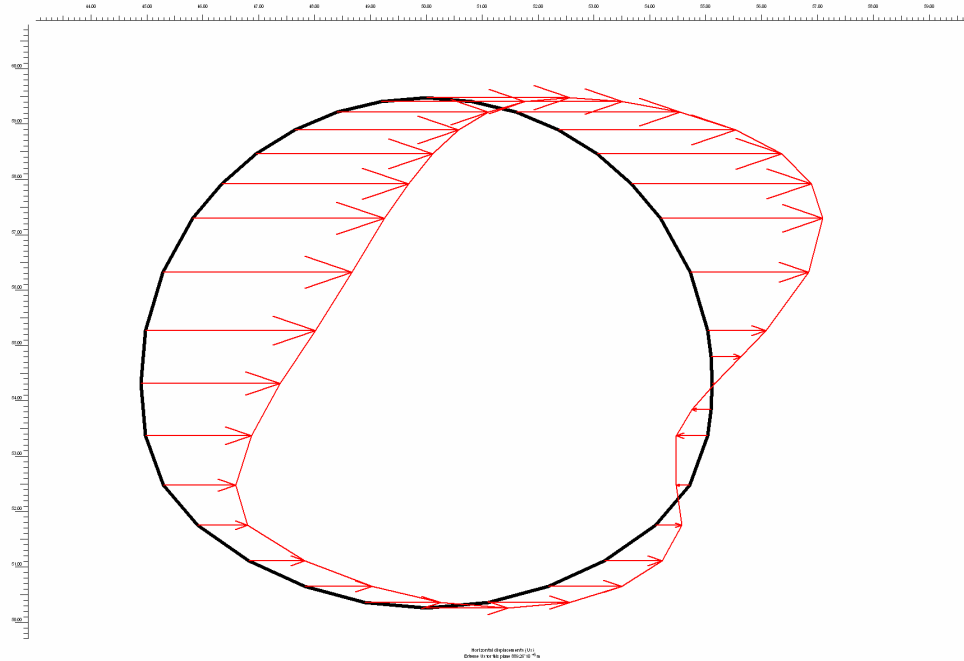


Figure 4.25 Horizontal displacement distribution of the tunnel lining for Analysis30 (e=20m, E=600 MPa)

4.4 Effect of Surface Loading to the Tunnel Lining

The result of the study in which the effects of the surface loading to the forces and deformations in the tunnel lining is investigated, is presented in this section. The height of the fill which represents the loading has been changed throughout the study. These fill heights are $h=5\text{m}$, $h=10\text{m}$ and $h=15\text{m}$. Four different E values, $E=150\text{ MPa}$, 300 MPa , 600 MPa and 900 MPa are used for each fill height, h . The results of the study are given in Table 4.3

The normal (axial) forces increase when a loading is applied in contrast to the excavation. The normal forces increase with increasing fill height and decrease with increasing Young's Modulus. The E vs. Axial Force diagram behavior is almost linear for the fill heights 5m and 10m , however the behavior for $h=15$ is different. The increase of the normal forces for $h=15\text{m}$

are identical with the ones for $h=10$ m when the Young's Modulus values 300 MPa, 600 MPa and 900 MPa are considered. On the other hand, there is a sharp increase in the normal force for $E=150$ MPa. (See Figure 4.26)

Table 4.3 Extreme forces and Displacements for the Mid-Plane

Set 3

Analysis	Normal Force (kN/m)	Bending Moment (kNm/m)	Shear Force (kN/m)	Vertical Displacement (mm)	Horizontal Displacement (mm)
Analysis 37	-1610	-40,44	-154,83	4,15	1,06
Analysis 38	-1790	-36,28	-162,38	8,32	2,13
Analysis 39	-1960	-55,93	-219,76	12,5	3,21
Analysis 40	-1530	-26,4	-100,63	2,23	0,54
Analysis 41	-1690	19,71	-104,35	4,48	1,08
Analysis 42	-1710	-20,43	106,39	4,75	1,14
Analysis 43	-1410	16,55	-59,38	1,2	0,26
Analysis 44	-1560	14,31	-61,19	2,4	0,52
Analysis 45	-1580	13,74	63,21	2,54	0,55
Analysis 46	-1330	-13,52	-39,91	0,83	0,17
Analysis 47	-1470	11,01	43,67	1,67	0,33
Analysis 48	-1480	10,62	46,34	1,77	0,35

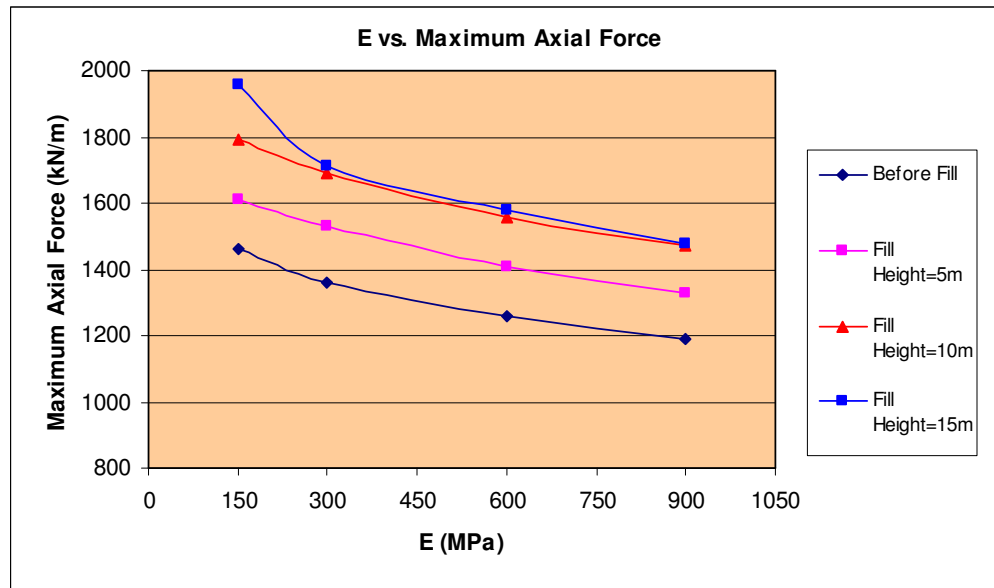


Figure 4.26 E vs. Axial Forces for Different Fill Heights

The initial value is -1460 kN/m for $E=150$ MPa and the normal forces increased with the following percentages; 10%, 23% and 34% for $h=5$ m, 10m and 15m respectively. The case for $E=300$ MPa is; 13%, 24% and 26% increases from the initial value -1360 kN/m for $h=5$ m, 10m and 15m respectively. The increases from the initial value -1260 kN/m for $E=600$ MPa are 12%, 24% and 25% and for $E=900$ MPa are 12%, 24% and 33% for $h=5$ m, 10m and 15m respectively. The h/B vs. normal force diagram (Figure 4.27) shows the change of the normal forces for different fill heights and for two extreme E values. As it can be seen in the Figure 4.27, the normal forces increase with increasing h/B ratios. For $E=900$ MPa, for ratios greater than 0.9, the magnitude of the normal force is almost constant.

The E vs. Bending Moment diagram in Figure 4.28 shows that the bending moments decrease when a loading is applied above the tunnel. The amount of decrease get larger as the fill height increases up to a level, however when the fill height is 15m, the amount of the decrease is less than the cases for $h=5$ m and $h=10$ m for $E=150$ MPa. The behavior is consistent with the variation trend of the normal forces. It can be said that for $E=150$ MPa, since the soil is relatively soft, the soil can not resist the forces due to the fill and a significant amount of the forces are exerted on the tunnel lining. The initial value of bending moment for $E=150$ MPa is -63.83 kNm/m and it decreases with the following percentages; 37%, 43% and 12% for $h=5$ m, 10m and 15m. The decreases from the initial value -37.92 kNm/m of bending moment for $E=300$ MPa are 30%, 46% and 49% for $h=5$ m, 10m and 15m respectively. The initial value for $E=600$ MPa is -21.29 kNm/m and the decreases as percentage are; 22%, 33% and 35% for $h=5$ m, 10m and 15 m respectively. The decreases for $E=900$ MPa are 17%, 32% and 35% where the initial value is 16.27kNm/m. Figure 4.29 shows the e/B vs. moment diagram. The change of the moments with increasing h/B ratios is different for soft soil and for stiff soil. The moments decrease with increasing h/B ratio in stiff soil, however for soft soil, the moments decrease up to $h/B=0.9$ and for greater values of h/B , they increase.

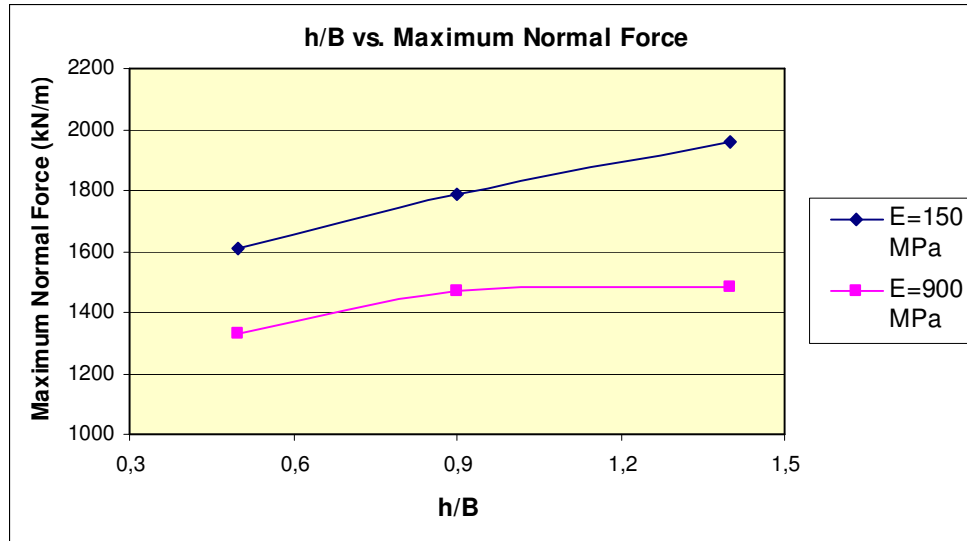


Figure 4.27 h/B vs. Normal Forces for two extreme E values

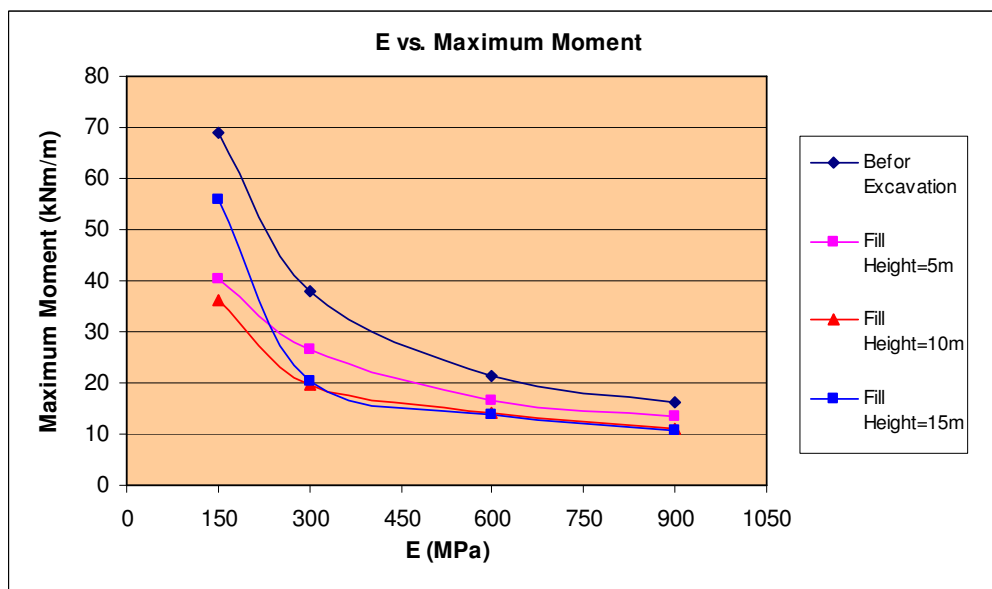


Figure 4.28 E vs. Bending Moments for Different Fill Heights

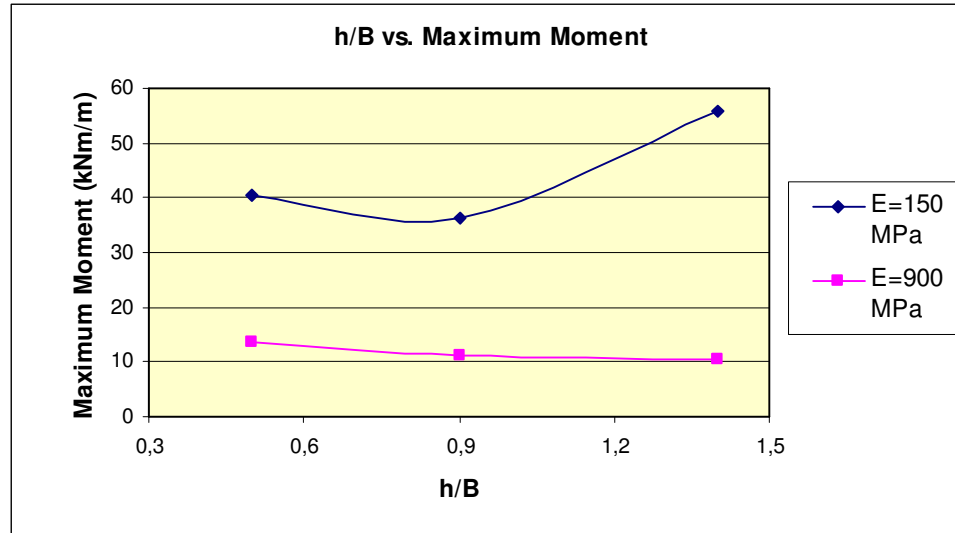


Figure 4.29 h/B vs. Moments for two extreme E values

The normal force and the bending moment couples in the mid-plane are shown in the interaction diagrams in Figure 4.30. Two extreme cases with $h/B=0,5$ and $h/B=1,4$ for $E=150$ MPa and $E=900$ MPa are illustrated. In the figure, it can be seen that the normal force and moment couples move to a safer area in the interaction diagram after the loading is applied. This is due to the increase in the moments and the decrease in the moments. The capacity of the lining is not exceeded within the limits of the fill heights considered in this study.

In Figure 4.31, all loading cases are presented in terms of the risk of the failure. The figure shows that there is not a failure risk for the loading cases.

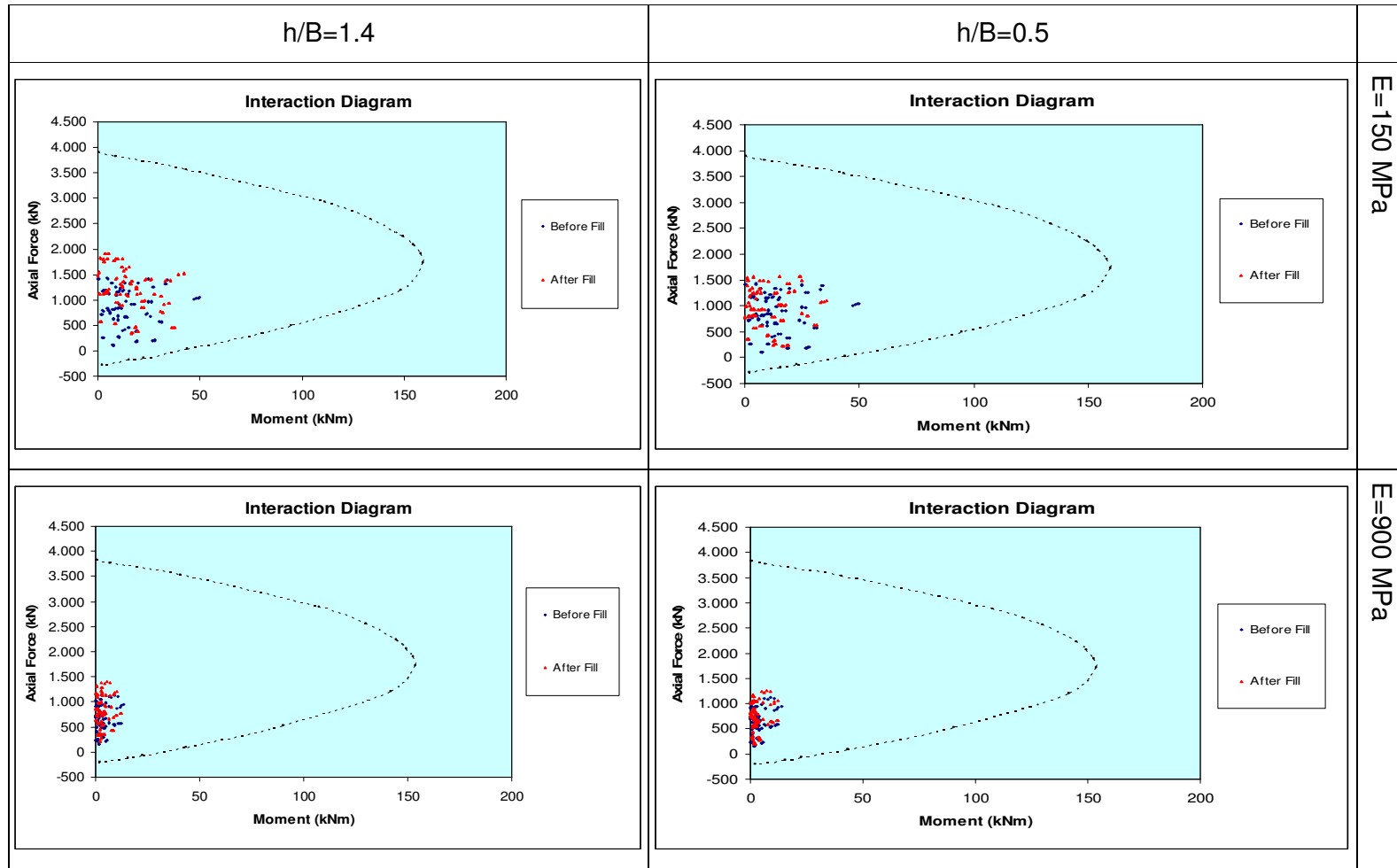


Figure 4.30 Interaction Diagrams for extreme values of h/B ratio and E



	E=150 MPa	E=300 MPa	E=600 MPa	E=900 MPa
h/B=0.5	✓	✓	✓	✓
h/B=0.9	✓	✓	✓	✓
h/B=1.4	✓	✓	✓	✓
 = The capacity of the lining not exceeded (No Failure)		 = The capacity of the lining exceeded (Failure)		

Figure 4.31 Risk of failure for different e/B ratios and E values

The shear forces are not greatly affected from the loading with different heights. Figure 4.32 shows that the E vs. Shear Force Diagram behavior is almost the same for all fill heights h. The only change occurs by fill height h=15 m and E=150 MPa. The initial value of the shear force for E=150 MPa is -159.56 kN/m and it increases to a value -219.76 kN/m, i.e. a 38% increase. Since the shear forces for other E values and fill heights do not vary actually, they will be only presented in Table 4.3 and not discussed in detail.

Vertical and horizontal displacements are very similar in the way that they vary. When the Figures 4.33 and 4.34 are compared it can be seen that the shape of the diagrams are not different from each other, the only difference is the magnitude of the displacements. The vertical and horizontal displacements increase with increasing fill height and decrease with increasing Young's Modulus. The displacements are similar for the fill heights 10m and 15m for E values greater than 300 MPa. The vertical displacements are 4.15mm, 8.32mm, 12.5mm for E=150 MPa; 2.23mm, 4.48mm, 4.75 mm for E=300 MPa; 1.2mm, 2.4mm, 2.54mm for E=600 MPa and 0.83mm, 1.67mm, 1.77 mm for E=900 MPa for fill height h=5m, 10m and 15m respectively.

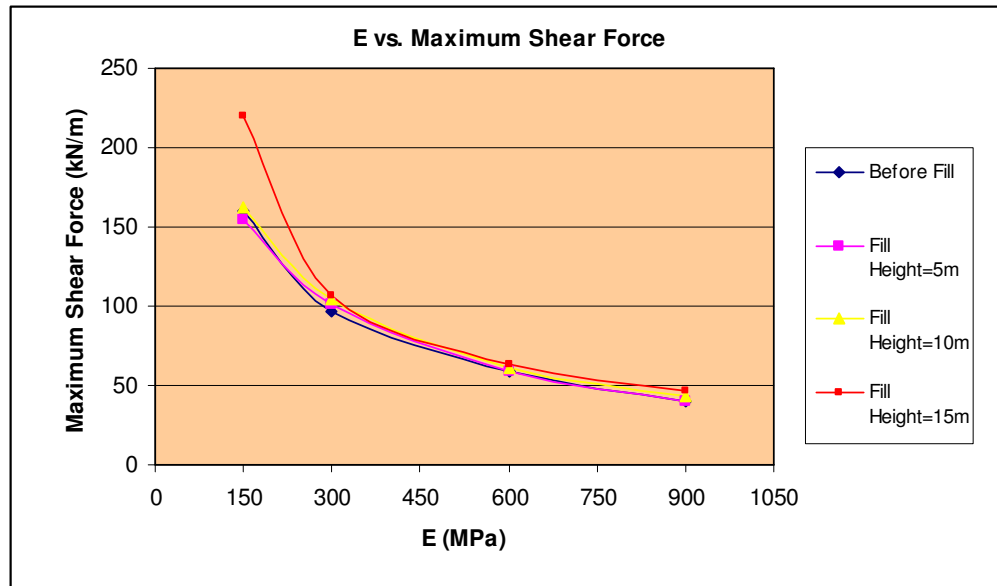


Figure 4.32 E vs. Maximum Shear Forces for Different Fill Heights

The horizontal displacements are 1.06mm, 2.13mm, 3.21mm for $E=150$ MPa; 0.54mm, 1.08mm, 1.14 mm for $E=300$ MPa; 0.26mm, 0.52mm, 0.55mm for $E=600$ MPa and 0.17mm, 0.33mm, 0.35 mm for $E=900$ MPa for fill height $h=5$ m, 10m and 15m respectively.

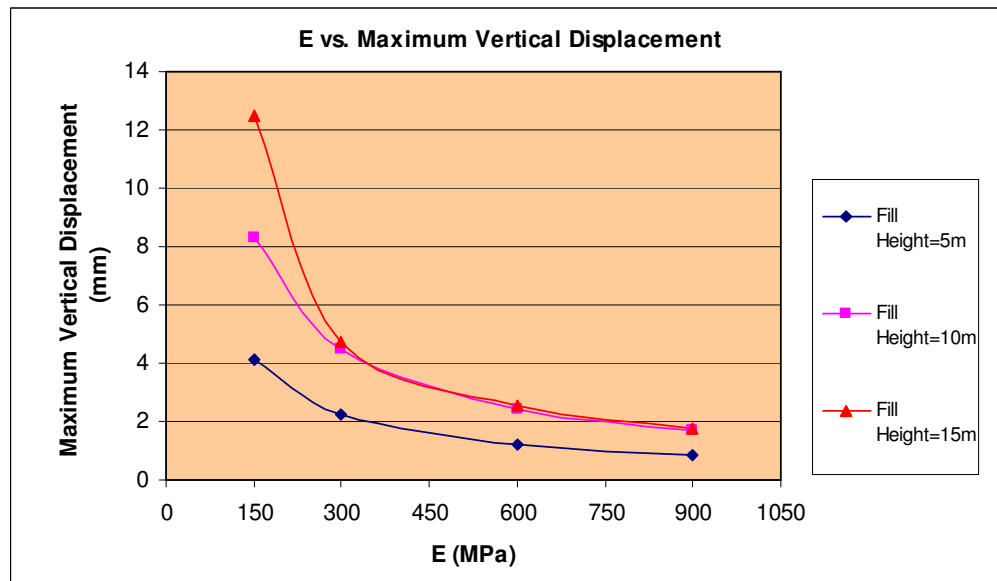


Figure 4.33 E vs. Vertical Displacements for Different Fill Heights

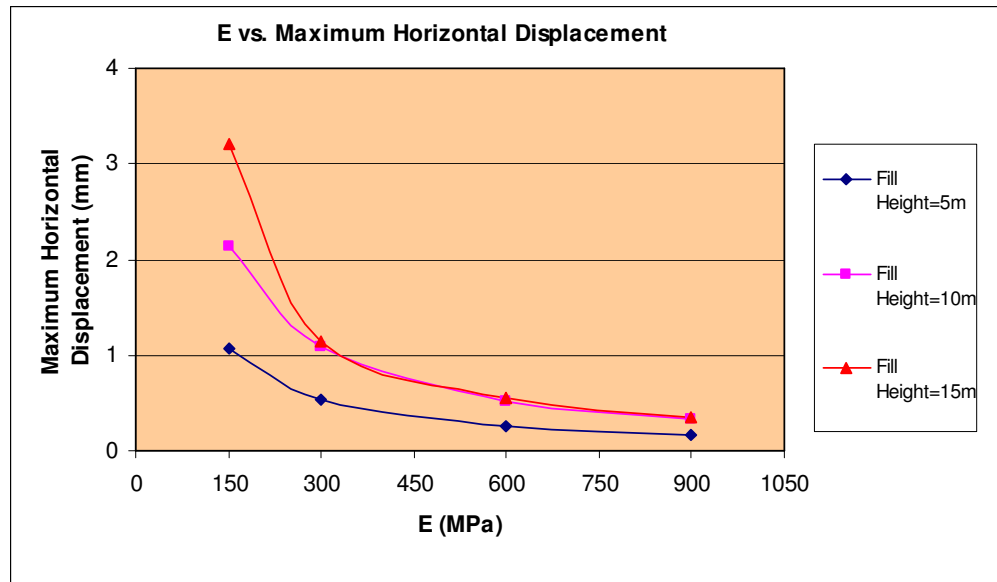


Figure 4.34 E vs. Horizontal Displacements for Different Fill Heights

CHAPTER 5

CONCLUSION

The influences of surface excavation and loading on existing tunnels have been investigated using the Plaxis 3D Tunnel program. A parametric study has been carried out where the parameters were the depth of the excavation, height of the embankment fill and the stiffness of the hosting medium. The followings are concluded.

- It is found that the force couples and the deformations differ significantly in staged construction model and in one-phase construction model. Therefore it is necessary to take into account the construction stages in the design of tunnels.
- The stresses and deformations are found to be dependent on the soil stiffness. It is found that higher magnitudes of normal forces and bending moments are exerted on tunnel lining in soils with lower magnitudes of deformation modulus as compared to stiffer soils.
- It has been shown that excavations over the tunnels have a negative effect on tunnel lining. This is due to the reduction of the normal forces and increase in the bending moments as a result of unloading due to the excavation.
- It is demonstrated that for softer soils ($E=150$ MPa) the capacity of the tunnel lining is exceeded for all values of excavation depth considered in this study. In case of stiffer soil ($E=900$ MPa), the critical excavation depth where the tunnel lining capacity is exceeded, is about $H/B < 0.7$ for the geometry and material properties in this study.

- It has been found that the increasing eccentricity has a positive effect on the tunnel lining capacity compared with the excavation with $e/B=0$. The critical eccentricity for soft soil ($E=150$ MPa) where the tunnel lining capacity is exceeded is about $e/B<1.8$ and for stiffer soil ($E=900$ MPa), none of the e/B values considered in this study is critical in terms of the tunnel lining capacity.
- It can be concluded that if the excavation axis moves away from the tunnel axis ($e/B \neq 0$), the stability of the tunnel becomes less critical as compared to the symmetrical excavation ($e/B=0$) over the tunnel. This is due to the fact that as the excavation moves away from the tunnel, unloading effects are less and therefore the reduction in the normal forces is less.
- It is found that a surcharge loading within the limits considered in this study ($h=5\text{m}-15\text{m}$) is not critical in terms of tunnel stability due to the increase in normal forces and decrease in moments as a result of surface loading.

REFERENCES

Abdel-Meguid, M., Rowe R.K., Lo K.Y., *3D Effects of Surface Construction over Existing Subway Tunnels*, The International Journal of Geomechanics, 2002, Vol. 2 Number 4, pp. 447-469

Barton N., Lien R., Lunde J., *Engineering Classification of Rock Masses for the Design of Tunnel Supports*, Rock Mechanics 6, Springer Verlag, 1974, pp. 48

Bieniawski Z.T., *Geomechanics Classification of Rock Masses and its Application in Tunneling*. Proceedings, 3rd International Conference on Rock Mechanics, Denver, 1974, Vol. IIA, pp. 27-32

Bobet A., *Analytical Solutions for Shallow Tunnels in saturated ground*, Journal of Engineering Mechanics, 2001, Vol. 127, No. 12, pp. 1258-1266

Britto A.M., Gunn M.J., *Critical State Soil Mechanics via Finite Elements*, 1987, Ellis Horwood Limited, West Sussex, pp. 36-44

Dolezalova M., *Tunnel Complex Unloaded by a Deep Excavation*, Computers and Geotechnics, 2001, Vol. 28, pp. 469-493

Farias M.M., Junior A.H.M., Assis A.P., *Displacement control in tunnels excavated by the NATM: 3-D numerical simulations*, Tunneling and Underground Space Technology, 2004, Vol. 19, pp. 283-293.

Franzius J.N., Potts D.M., *Influence of mesh geometry on three dimensional finite-element analysis of tunnel excavation*, International Journal of Geomechanics, 2005, Vol. 5, pp. 256-266

Galli G., Grimaldi A., Leonardi A., *Three-dimensional modelling of tunnel excavation and lining*, Computer and Geotechnics, 2004, Vol. 31, pp. 171-183.

Gioda G., Swoboda G., *Developments and applications of the numerical analysis of tunnels in continuous media*, International Journal for Numerical and Analytical Methods in Geomechanics, 1999, Vol. 23, pp. 1393-1405.

Gnilsen R., *Underground Structures Design and Instrumentation* (ed. Sinha R.S.), 1989, Elsevier, Amsterdam, pp. 84-128

ICE Design and Practice Guides, *Sprayed Concrete Linings (NATM) for Tunnels in Soft Ground*, 1996, Thomas Telford, pp.3-42

Jing L., Hudson J.A., *Numerical methods in rock mechanics*, International Journal of Rock Mechanics & Mining Sciences, 2002, Vol. 39, pp. 409-427.

Kolymbas D., *A Rational Approach to Tunneling*, 2005, Elsevier, Amsterdam, pp. 56-67

Loganathan N., Poulos H.G., *Analytical prediction for tunneling-induced ground movement in clays*, Journal of Geotechnical and Geoenvironmental Engineering, 1998, Vol. 124, pp. 846-856.

Main D., Herle I., *Numerical analysis of a tunnel in London clay using different constitutive models*, International Journal for Numerical and Analytical Methods in Geomechanics, 1995, Vol. 17, pp. 149-165

Mair R.J., Taylor R.N., Bracegirdle A., *Subsurface settlement profiles above tunnels in clays*, Géotechnique, 1993, Vol. 43, pp. 315-320.

McCusker T.G., *Underground Structures Design and Construction* (ed. Sinha R.S.), 1989, Elsevier, Amsterdam, pp. 403-415

Megaw T.M., Bartlett V., *Tunnels: Planning, Design, Construction*, 1981, Volume1, Ellis Horwood Limited, West Sussex, pp.11-18

Nakai T., Xu L., Yamazaki H., *3D and 2D model tests and numerical analyses of settlements and earth pressures due to tunnel excavation*, Soils and Foundations, 1997, Vol. 37, pp. 31-42.

Nam S.W., Bobet A., *Liner stresses in deep tunnels below the water table*, Tunneling and Underground Space Technology, 2005 Volume.21, pp.626-635

Oreste P. P., Peila D., Pama A., *Numerical study of low depth tunnel behavior*, World Tunnel Congress, Challenges for the 21st Century, 1999, Balkema, Oslo, pp.155-162

Peck R.B., *Deep excavations and tunneling in soft ground*, Proc. 7th Int. Conf. Soil Mech., Mexico, State of the art 3, 1969, pp.225-290

Plaxis 3D Tunnel *User's Manual*, 2004, Delft, Delft University of Technology&PLAXIS B.V.

Plaxis 3D Tunnel *Reference Manual*, 2001, Delft, Delft University of Technology&PLAXIS B.V

Potts D.M., Addenbrooke T.I., (revised by Mair & Taylor), *The influence of an existing surface structure on the ground movements due to tunneling*, Geotechnical Aspects of Underground Construction in Soft Ground, 1996, Vol. 22, pp. 78-93

Potts D.M., Zdravkovic L., *Finite element analysis in geotechnical engineering-theory*, 2001, Thomas Telford, London, pp.135-167

Roscoe K.H., Burland J.B., *On the generalized stress-strain behavior of wet clay*, Engineering Plasticity, Cambridge University Press, 1968

Roscoe K.H., Schofield A.N., *Mechanical Behavior of an idealized wet clay*, Proc. 2nd European Conf. Soil Mech., 1963, pp.47-54

Schmidt B., *Settlements and ground movements associated with tunneling in soil*, PhD thesis, 1969, University of Illinois

Schwartz C. H., Einstein H.H., *Improved Design of Tunnel Supports, Simplified Analysis for Ground Structure Interaction in Tunneling.*, Report No. UMTA-MA-06-0100-80-4. U.S. Department of Transportation, Urban Mass Transportation Administration, 1980, Vol.1, pp.427

Sinha R.S., *Underground Structures Design and Instrumentation* (ed. Sinha R.S.), 1989, Elsevier, Amsterdam, pp. 17-19

Terzaghi K., *In Rock Tunneling with steel supports*, Proctor, R.V. and White T.L., *Commercial Shearing*, 1946, Ohio, pp.278

Verruijt A., Booker J.R., *Surface settlements due to deformation of a tunnel in an elastic half plane*, Geotechnique, 1996, Vol.46, No.4, pp-753-756

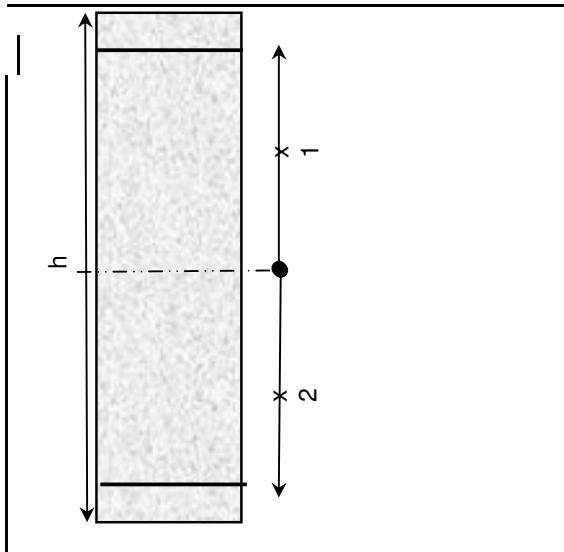
Verruijt A. *A complex variable solution for a deforming circular tunnel in elastic half-plane*, International Journal for Numerical and Analytical Methods in Geomechanics, 1997, Vol. 21, pp. 77-89

APPENDIX A

TUNNEL LINING CAPACITY CALCULATION SAMPLE

Section dimensions
h=30cm w=100 cm

Material		Properties
$f_{cd} = 17000 \text{ kPa}$	Econcrete = 30250000 kPa	$\epsilon_{concrete} = 0.003$
$f_{yd} = 435000 \text{ kPa}$	Esteel = 200000000 kPa	$\epsilon_{steel,y} = 0.002175$



$$A_{S1} = 4 \text{ cm}^2 \times 1 = 10$$

$$A_{S2} = 4 \text{ cm}^2 \times 2 = -10$$

APPENDIX B

INTERACTION DIAGRAMS

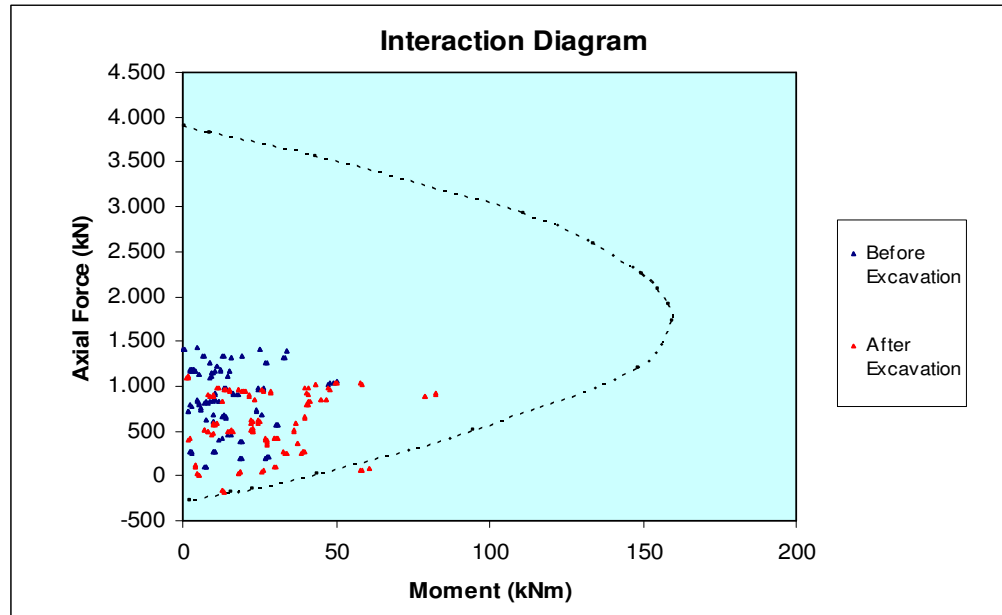


Figure A.1 Interaction Diagram for Analysis2 ($E=150$ MPa, $d=6$ m, $H/B=1.3$, $e=0$ m)

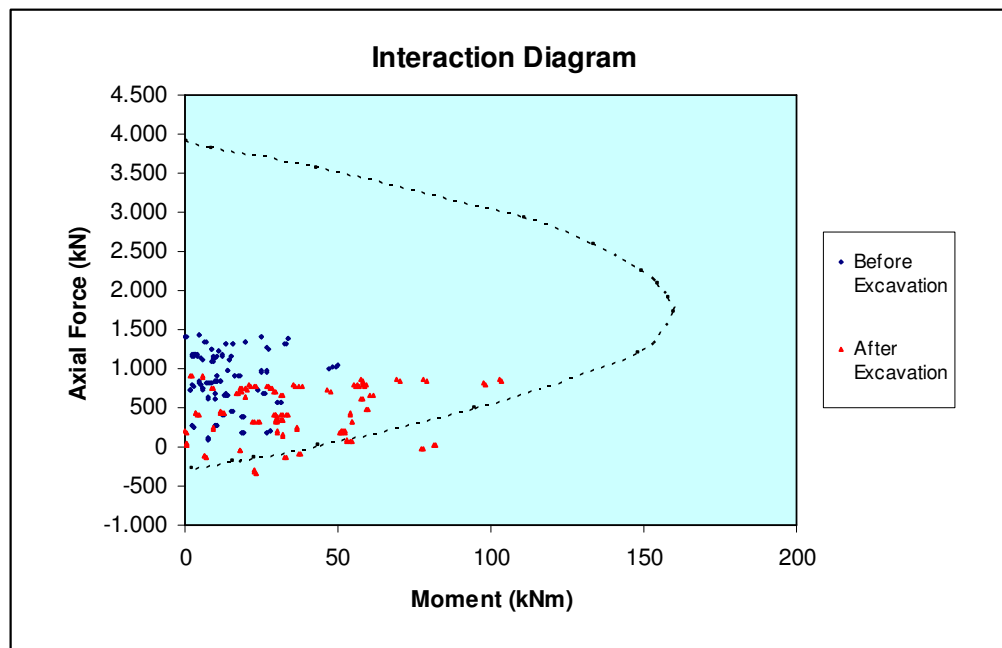


Figure A.2 Interaction Diagram for Analysis3 ($E=150$ MPa, $d=9$ m, $H/B=1.0$, $e=0$ m)

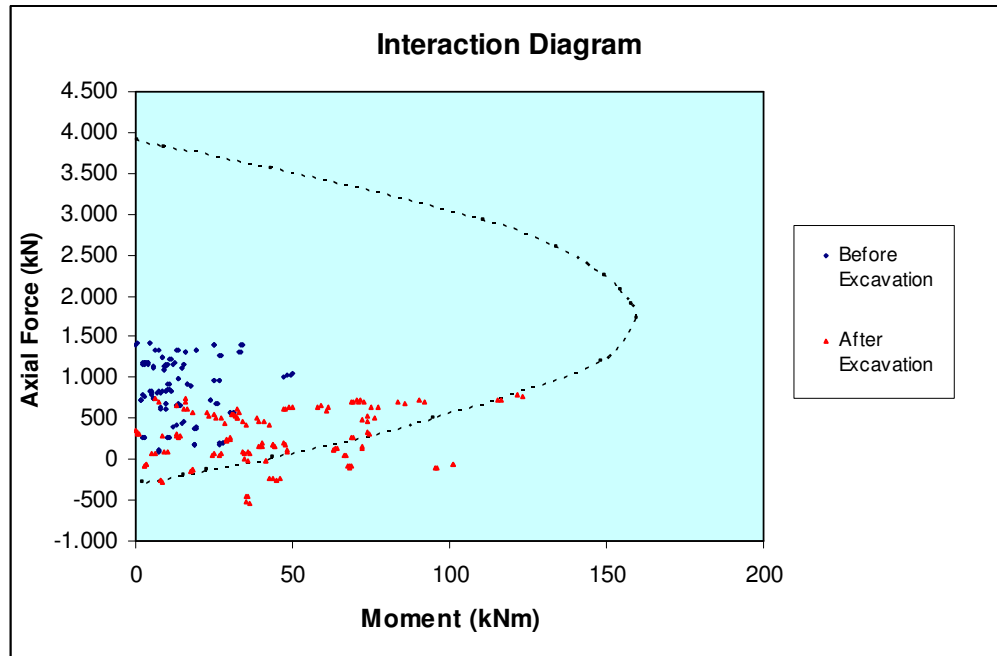


Figure A.3 Interaction Diagram for Analysis4 ($E=150$ MPa, $d=12$ m, $H/B=0.7$, $e=0$ m)

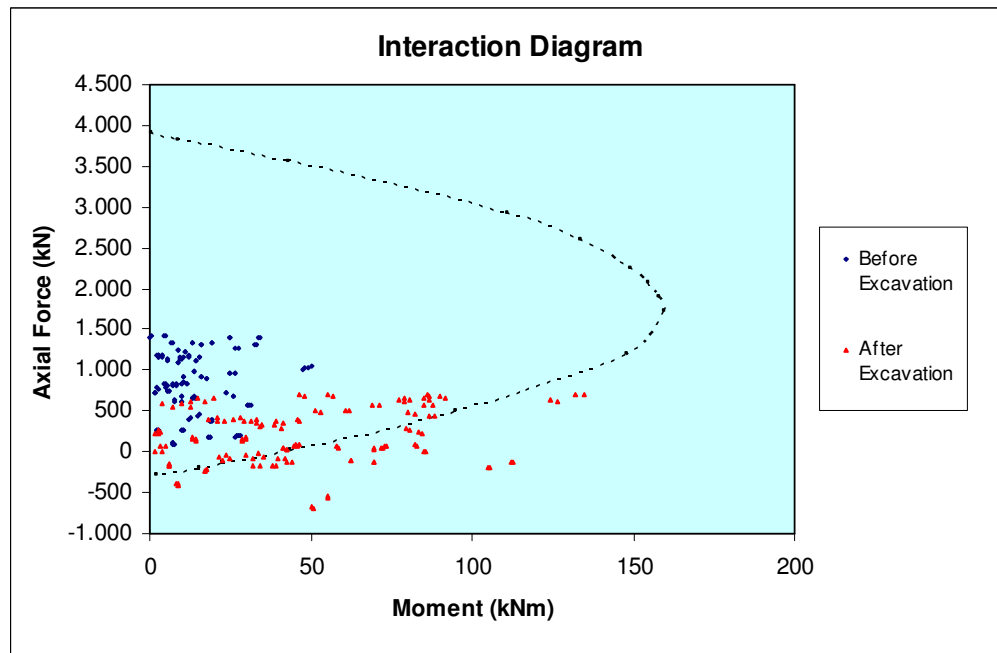


Figure A.4 Interaction Diagram for Analysis5 ($E=150$ MPa, $d=15$ m, $H/B=0.5$, $e=0$ m)

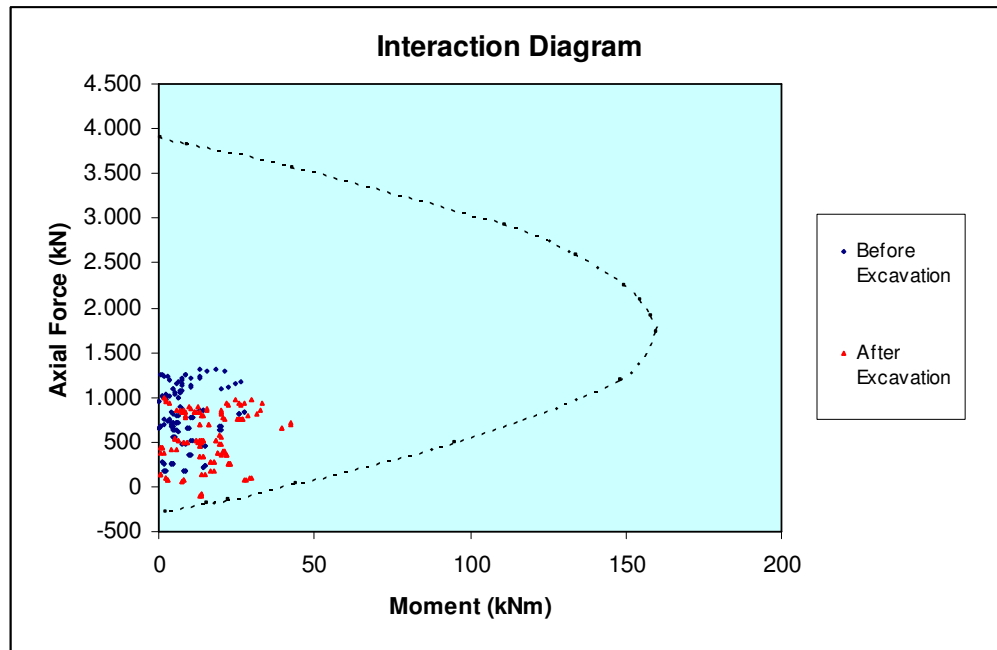


Figure A.5 Interaction Diagram for Analysis7 ($E=300$ MPa, $d=6$ m, $H/B=1.3$, $e=0$ m)

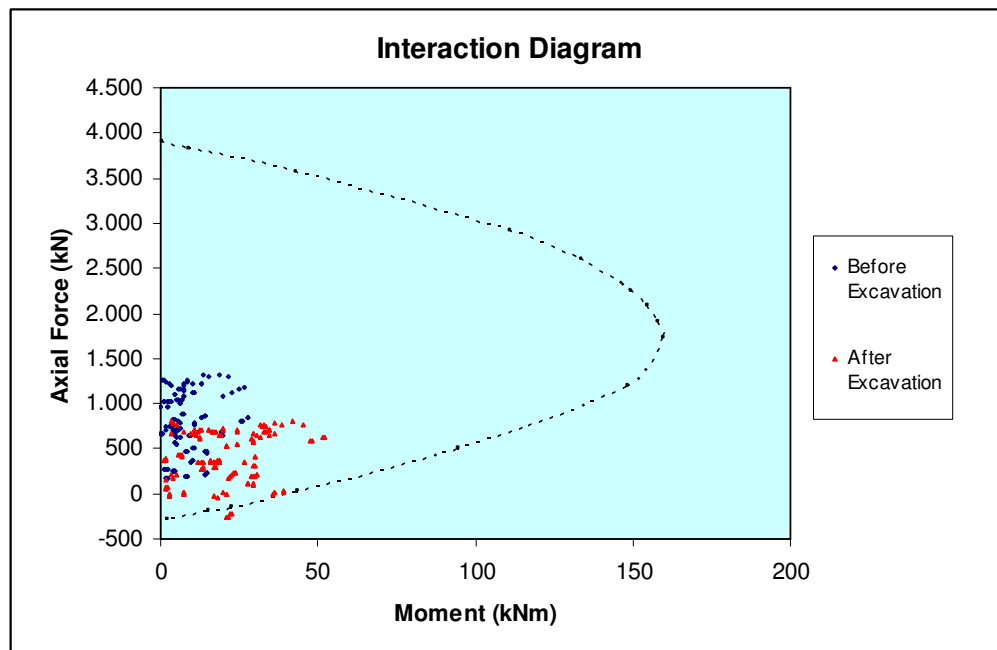


Figure A.6 Interaction Diagram for Analysis8 ($E=300$ MPa, $d=9$ m, $H/B=1.0$, $e=0$ m)

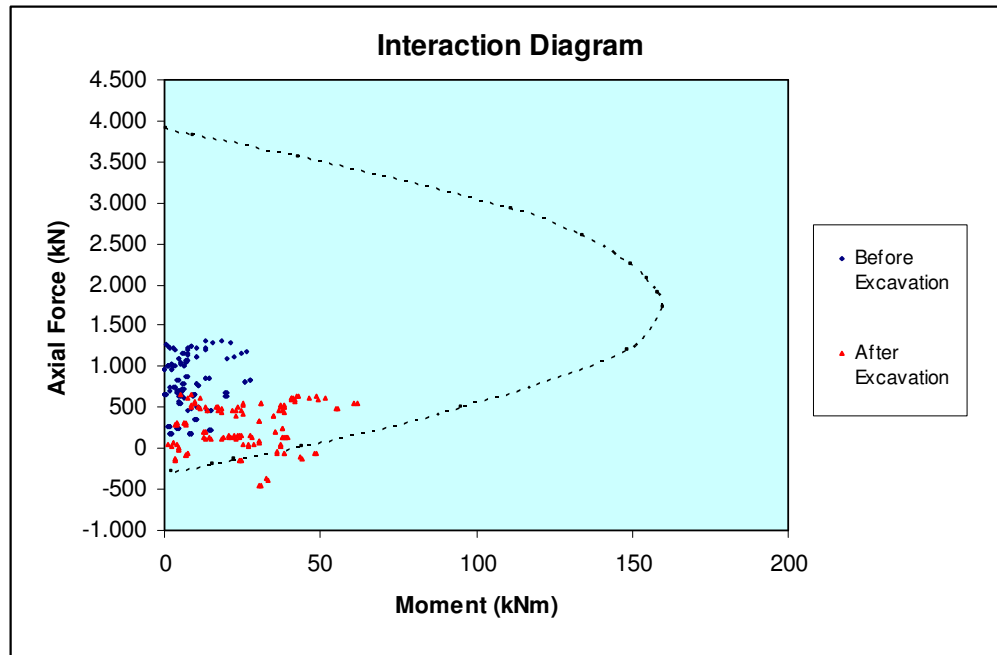


Figure A.7 Interaction Diagram for Analysis9 ($E=300$ MPa, $d=12$ m, $H/B=0.7$, $e=0$ m)

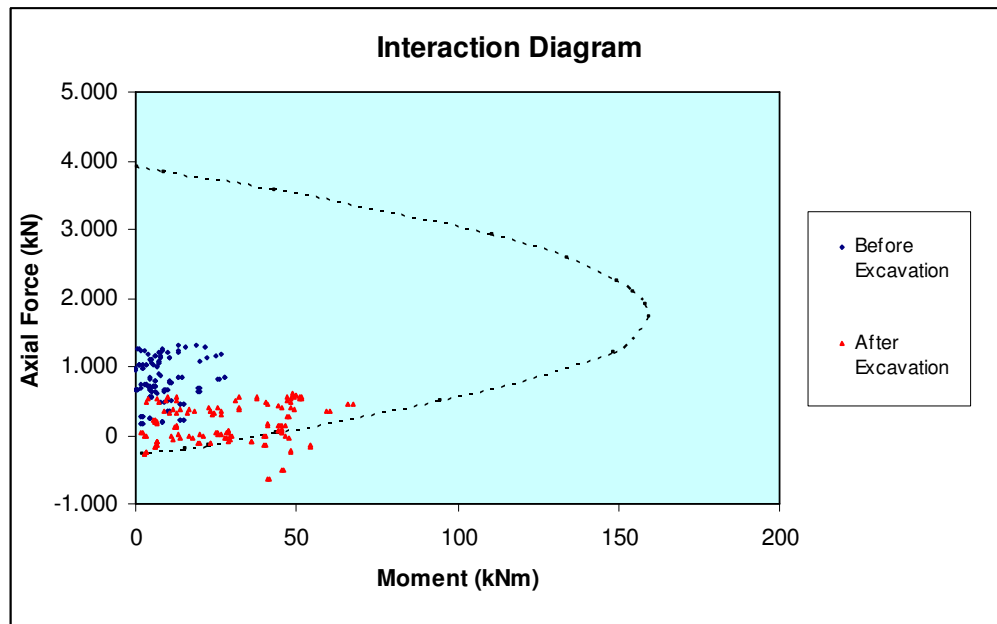


Figure A.8 Interaction Diagram for Analysis10 ($E=300$ MPa, $d=15$ m, $H/B=0.5$, $e=0$ m)

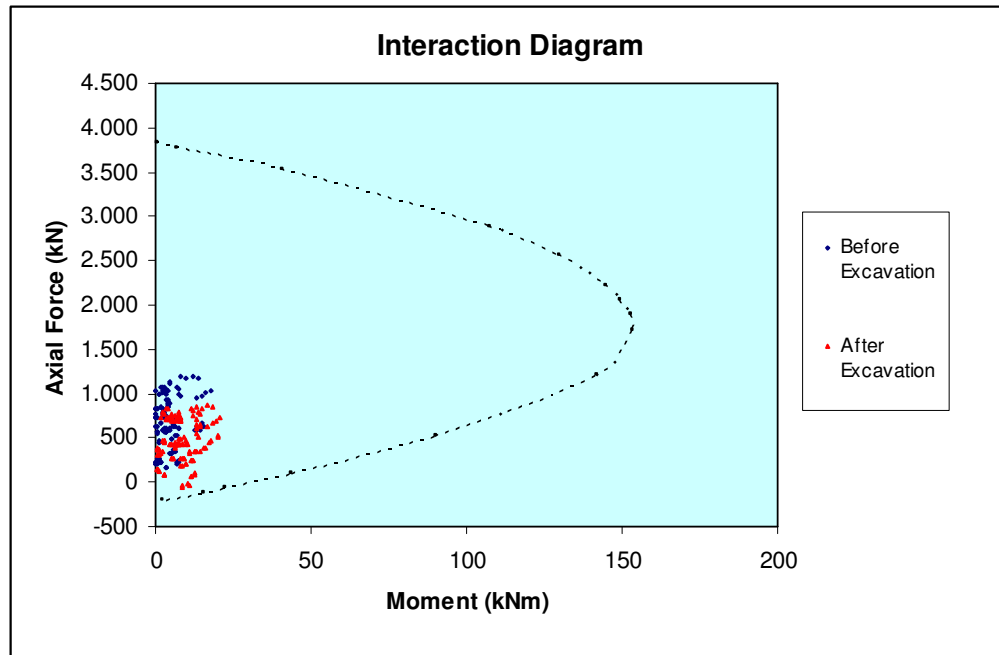


Figure A.9 Interaction Diagram for Analysis12 ($E=600$ MPa, $d=6$ m, $H/B=1.3$, $e=0$ m)

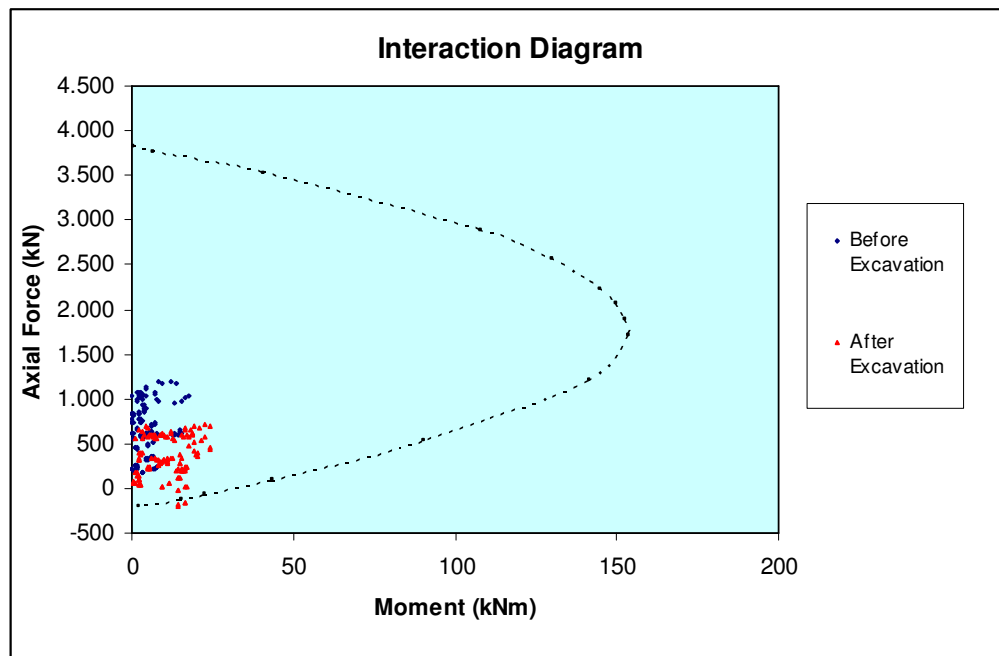


Figure A.10 Interaction Diagram for Analysis13 ($E=600$ MPa, $d=9$ m, $H/B=1.0$, $e=0$ m)

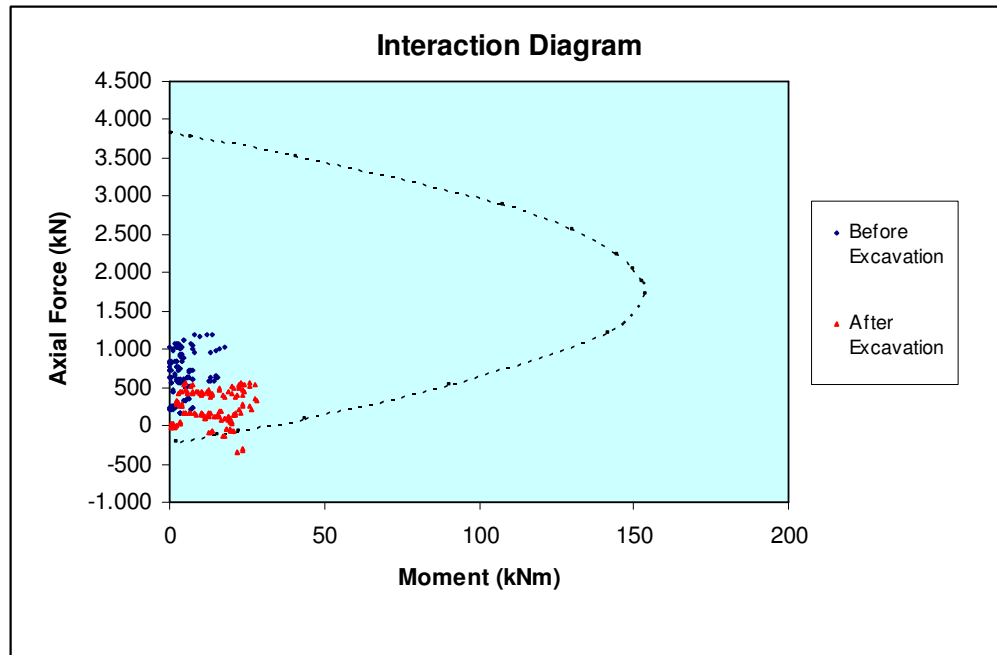


Figure A.11 Interaction Diagram for Analysis14 ($E=600$ MPa, $d=12$ m, $H/B=0.7e=0$ m)

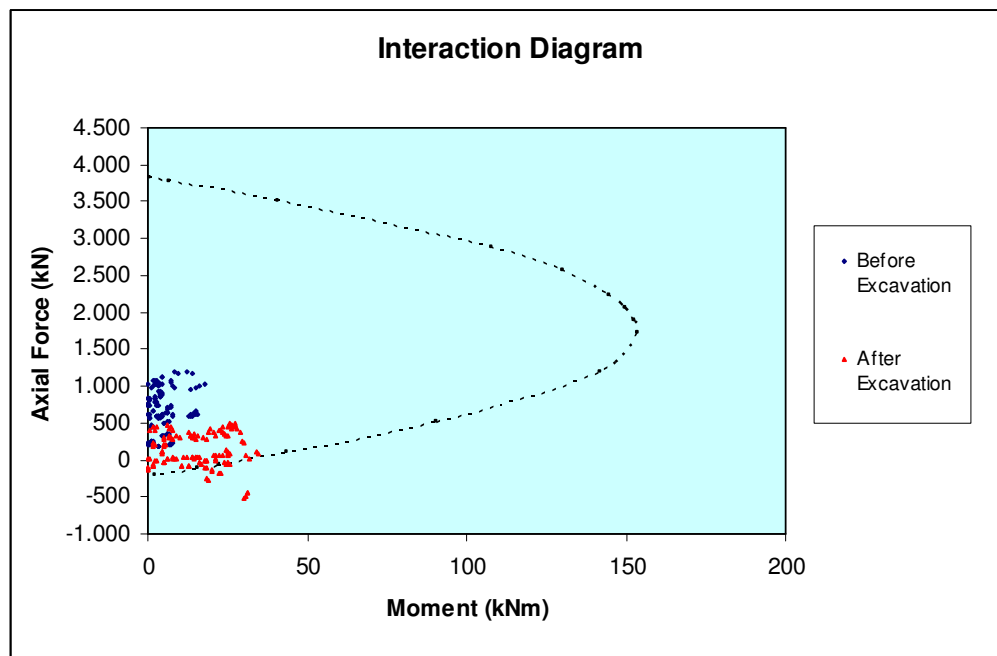


Figure A.12 Interaction Diagram for Analysis15 ($E=600$ MPa, $d=15$ m, $H/B=0.5$, $e=0$ m)

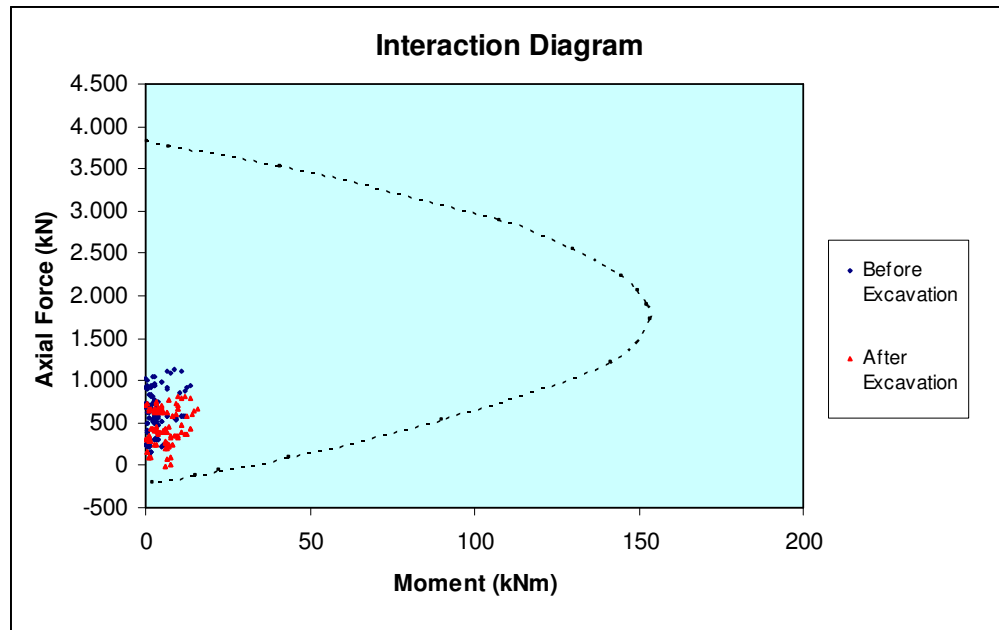


Figure A.13 Interaction Diagram for Analysis17 ($E=900$ MPa, $d=6$ m, $H/B=1.3$, $e=0$ m)

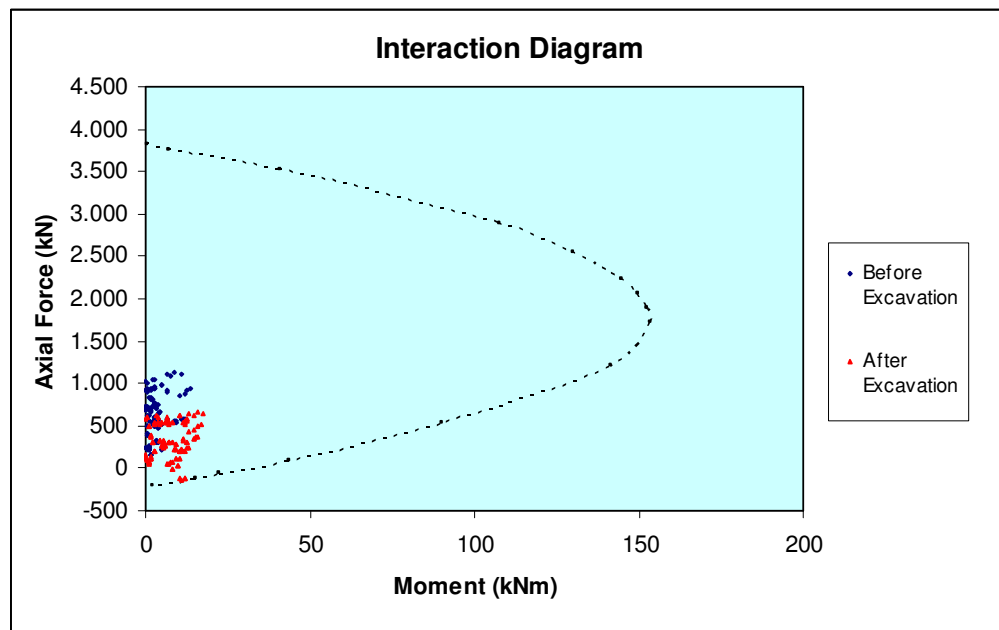


Figure A.14 Interaction Diagram for Analysis18 ($E=900$ MPa, $d=9$ m, $H/B=1.0$, $e=0$ m)

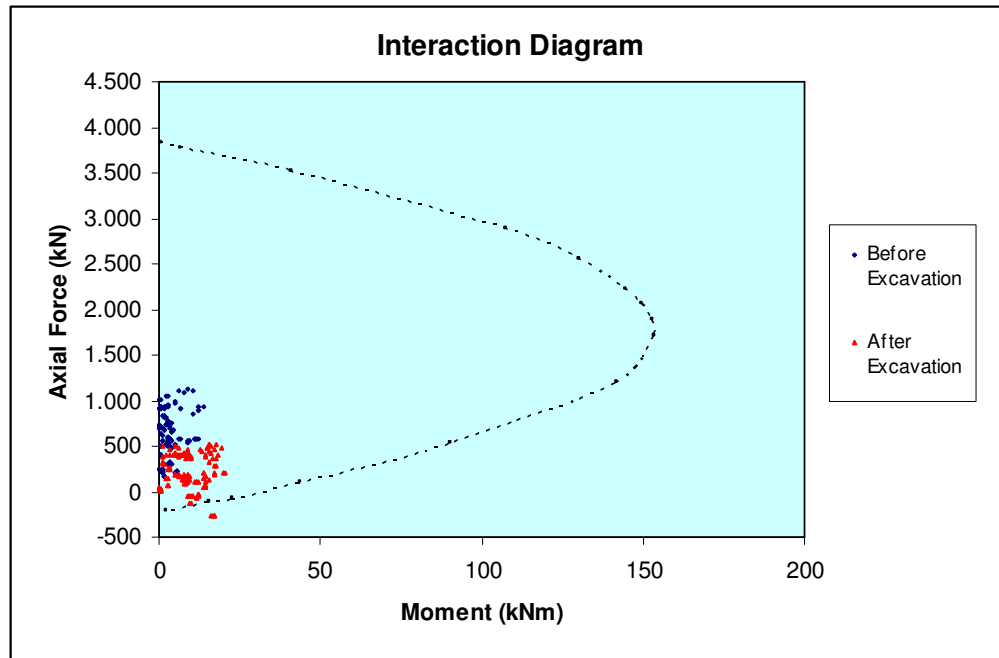


Figure A.15 Interaction Diagram for Analysis19 ($E=900$ MPa, $d=12$ m, $H/B=0.7$, $e=0$ m)

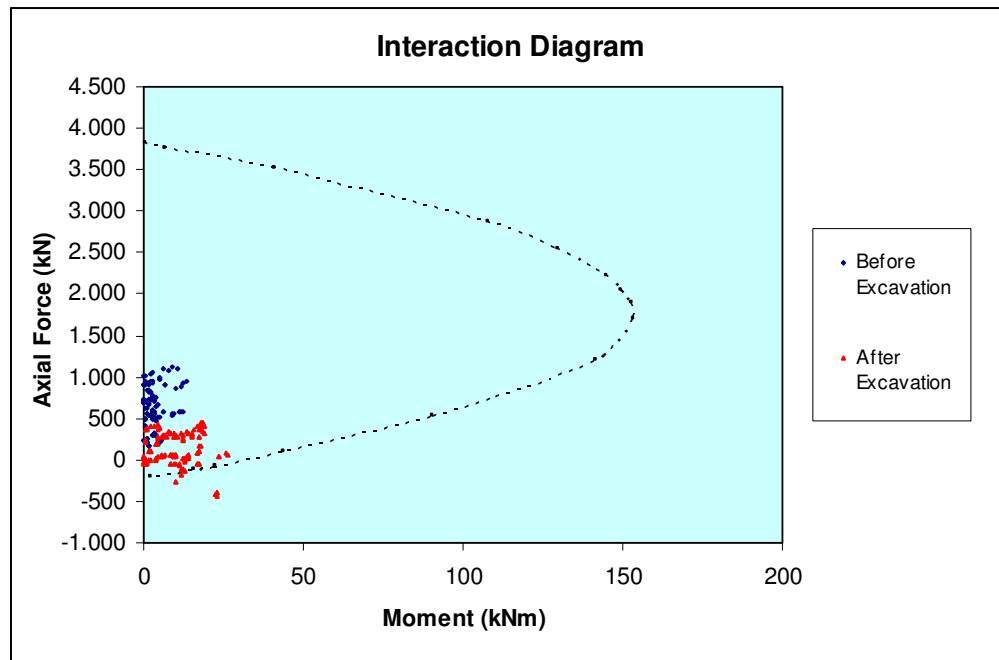


Figure A.16 Interaction Diagram for Analysis20 ($E=900$ MPa, $d=15$ m, $H/B=0.5$, $e=0$ m)

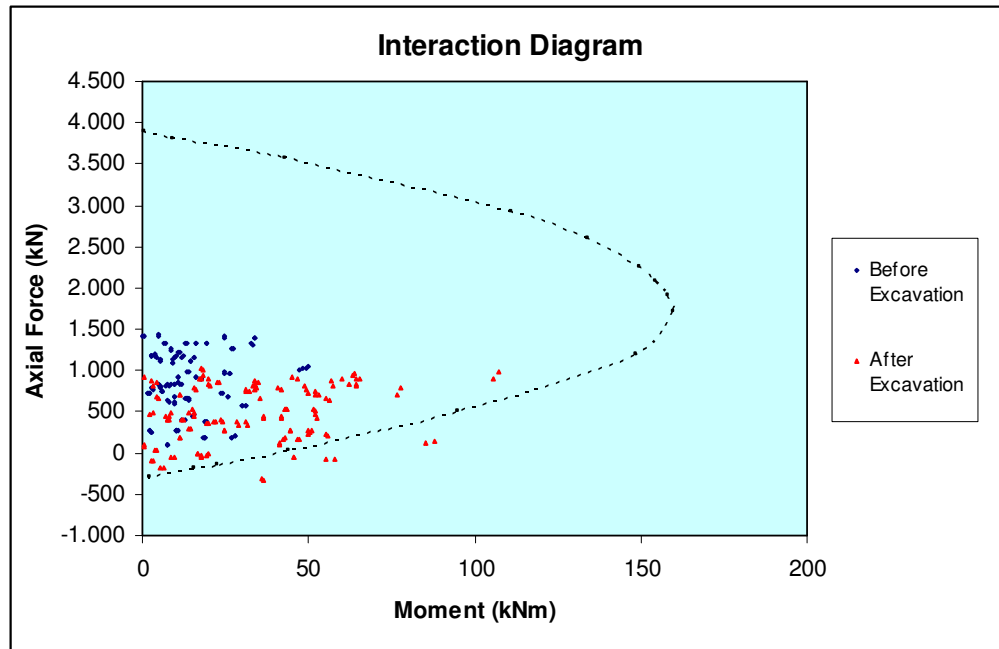


Figure A.17 Interaction Diagram for Analysis21 ($E=150$ MPa, $e=10$ m, $e/B=0.9$)

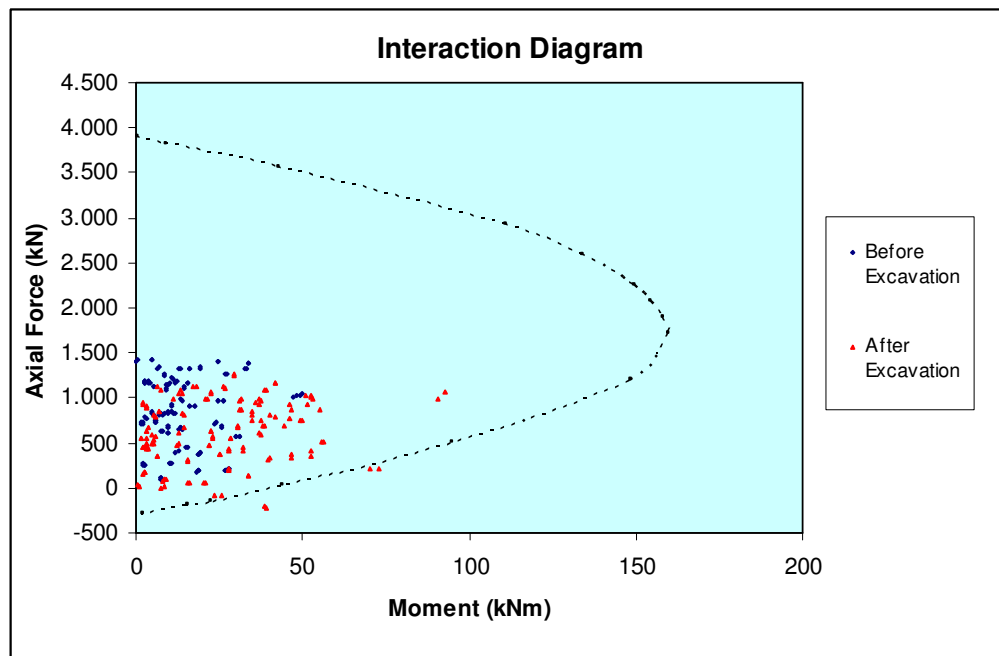


Figure A.18 Interaction Diagram for Analysis22 ($E=150$ MPa, $e=20$ m, $e/B=1.8$)

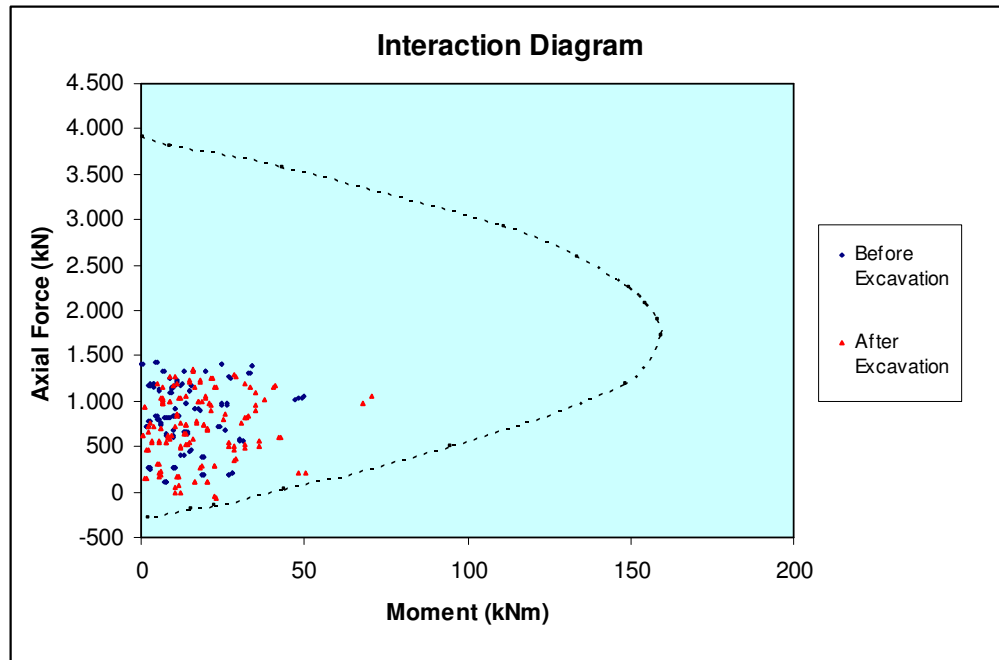


Figure A.19 Interaction Diagram for Analysis23 ($E=150$ MPa, $e=30$ m, $e/B=2.7$)

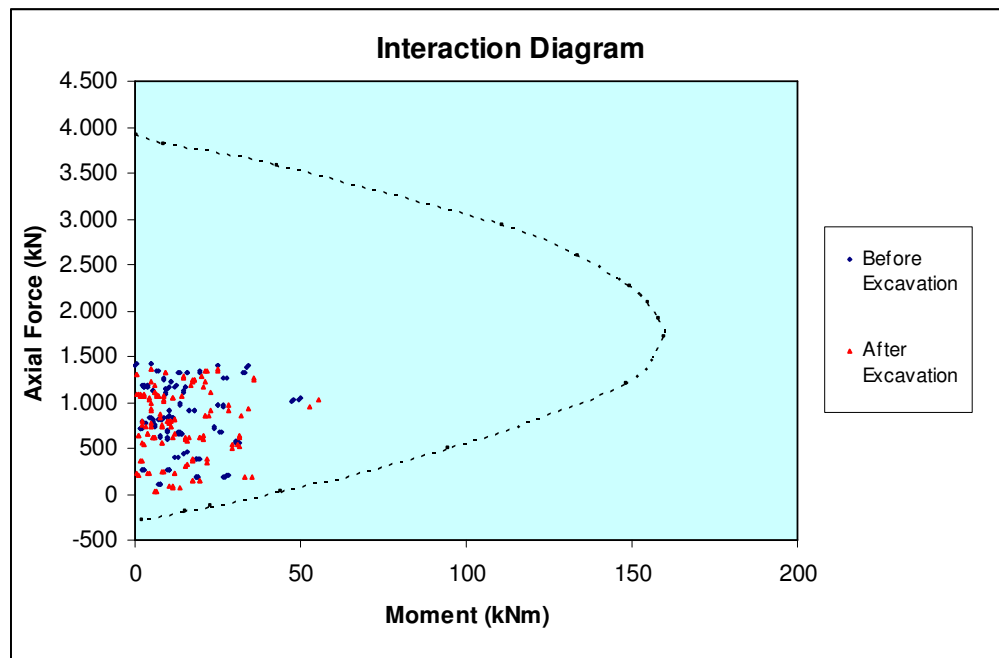


Figure A.20 Interaction Diagram for Analysis24 ($E=150$ MPa, $e=40$ m, $e/B=3.6$)

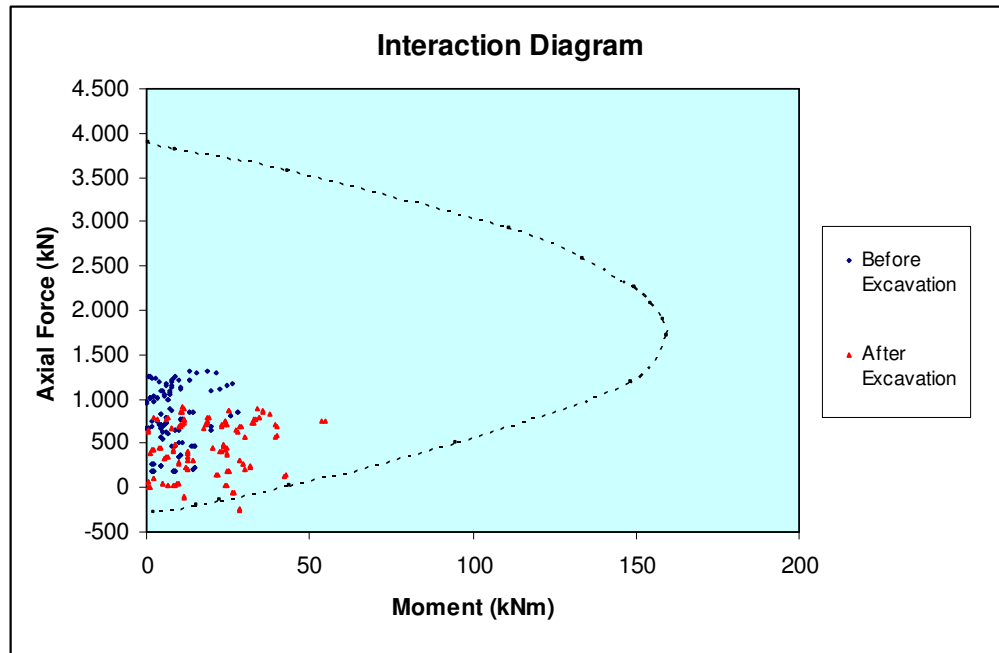


Figure A.21 Interaction Diagram for Analysis25 ($E=300$ MPa, $e=10$ m, $e/B=0.9$)

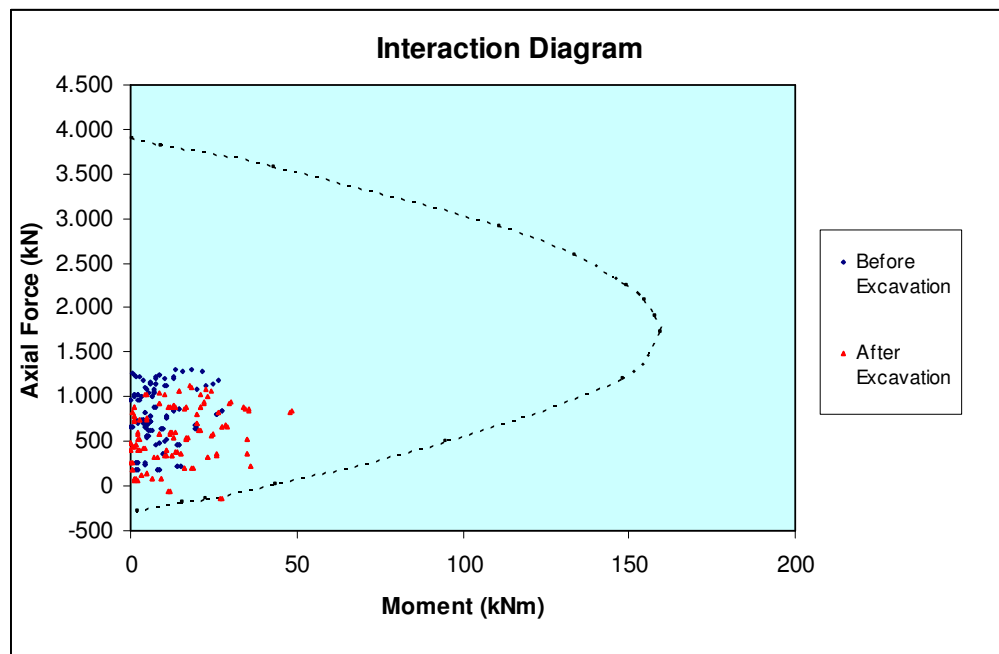


Figure A.22 Interaction Diagram for Analysis26 ($E=300$ MPa, $e=20$ m, $e/B=1.8$)

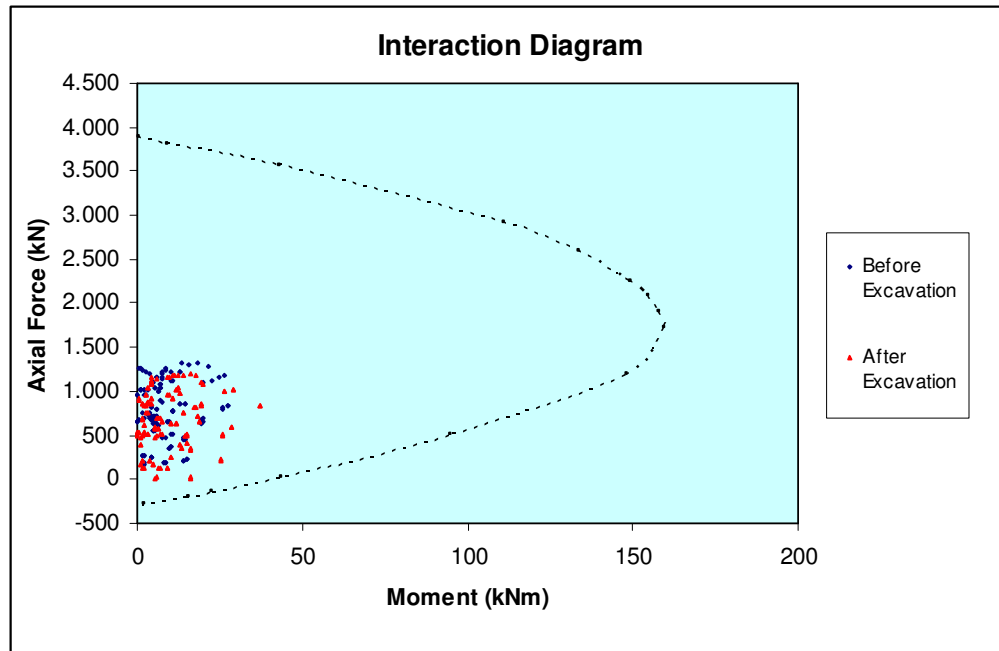


Figure A.23 Interaction Diagram for Analysis27 ($E=300$ MPa, $e=30$ m, $e/B=2.7$)

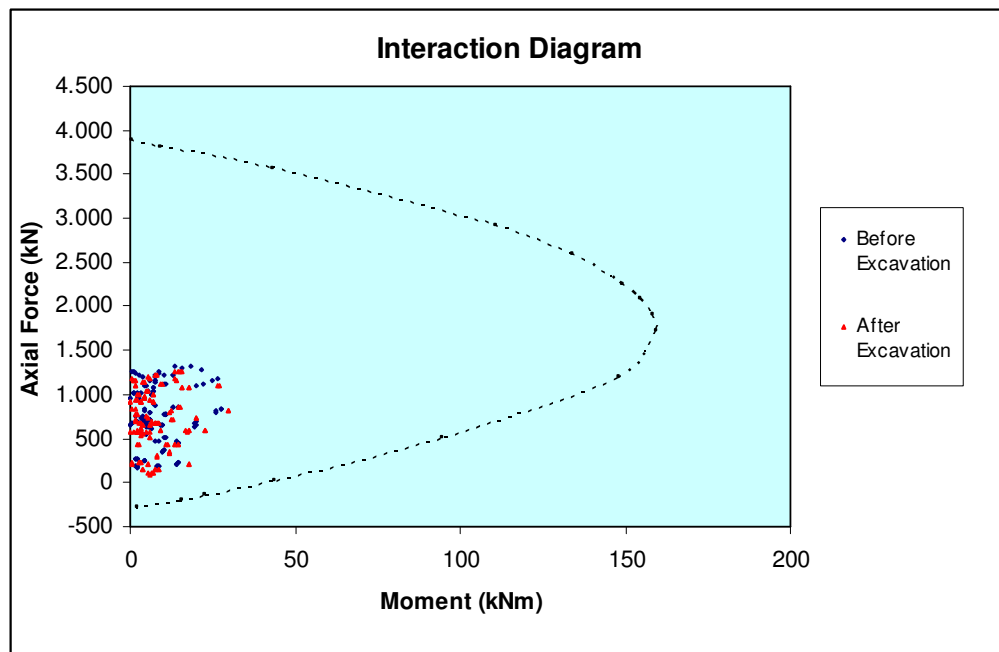


Figure A.24 Interaction Diagram for Analysis28 ($E=300$ MPa, $e=40$ m, $e/B=3.6$)

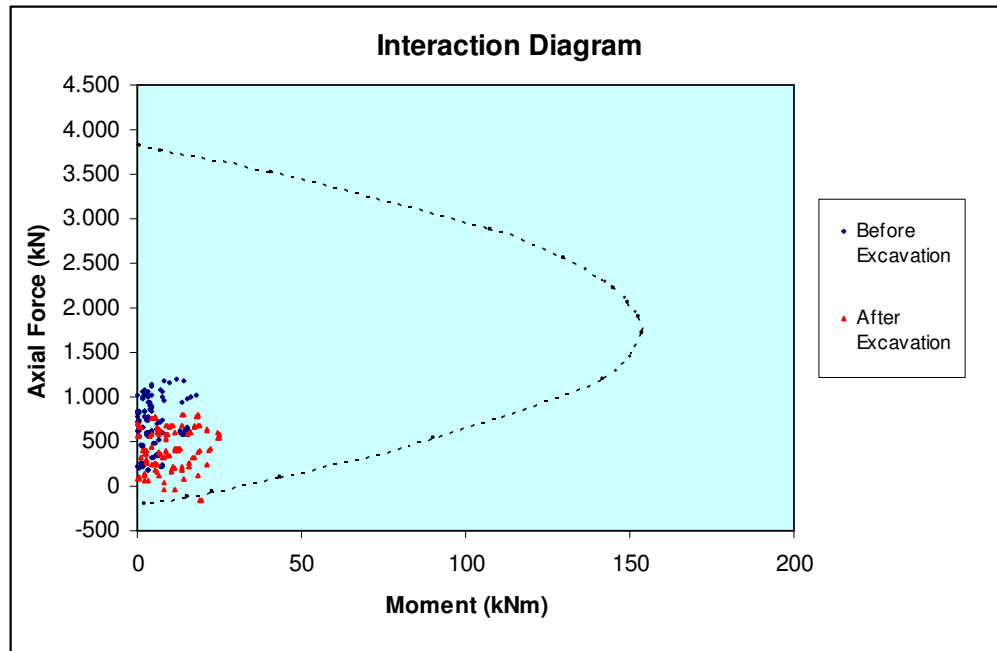


Figure A.25 Interaction Diagram for Analysis29 ($E=600$ MPa, $e=10$ m, $e/B=0.9$)

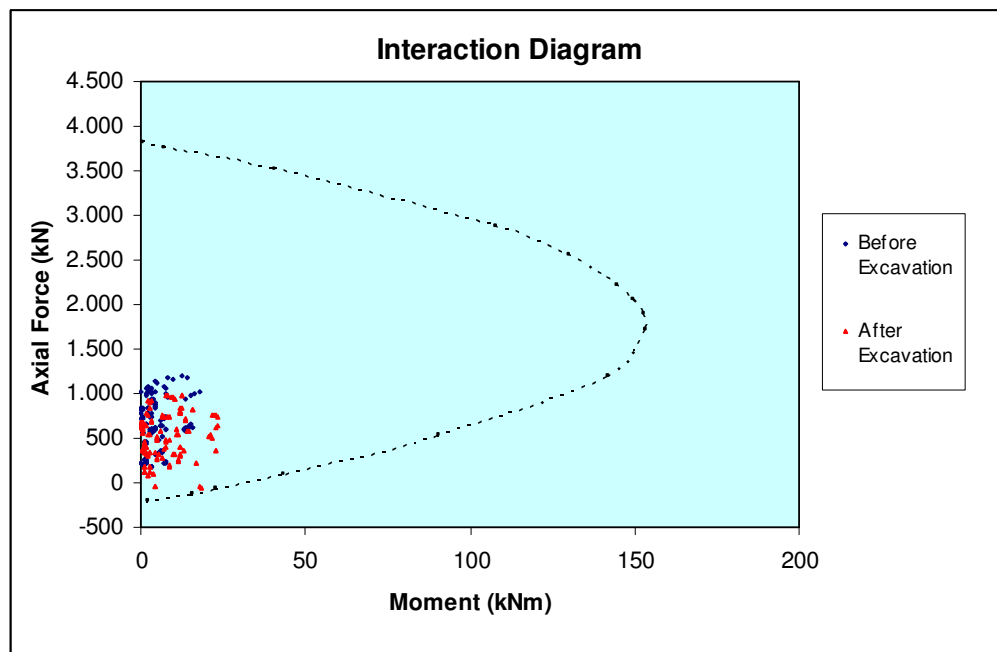


Figure A.26 Interaction Diagram for Analysis30 ($E=600$ MPa, $e=20$ m, $e/B=1.8$)

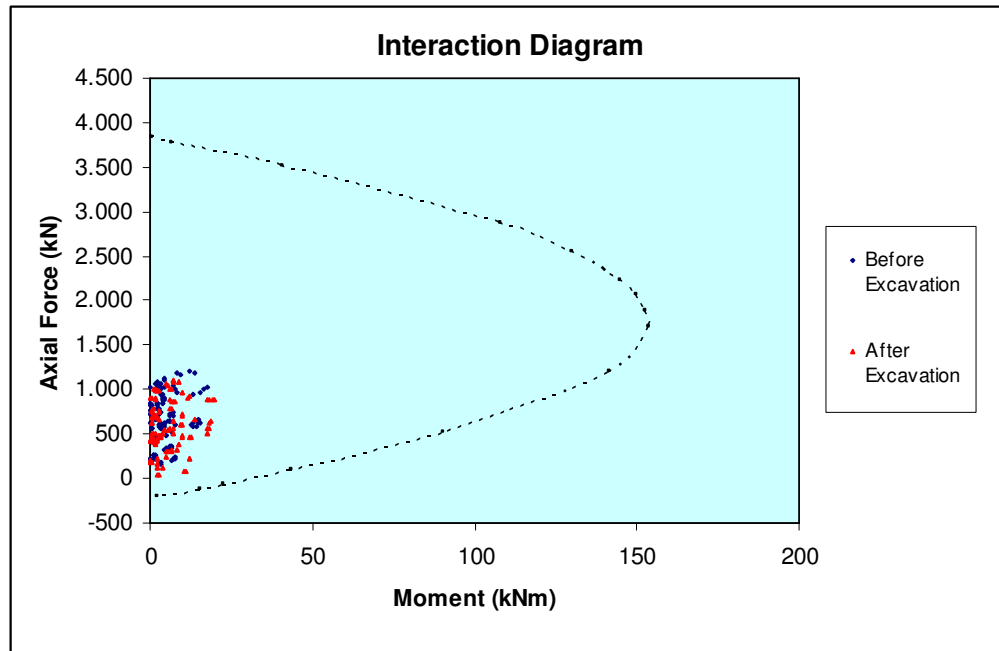


Figure A.27 Interaction Diagram for Analysis31 ($E=600$ MPa, $e=30$ m, $e/B=2.7$)

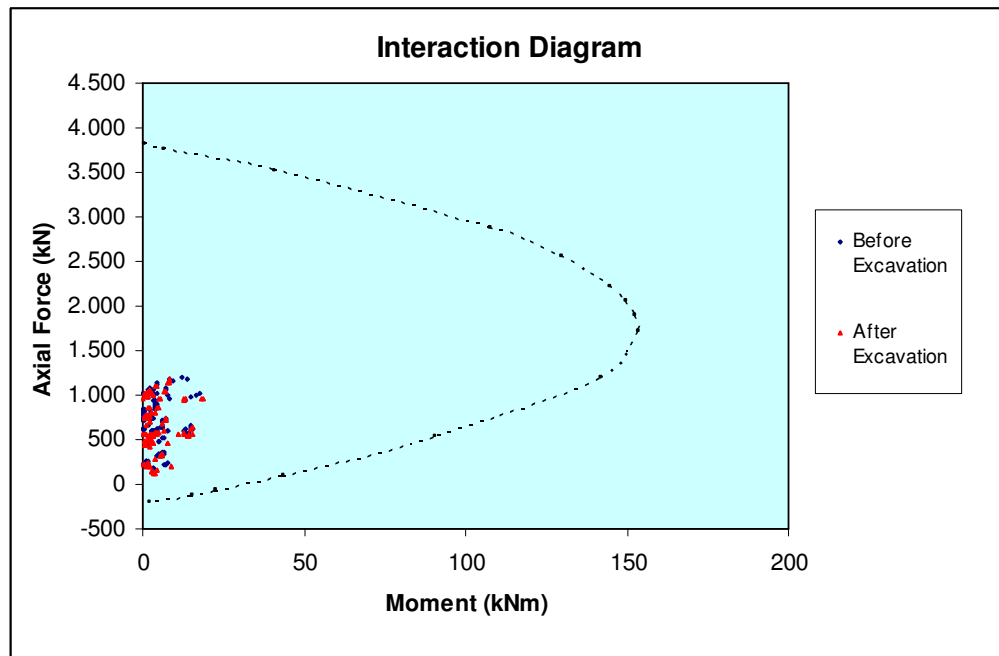


Figure A.28 Interaction Diagram for Analysis32 ($E=600$ MPa, $e=40$ m, $e/B=3.6$)

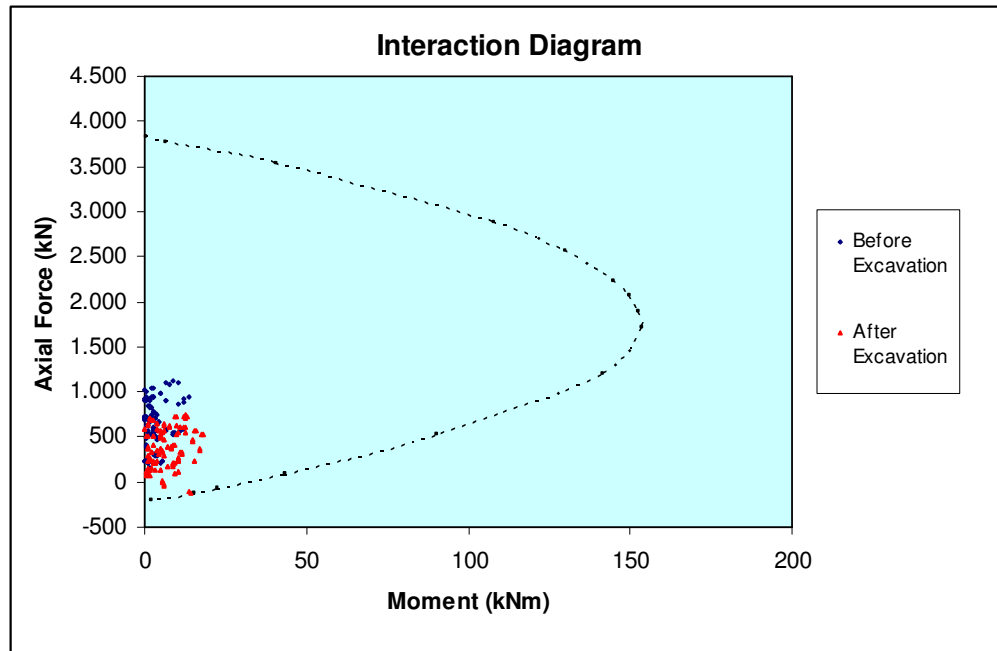


Figure A.29 Interaction Diagram for Analysis33 ($E=900$ MPa, $e=10$ m, $e/B=0.9$)

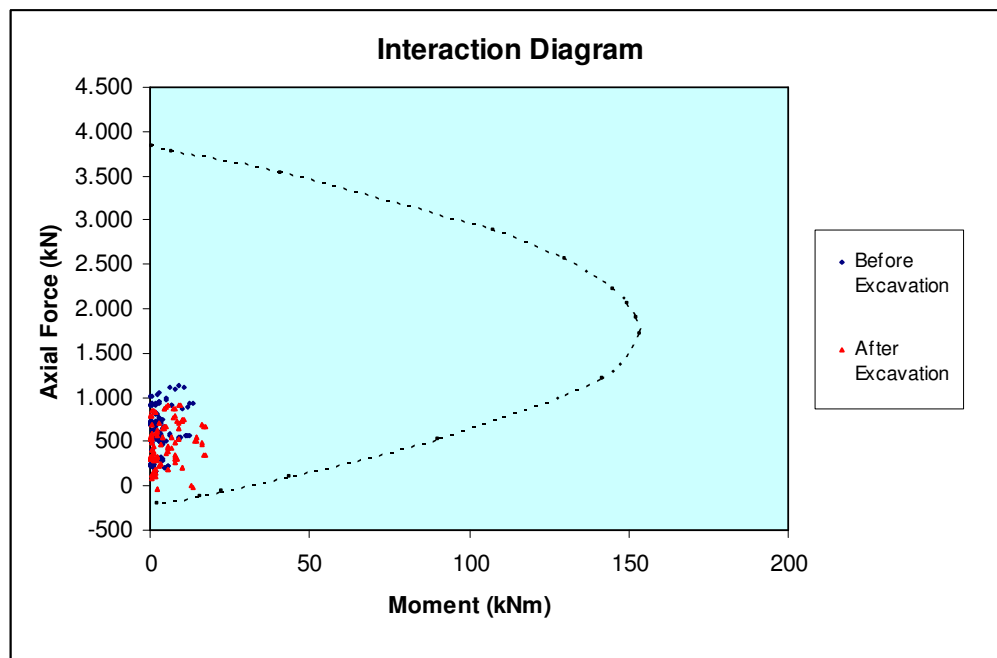


Figure A.30 Interaction Diagram for Analysis34 ($E=900$ MPa, $e=20$ m, $e/B=1.8$)

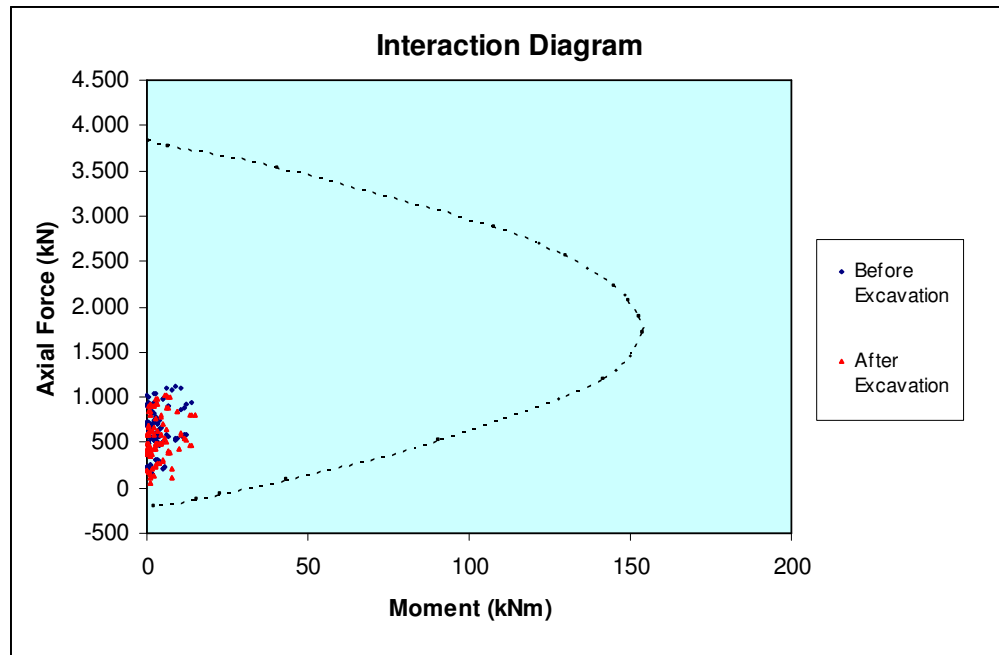


Figure A.31 Interaction Diagram for Analysis35 ($E=900$ MPa, $e=30$ m, $e/B=2.7$)

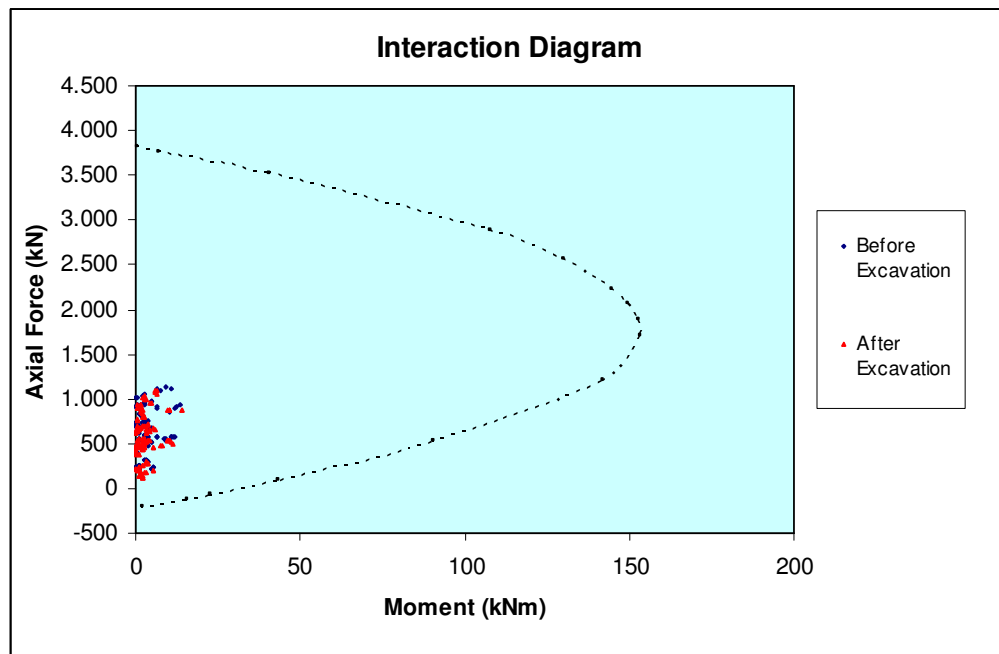


Figure A.32 Interaction Diagram for Analysis36 ($E=900$ MPa, $e=40$ m, $e/B=3.6$)

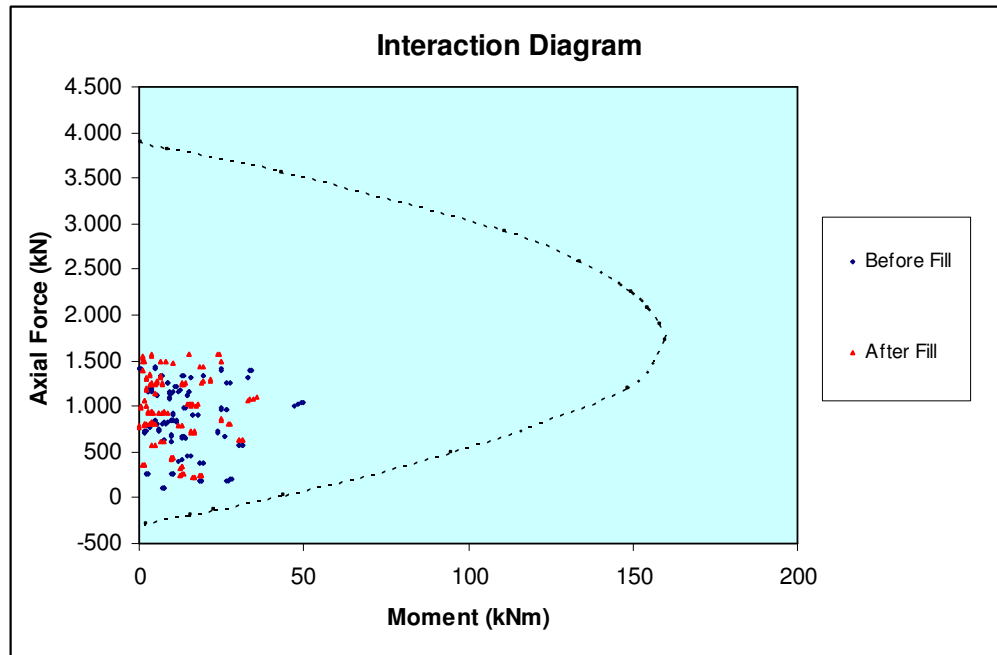


Figure A.33 Interaction Diagram for Analysis37 ($E=150$ MPa, $h=5$ m, $h/B=0.5$)

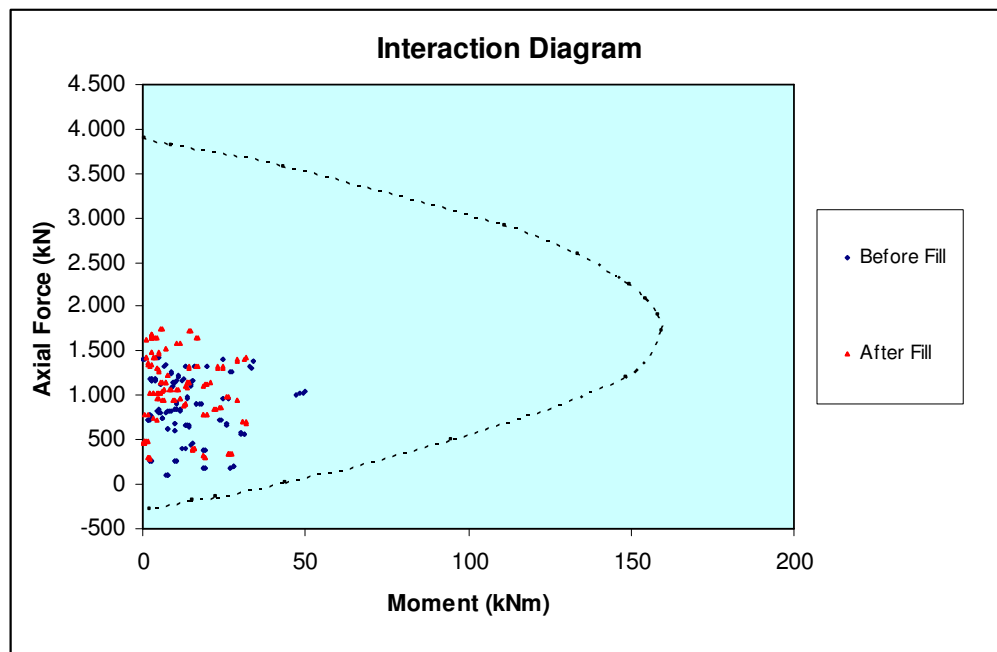


Figure A.34 Interaction Diagram for Analysis38 ($E=150$ MPa, $h=10$ m, $h/B=0.9$)

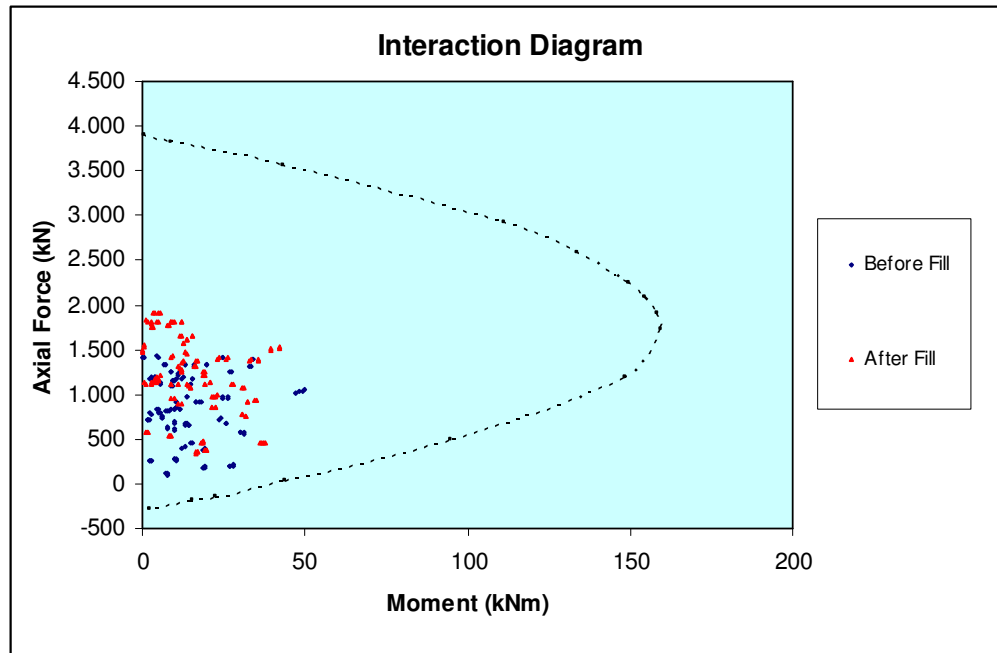


Figure A.35 Interaction Diagram for Analysis39 ($E=150$ MPa, $h=15$ m, $h/B=1.4$)

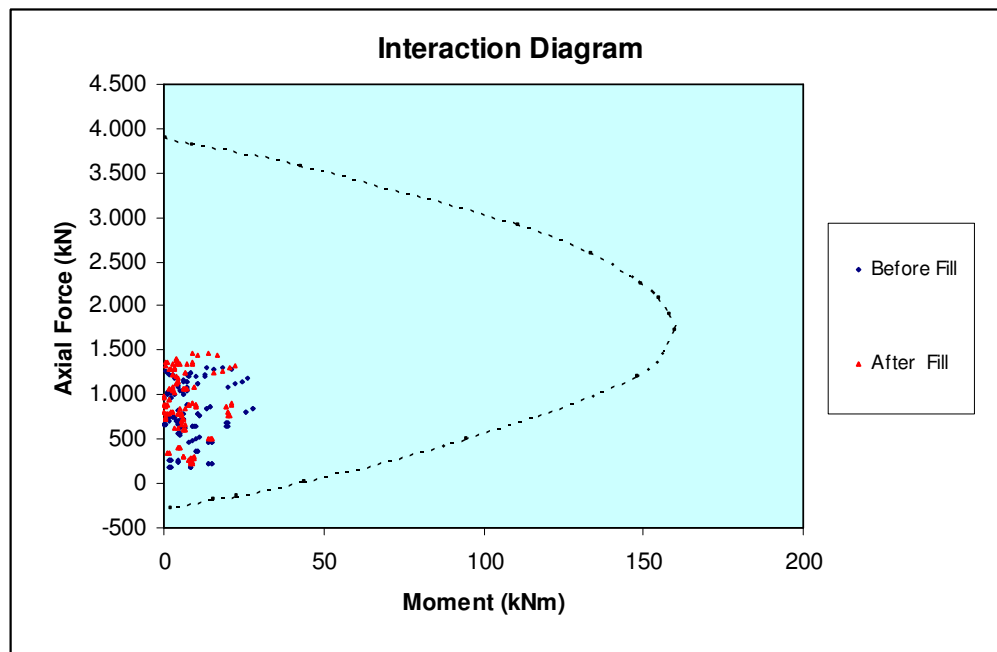


Figure A.36 Interaction Diagram for Analysis40 ($E=300$ MPa, $h=5$ m, $h/B=0.5$)

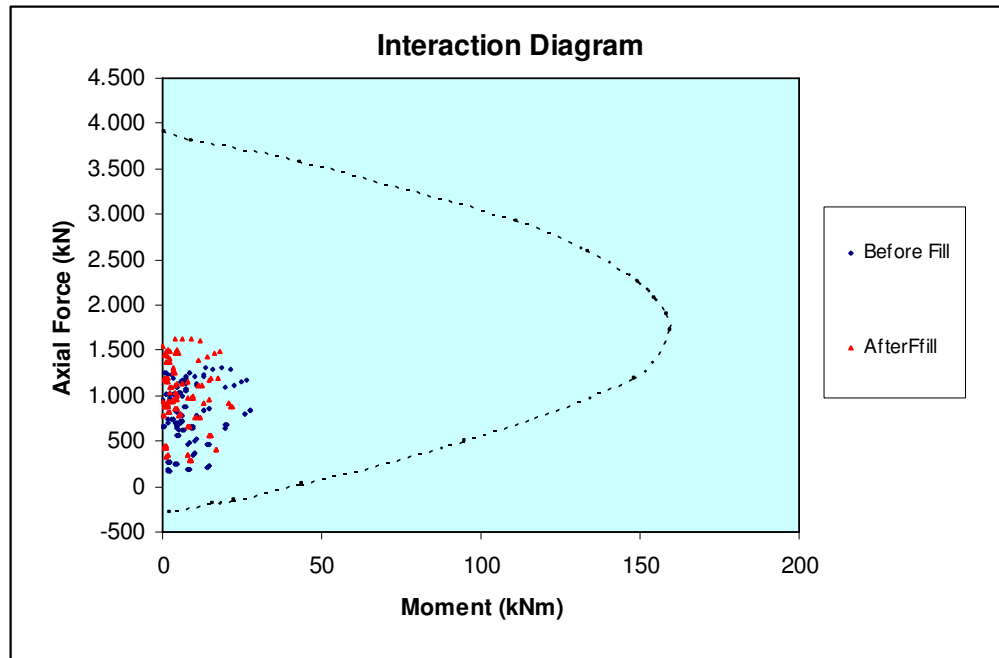


Figure A.37 Interaction Diagram for Analysis41 ($E=300$ MPa, $h=10$ m, $h/B=0.9$)

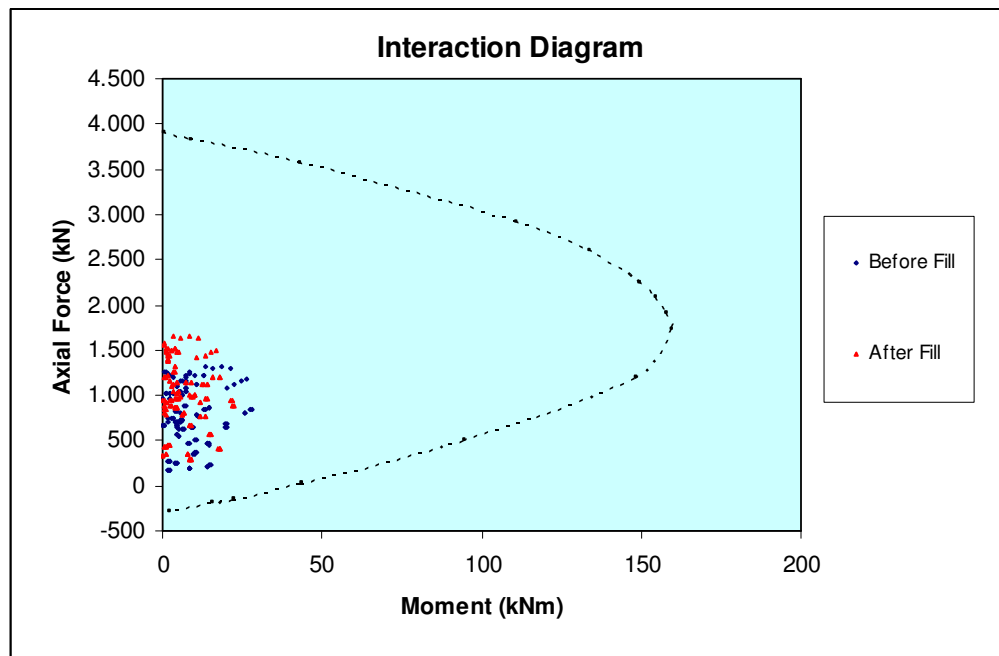


Figure A.38 Interaction Diagram for Analysis42 ($E=300$ MPa, $h=15$ m, $h/B=1.4$)

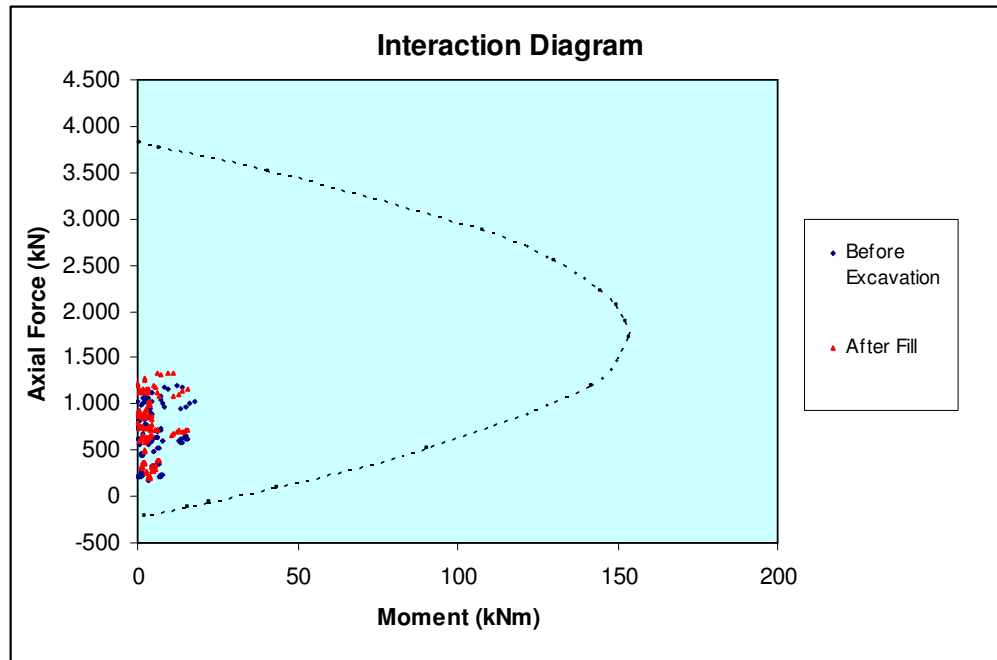


Figure A.39 Interaction Diagram for Analysis43 ($E=600$ MPa, $h=5$ m, $h/B=0.5$)

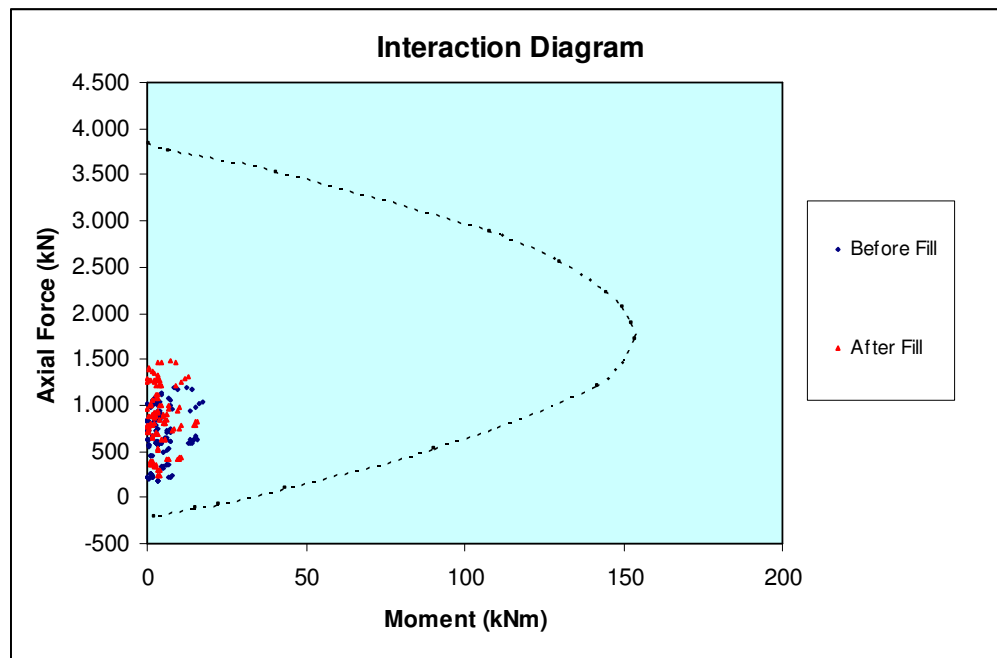


Figure A.40 Interaction Diagram for Analysis44 ($E=600$ MPa, $h=10$ m, $h/B=0.9$)

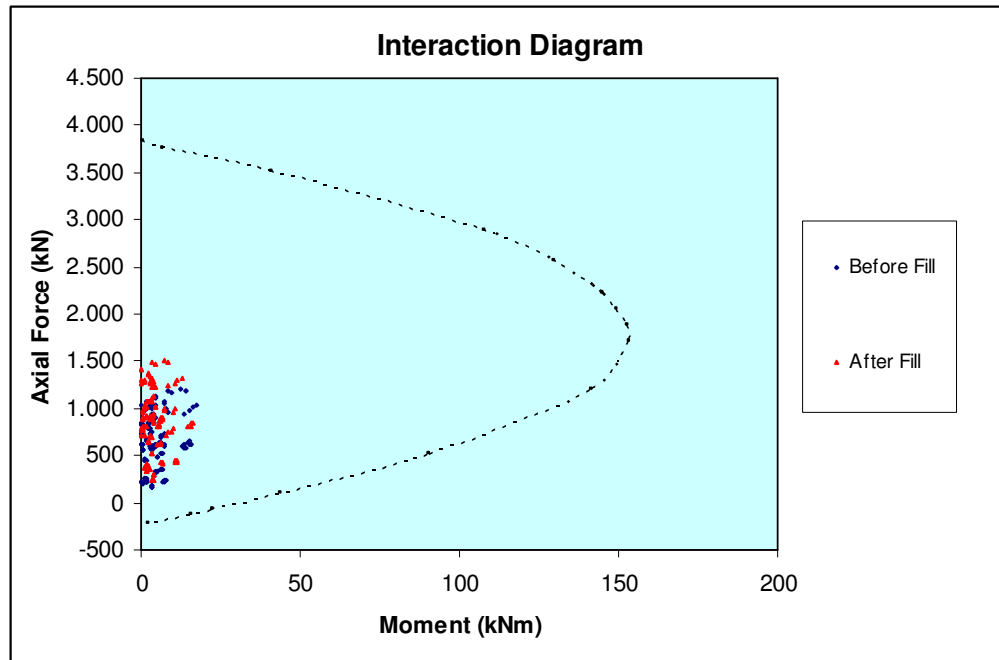


Figure A.41 Interaction Diagram for Analysis45 ($E=600$ MPa, $h=15$ m, $h/B=1.4$)

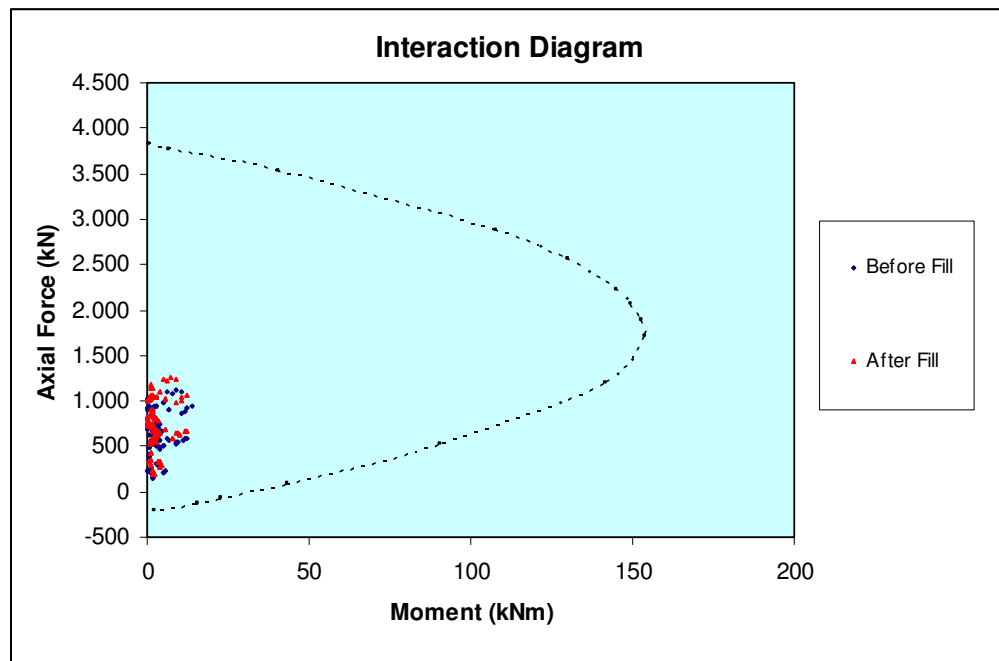


Figure A.42 Interaction Diagram for Analysis46 ($E=900$ MPa, $h=5$ m, $h/B=0.5$)

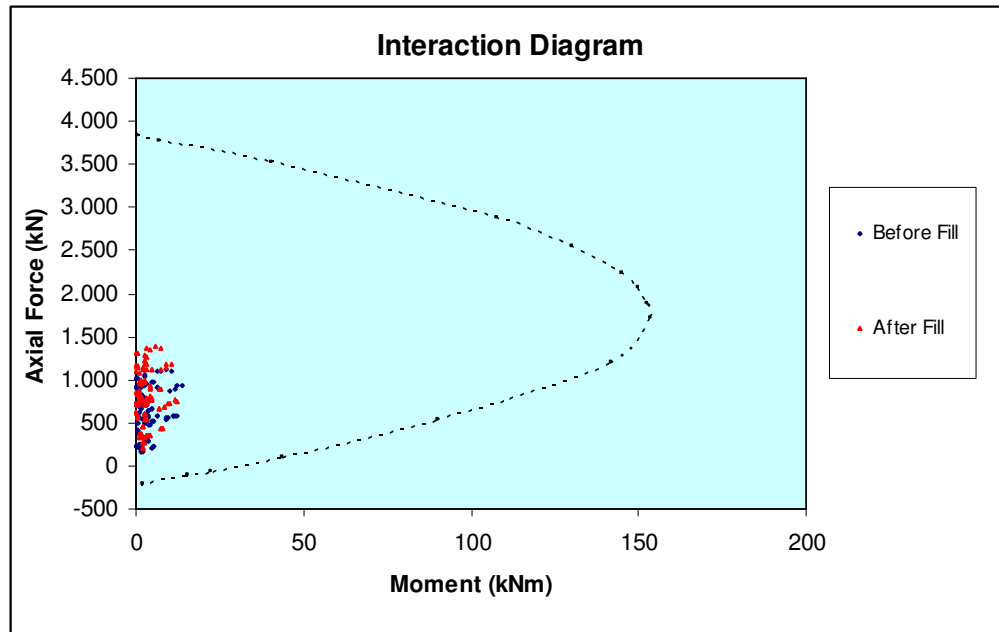


Figure A.43 Interaction Diagram for Analysis47 ($E=900$ MPa, $h=10$ m, $h/B=0.9$)

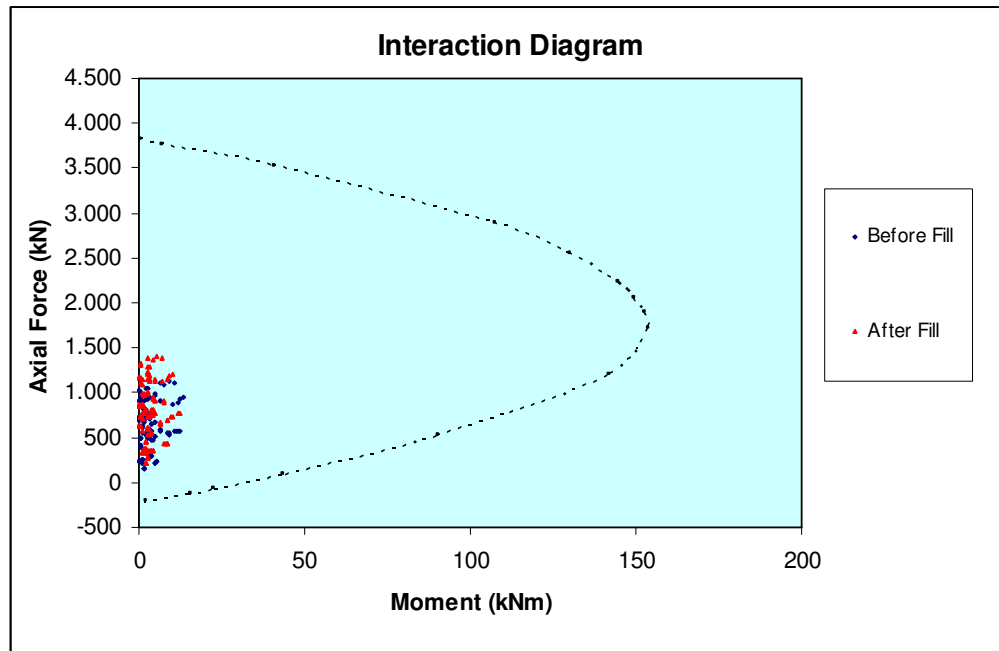


Figure A.44 Interaction Diagram for Analysis48 ($E=900$ MPa, $h=15$ m, $h/B=1.4$)